Performance of granulated foam glass in cement matrix composite material

A Dissertation Submitted in Partial Fulfillment of the Requirements for the Doctor of Philosophy degree in Ceramics Engineering as a Part of Stipendium Hungaricum Scholarship in Material Science and Technology

PhD Candidate

Masoud Osfouri

Supervisor

Dr. Simon Andrea, Associate Professor

Institute of Energy, Ceramics and Polymer Technology

Faculty of Materials and Chemical Engineering

University of Miskolc

Miskolc, Hungary

2025

'I'm always looking to the lightweight superproduct that you apply and almost don't see. That's the ultimate, at least for me.'

Francois Nars

ACKNOWLEDGEMENT

Table of contents

List of figures

List of tables

List of abbreviations

Abbreviation	Definition
AAS	Alkali-Activated Slag
ACI	American Concrete Institute
ASR	Alkali-Silica Reaction
ASTM	American Society for Testing and Materials
CMFGC	Cement Matrix–Foam Glass Composite
CRT	Cathode Ray Tube
DOE	Design Of Experiments
DSC	Differential Scanning Calorimeter
DTA	Differential Thermal Analysis
EDS	Energy Dispersive X-Ray Spectroscopy
FGA	Foam Glass Aggregate
FM	Fineness Modulus
FWHM	Full Width at Half Maximum
ICDD	International Center for Diffraction Data
ISO	International Organization for Standardization
LICA	Light expanded clay aggregate
LOI	Loss On Ignition
MCDM	Multi-Criteria Decision Making
N	Normal (in measuring the solution)
OPC	Ordinary Portland Cement
PDF	Powder Diffraction File Database
PMC	Polymer Matrix Composite
RH	Relative Humidity
S/N	Signal-To-Noise Ratio
SEM	Scanning Electron Microscopy
SLS	Soda-Lime Silicate
TG	Thermogravimetry
T_g	Glass Transition Temperature
T_{EX}	The starting temperature of expansion
T_{MH}	Maximum height temperature
T_{MA}	Maximum area temperature
T_{Avg}	The average of maximum height and maximum area temperature
TGA	Thermogravimetric Analysis
WSM	Weighted Sum Model
XRD	X-Ray Diffraction

Introduction

The researcher's and engineers' efforts to create new materials have led to the invention of foam glass and its establishment in various industries. This material is a promising replacement for traditional aggregates in concrete, offering a balance of strength, weight reduction, and environmental benefits.

Concrete and cement matrix composites are an integral part of human life, increasingly used in construction and infrastructure projects in all countries. It is said that concrete has the highest per capita consumption of any manufactured material in the world. Currently, around 30 billion tons of this widely used man-made material are produced globally each year. This means that about four and a half tons of concrete are produced annually for each person. According to statistics, concrete accounts for approximately 70 percent by the weight of all construction materials. In Europe, concrete consumption is significant, with about two and a half billion tons produced annually. In the United States, concrete use in construction is common, with about 300 million tons produced annually. Today, China leads global concrete production, having produced more concrete in the last three years than the United States has in the past century.

The ubiquitous presence of cement matrix composite materials in our daily environments, buildings, bridges, towers, dams, and all construction projects is evident. Concrete is a material that, despite its low cost, possesses specific engineering properties. Its high compressive strength, ease of use, and readily available raw materials contribute to its widespread use. However, the inherent density of concrete, due to its sand and gravel content, results in heavy structures. Primarily, the significant weight of concrete increases the dead load of structures, necessitating very strong foundations and support systems. Using lightweight concrete can reduce the cost of foundation construction by up to 30 percent. Additionally, reducing the weight of concrete can lower transportation and handling costs. In earthquake-prone areas, the heavy mass of concrete structures can cause significant casualties; for example, the collapse of heavy concrete buildings during the 1999 Izmir earthquake in Turkey resulted in the deaths of over 17,000 people. Furthermore, traditional concrete lacks high thermal and acoustic insulation properties, leading to increased energy consumption for heating and cooling buildings and raising operational costs by up to 60 percent.

These factors have led engineers and researchers to focus on lightweight concrete. The extraction of natural stones for use as aggregates in concrete also causes significant environmental issues, which is a major concern for humanity today. Of course, with the advancement of civilizations, environmental degradation is occurring in various forms across the globe. This issue has

increasingly captured the attention of scientists, researchers, and governments today. One of the major challenges humans face is the problem of waste glass. Waste glass, being non-degradable, significantly harms the environment, remaining intact for thousands of years and contributing to the growing problem of waste density. In Europe, about 12 million tons of waste glass are produced annually. Although European countries are more focused on recycling waste than many other countries, only about 70 percent of waste glass is recycled, with around 3.6 million tons ending up in landfills. Waste glass in landfills can leach harmful chemicals into the soil and groundwater, potentially contaminating drinking water and harming wildlife. Moreover, producing glass from raw materials is energy-intensive and requires large amounts of natural resources like sand, soda ash, and limestone, and the production process emits a significant amount of carbon dioxide. For example, producing one ton of new glass emits about 385 kilograms of carbon dioxide. Additionally, discarded glass can cause physical injuries to humans and animals. Therefore, increasing recycling rates and finding innovative applications for waste glass are crucial steps toward sustainable waste management.

One product made from recycled glass is foam glass. Foam glass, available in various shapes and qualities, has special applications in insulation, filtration as a liquid absorber, and as lightweight construction material. One recent application attracting industrial attention is using it as an aggregate in lightweight concrete and cement matrix composite materials. Although this application is still in its early stages, extensive research is ongoing, and no studies have yet examined the use of granular foam glass for producing structural lightweight concrete. This study investigates the feasibility of producing and utilizing granular foam glass with optimized properties on a laboratory scale. The study is divided into two parts: the first part involves research on foam glass and examines the properties of foam glass made from different compositions and production conditions, ultimately presenting an innovative method for laboratory-scale production of foam glass granules. The second part focuses on the incorporation of foam glass granules into a cement matrix and examines the resulting composite's properties.

1. State of the Art

The primary focus of this thesis lies in two interrelated areas: the investigation of foam glass and the development of structural lightweight cement matrix composites incorporating foam glass granules. Before presenting the core contributions of the research, this chapter first reviews the concept of lightweight concrete, its applications, existing research, knowledge gaps, and relevant innovations in the field. It then introduces foam glass as a relatively new and promising material in construction, summarizing the findings of prior studies. The discussion proceeds with an exploration of the use of granular foam glass in cementitious systems and its integration into the design of structural composites.

In this study, instead of using the term "lightweight concrete," the term cement matrix foam glass composite (CMFGC) is introduced to better reflect the experimental and innovative nature of the material system. Unlike conventional concrete, which is governed by strict standards regarding mixture proportions, aggregate types, and performance criteria, this research adopts a more flexible approach to explore the fundamental behavior of foam glass in a cementitious environment. Since this is a pioneering and foundational study aimed at guiding future research, in certain cases the formulations do not strictly adhere to standard concrete specifications. Therefore, the term CMFGC is used throughout this thesis to accurately describe the cement matrix composite material and to distinguish it from conventional lightweight concrete.

1.1. The role of lightweight aggregate

Lightweight concrete, an alternative to conventional concrete, has gained traction in the construction industry due to its unique properties and versatility. Unlike conventional concrete, which typically weighs around 2400 kg/m^3, lightweight concrete boasts a significantly lower density, ranging from 400 to 2000 kg/m^3 [1]. This remarkable weight reduction is achieved by employing lightweight aggregates, such as light-expanded clay aggregate (LICA), slate, or artificial lightweight aggregates in place of conventional aggregate.

As it is shown in Figure 1 lightweight concrete encompasses three primary types: foamed concrete, no-fines concrete, and lightweight aggregate concrete [1]. Foamed concrete, with a density between 400 and 1200kg/m^3, is produced by introducing air bubbles into the cement paste [2]. No-fines concrete, characterized by a density range of 700 to 1500 kg/m^3, is produced by introducing air bubbles into the cement paste sand from the concrete mix [3, 4]. The third type is lightweight aggregate concrete. This type of lightweight concrete, which includes most lightweight concrete varieties, has a density ranging between 500 to 2000 kg/m³[5-8].

Figure 1. Three typical types of lightweight concretes. a) foamed concrete [9], b) no-fine concrete [10], and c) lightweight aggregate concrete [11]

The allure of lightweight concrete stems from its array of advantages over conventional concrete. Its reduced weight, up to 50% less than conventional concrete, translates into significant construction cost savings, particularly for high-rise buildings [5-8, 12, 13]. Additionally, lightweight concrete's enhanced thermal conductivity promotes energy efficiency by keeping buildings cooler in summer and warmer in winter [14-17]. Furthermore, its improved fire resistance and seismic performance make it a safer choice for construction [18-20]. The versatility of lightweight concrete extends to a wide spectrum of applications. In building construction, it commonly finds use in floors, walls, roofs, and precast concretes. Infrastructure projects, including bridges, tunnels, and retaining walls, also benefit from lightweight concrete properties. Moreover, industrial applications, such as tanks, silos, and flooring, utilize lightweight concrete for its lightweight and durable nature [1, 8, 12, 14, 16, 21-24]. With the growing global demand for sustainable construction materials intensifying, lightweight concrete is poised to play an increasingly prominent role in the construction industry. Its versatility, sustainability, and performance advantages make it a valuable asset in the pursuit of greener and more resilient structures. Based on the strength and load-bearing capacity of lightweight concretes, they are generally classified into three categories: non-structural lightweight concrete, semi-structural lightweight concrete with medium strength, and structural lightweight concrete [1, 16, 25-27].

Non-structural lightweight concrete refers to concretes with compressive strength less than 9.5MPa, and their density is usually below $800 \, kg/m^3$. This category of concrete is highly effective in separating blades and thermal and sound insulation on floors. Such concrete can be utilized in walls, floors, and various ceiling systems when combined with other materials [28, 29]. Primarily of the cellular lightweight concrete or open-structure lightweight concrete type, this concrete may also include lightweight aggregate concretes within this range of strength and density [30]. The addition of natural aggregates to the lightweight aggregate concrete mix design increases

the weight and strength of the concrete. However, to achieve optimal thermal insulation properties, the density is limited to 800 kg/m^3 [7, 31, 32].

When constructing and using non-structural lightweight concrete, the aim is to enhance thermal insulation properties while reducing weight. Extensive research has been conducted on the relationship between the density of lightweight concrete and its thermal conductivity, generally showing that by increasing the density, thermal conductivity rises. Additionally, mechanical strength has a direct relationship, implying that an increase in concrete density is expected to result in increased compressive strength [2, 12, 18, 21, 22, 28, 31].

Overall, the compressive strength of concrete specifies its potential applications. A compressive strength of less than 1 MPa is suitable for insulating underground pipes, while concrete with higher strength, up to approximately 3.5 MPa, can be used for flooring [7, 33]. It is worth noting that lightweight concrete's shrinkage during drying is a significant issue in most cases [7].

Semi-structural lightweight concretes, with a range of density varying from 700 to 1400 kg/m^3, constitute the second category. These concrete exhibit compressive strengths ranging from 5 to 15 MPa, and are typically lightweight aggregate or open-structure concretes [34]. To reduce density, fine aggregates are either removed from the concrete or natural and artificial lightweight aggregates are used. These concretes are commonly employed in hollow concrete blocks and flooring applications [35].

The third type of lightweight concretes is its structural type. The density of this type is less than 2000 kg/m^3 and a compressive strength of more than 17 MPa and less than 80 MPa. Typically, the density of these concretes is in the range of 1400 to 2000 kg/m^3. Most structural lightweight concretes belong to the lightweight aggregate concrete family [1, 5, 26, 28].

Achieving a compressive strength of 17 MPa or more is possible with many artificial lightweight aggregates and some natural lightweight aggregates [1]. As mentioned earlier, the strength of concrete is usually related to its density. It should be noted that the concrete's density is primarily influenced by the density of the aggregates used, with lighter materials leading to a reduction in the overall density of the concrete. However, it is important to know the use of heavier lightweight aggregates does not necessarily increase the compressive strength of the concrete, and the use of lightweight aggregates with a strength commensurate with the required strength of the lightweight concrete is desirable to achieve the minimum density and maximum desired strength [1, 33, 36]. Various natural lightweight aggregates have been used by industries and researchers to date for making lightweight concrete. All of these

lightweight aggregates have a porous structure in which gas cells inside them reduce the density of the aggregate [37, 38]. One of the lightweight porous aggregates that can be used in concrete is foam glass.

Knowledge gap: is it possible to develop a structural lightweight cement matrix composite material *using granulated foam glass?*

1.2. Introduction of foam glass

Foam glass is a porous material with a glass matrix containing millions of bubbles of varying sizes. Figure 2 illustrates conventional types of foam glass material in the market and its typical porous structure. Foam glass is fire-resistant, extremely lightweight, and behaves almost like rigid materials in terms of dimensional stability. It is an insulator for both sound and temperature, is non-toxic, and can be easily machined. Additionally, depending on the manufacturing method and materials used, foam glass can be either moisture-resistant or permeable.
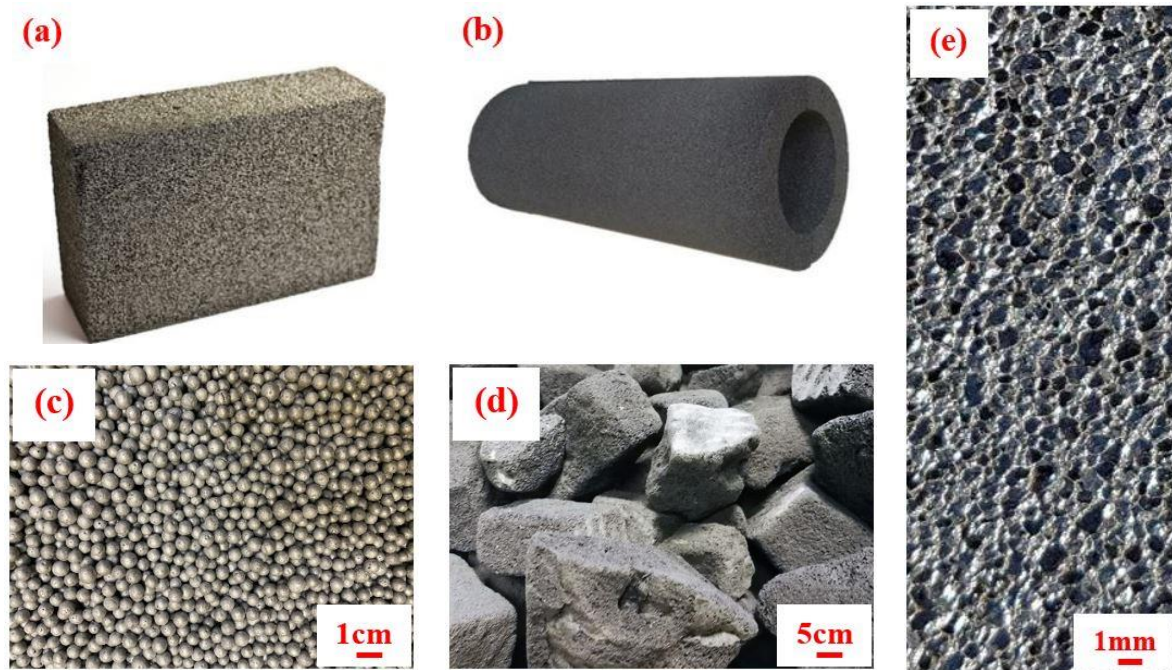
Figure 2. The conventional types of foam glass in the market, a) block [39], b) pipe insulator [40], c) granules [41], d) gravels. e) the typical porous structure of foam glass [42]

The properties of foam glass have led to its use in various industries, including road construction, petrochemicals, pipelines for transporting very hot and very cold gases and liquids, foundations for sports facilities and buildings, dam construction, and any industry where its properties can meet their specific needs [43]. This lightweight material is commonly used for heat resistance and sound insulation [44, 45]. The foam glass could be a tailoring material, which means according to the desired application, the engineers can produce it as open/close-pored porous material. If heat insulation is required, more close porosity could be

an advantage [46-48]. The close-pored foam glass is usually used as the heat insulator of high or very low-temperature fluid transfer pipes. The apparent bulk density of this type of foam glass ranges from 120 and 165 kg/m^3 and the thermal conductivity is around 0.05 W/m·K. The compressive strength of this type of foam glass lies between 0.7 -1 MPa [49-51]. According to a claim the closed-porous foam glass (the closed porosity is at least 90 percent by volume) could be utilized in building industries due to its thermal conductivity of less than 0.1 W/m·K and compressive strength exceeding 0.5 MPa, along with its high water resistance [52, 53]. On the other hand, the open-porous foam glass with more than 50 vol% could be a good candidate as a sound insulator material [54].

The following section will provide explanations about foam glass, a short literature review about it, and an examination of the existing knowledge gaps. However, the main knowledge gap, which will be elaborated on in detail and is the main focus of this research, is that no structural lightweight CMFGC has yet been produced using granular foam glass. This research ultimately aims to explore the feasibility of creating structural lightweight CMFGC using granular foam glass. Following this section, the results of previous studies and the knowledge gaps related to foam glass research, as well as the investigations into lightweight concrete incorporating foam glass, will be discussed in detail.

Generally, the waste glass which cannot recycled into glass again is the main raw material for foam glass. Most foam glass factories use window or bottle glass cullets as raw material. However, in some foam glass factories virgin glass is used as a feed glass component. In the process of making foam glass (as sketched in Figure 3), First, the glass is ground into a fine powder. Then a foaming agent is added to the grounded glass. Subsequently, the powder mixture is heated, causing the glass particles to first soften and then produce foam glass due to the decomposition of the foaming agent.
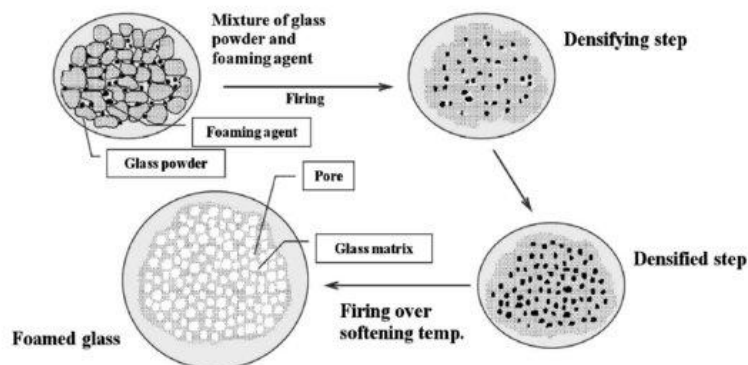
Figure 3. The foaming process of foam glass [55]

Various parameters influence the characteristics of the foam glass. Parameters such as particle size of raw materials, the weight percentage of the foaming agent, the material used as the foaming agent and glass, additional additives to the powder, firing temperature, and dwell time in the furnace, among others, affect the quality of the foam glass. Various studies have been conducted to investigate the impact of these parameters on foam glass, and the results of these studies were used to guide the direction of this research.

Knowledge gap and research question:

What is the difference in foam glasses made from virgin and waste glasses?

1.3. Effect of particle size of raw material on foam glass

Dong Sheng et al. [56] used in their study carbon black as a foaming agent, and the properties of the foam glass were examined concerning the change of particle size of the foaming agent and the heating rate. The results indicated that an increase in the heating rate could lead to a decrease in the uniformity of the foam cells. Also, they concluded that the optimal particle size when the heating rate is 8ºC/min is 0.15mm.

König et al. [57] used MnO_2 and carbon as the foaming agent in their experiments. They investigated the effect of varying the particle size of glass on the physical properties of the foam and its cells' structure. Their research results showed that a reduction in MnO_2 content led to a decrease in the foaming of the samples. Additionally, they demonstrated that reducing the particle size resulted in an increase in cell size, to the extent that when using glass powder smaller than 33 μm, foam glass with a density of 150 kg/m^3 could be produced. It happens due to the faster coalescence process. Another important claim of their study was that increasing the close porosity causes decreasing the thermal conductivity of foam glass, also if the trapped gas changes to CO_2 the thermal conductivity of the foam glass decreases.

Based on previous research, it can be stated that the particle size of the raw materials used to produce foam glass significantly affects its final properties. These studies have shown that reducing the particle size decreases the cell size of the foam glass and makes the cell distribution more uniform. This is because smaller particles pack more densely, leaving less space for larger cells to form during the foaming process. Particle size also influences the density of the foam, with smaller particle sizes resulting in higher foam density. This is due to the increased total surface area as particle size decreases, which enhances bonding between powder particles during the firing process. However, it is important to note that there is an optimum particle size; if the particle size is too small, it can inhibit the formation of gas cells within the foam glass, reducing porosity. Changes in particle size also affect thermal

conductivity: smaller and more homogeneous particle sizes in the foam glass raw materials create a greater number of tortuous paths within the foam, increasing its resistance to heat transfer. Compressive strength is also impacted by particle size. A well-distributed particle size can improve strength, as smaller particles can fill gaps between larger ones, creating a more cohesive structure. It has also been claimed that producing foam glass using finer glass powder requires lower sintering temperatures [57-62].

Previous studies have typically employed full-factorial experimental designs to investigate this topic [44-46, 50, 63-76]. As is evident, the particle size of raw materials significantly affects the properties of foam glass. One aspect of this research explores the impact of particle size on foam glass. While effective, full-factorial designs require significant time, energy, materials, and financial resources. Statistical design of experiments (DOE) offers a more efficient approach, reducing the number of required experiments while maintaining precision.

However, no existing research has applied statistical DOE to optimize particle size for foam glass production. This knowledge gap is addressed in this study using the Taguchi DOE method. The Taguchi method allows for the determination of precise trends and high-accuracy predictions with fewer experiments by utilizing specific orthogonal arrays, thereby reducing the number of experiments by up to one-fifth. Consequently, this method significantly reduces research costs in this field while also saving time, energy, and human resources.

Knowledge gap and research question:

How can the Taguchi design of experiments (DOE) can be used to optimize particle size for foam glass, given that no previous research has applied statistical DOE for this purpose?

1.4. Foaming agents and additives in foam glass

So far, numerous studies have been conducted on the feasibility of using various materials as foaming agents [65, 77-79]. SiC, eggshell, sodium hydroxide, calcium sulfate ($CaSO_4$), coal, graphite, aluminum slag, and calcium carbonate ($CaCO_3$) are the most common foaming agents. The redox foaming agents (eg. carbon black, and SiC) contain carbon and during the oxidation reaction, they dissolve, release gases, and make foam glass. These types of foam glass contain more closed pores in comparison to the neutralization foaming agent-based foam glasses [44, 65, 80-83].

The material that is used as a foaming agent leads the final product to end up with different types of gases filled in the cells. CO_2 due to its non-toxic nature and low thermal conductivity, is the best gas for foaming glass. O_2, N_2, and water vapor are other gases that are produced from the decomposition of different foaming agents [48, 67, 80, 81, 84-86]. Generally,

the decomposition of carbonates produces CO_2 and the other foaming agent that produces CO_2 and is very commonly used in this field is SiC [65, 72, 76, 87-90]. When SiC is used as a foaming agent the released gas is a mixture of CO_2 and CO [57]. In some research, an oxidizing agent like Fe_2O_3, different sulfates, and MnO_2 are added to the raw material of foam glass to facilitate the decomposition of the foaming agent [64, 66, 91, 92].

Since one of the main principles of using foam glass is to recycle the waste into a valuable and applicable material, some research is carried out by replacing the conventional foaming agents with waste foaming agents. Soot is a waste material produced widely in the industries. Some studies carried out on using soot as a foaming agent in foam glass [93-97]. It is claimed that soot as a foaming agent allows to achievement of a significantly higher quality of foam glass that has lower water absorption and higher compressive strength in comparison to carbonate foaming agents [98]. Using the soot as a foaming agent can increase the probability of forming close pores in foam glass [99]. Since the viscosity of glass supercooled liquid changes in a large range [100], using different foaming agents with different decomposition temperatures simultaneously could form a foam with various properties [101, 102]. Likewise, adding additives may play the role of characteristics modifier and change the properties of final foam glass products. Researches show that the presence of MgO and Al_2O_3 in the structure of glass causes an increase in the viscosity during sintering, and the formation of bubbles becomes more hindered [74]. So, adding Al_2O_3 to foam glass components could modify some properties of the foam glass like compressive strength [103, 104].

Cement factories produce significant amounts of soot annually. The soot generated in these factories contains large quantities of oxides, with carbon black and calcium carbonate being the primary constituents. Based on previous research on soot and calcium carbonate, it appears that soot from cement factories could act as a foaming. However, no studies have been conducted so far on the use of waste soot from cement factories for foam glass production.

This raises an important question: Can the soot from cement factories serve as a foaming agent that makes uniformly distributed cells, low density, high compressive strength, and low thermal conductivity foam glass? Part of this research focuses on the combined use of soot from cement factories and silicon carbide as foaming agents, along with alumina as a modifying additive, to investigate their effects on the properties of foam glass.

Knowledge gap and research question: *Can the soot from cement factories serve as a foaming agent that makes uniformly distributed cells, low density, high compressive strength, and low thermal conductivity foam glass? In chapters 2.2.4 and 3.2.5 part of this research focuses on*

the combined use of cement factory soot and silicon carbide as foaming agents, along with alumina as a modifying additive, to investigate their effects on the properties of foam glass.

1.5. Sintering parameters effect and crystallization of foam glass

Another focus of some research is the impact of crystallization on the properties of foam glass. If the composition of the glass enables crystallization during production, the possibility of the formation of closed pores will be reduced. Therefore, extensive studies are needed to determine the optimal sintering temperature for producing closed-pore foam glass [57].

In one of the studies conducted to produce strong foam glass with a compressive strength greater than 10 MPa and high thermal insulation, the idea of crystallizing foam glass by using the systems of $Na_2O-Al_2O_3-SiO_2$, and $Na_2O-CaO-SiO_2$ was explored. The results of the study indicated that if more than 20% of the foam glass crystallizes, it can reduce pore size, with an ideal porosity size of less than 1.55 mm. Additionally, crystallizing the foam glass increased the thickness of the cell walls up to 50 μm. Ultimately, the study concluded that crystallized foam glass possesses higher compressive strength [105].

In another study, it was reported that crystal-foamed materials are 3-4 times stronger than amorphous foam glass due to the presence of nanocrystals within the matrix. This research has demonstrated that the properties of foam glass-ceramic are influenced by the quantity and size of the crystalline phase. Enhancing mechanical strength, compared to amorphous foam glass, is achievable when the crystals' size is less than 1 μm [106].

Likewise in a study, they focused on creating foam glass-ceramic using waste materials and investigated the effects of sintering temperature on the final product. The precursor used was waste soda lime silicate (SLS) glass (94 wt%), and the foaming agent was eggshells (ES) (6%). The mixture was sintered at different temperatures (700, 800, and 900°C) for 60 minutes, and the resulting foam glass-ceramic was analyzed for crystal formation, microstructure, and mechanical properties. The findings identified crystalline phases such as cristobalite (SiO_2) and wollastonite ($CaSiO_3$) after sintering. At 800°C, the material achieved the lowest density (0.421 g/cm³), highest expansion (92%), and lowest compressive strength (0.42 MPa), indicating a highly porous structure with good expansion but reduced strength. Higher sintering temperatures resulted in decreased expansion and increased strength, likely due to pore closure from higher melt viscosity. Overall, a strong correlation between porosity, mechanical strength, and the crystal phases formed was observed [107]. In glasses, when the crystallization conditions are achieved, the primary crystals formed are quartz, diopside, anorthite, and wollastonite. Figure 4 shows the SEM micrographs of these crystals.
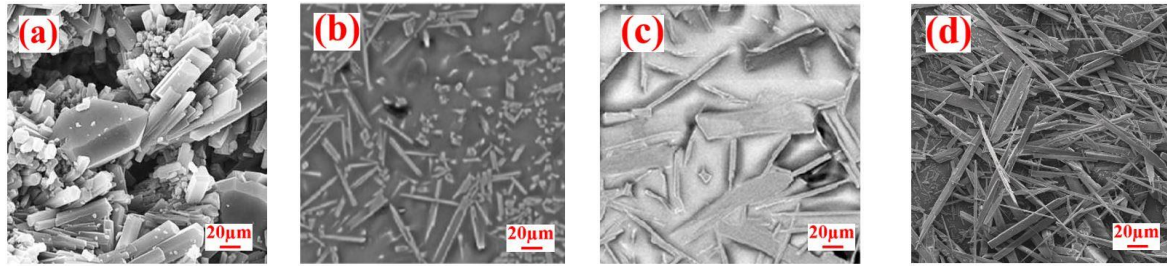
Figure 4. The SEM of probable crystals in soda-lime glass-ceramics a) quartz [108], b), diopside [109] c) anorthite [109], and d) wollastonite [110]

Studies show that the crystallinity of foam glass significantly impacts its properties. One method to alter the crystalline structure of materials is through thermal treatment. This approach has been used in previous research for the production of glass ceramics or crystalline glasses. A common finding across these studies is that certain glasses that can undergo crystallization with thermal treatment must be fired to a temperature between the softening point and the glass transition temperature (Tg) [111]. Given sufficient time, the amorphous structure of the glass will transform into a crystalline structure. The crystallization temperature of the glass is determined using Differential Scanning Calorimetry (DSC), from which the crystallization temperature is read [112, 113].

To date, a limited number of studies have been conducted on the crystallization of foam glass, achieving some success in crystallizing portions of the foam glass structure [114-116]. All previous studies on crystalline foam glass have utilized one of two methods to achieve crystallization. Either an additive was introduced into the foam glass preform powder to create crystalline foam glass, or glass powders with inherent crystallization properties were used. The glass powder employed in this research is soda-lime glass, which, according to conventional thermal treatment methods, typically lacks the ability to crystallize.

Knowledge gap and research question:

Given the extensive variety of glass structures, the question remains: Is it possible to crystallize the foam glass produced in this study through thermal treatment? If this is achievable, it could enhance the mechanical properties of the foam glass. Part of this research, supervised by Professor Edgar Zanotto at the University of São Carlos in Brazil, explored this possibility. Sections 2.2.7 and 4.8 focus on the analysis of this subject.

1.6. Fabrication methodology of foam glass

There are different methods for preparing foam glass, but typically, the laboratory production of foam glass involves a mixture of dried glass powder, a foaming agent, and other additives. The mixed powder is then compacted and placed in a furnace to produce the final foam glass product [117]. The typical production process is shown in Figure 5. Among these steps, pressing the glass powder and molding it is particularly time-consuming and energy-intensive, requiring the use of a press with a capacity of over 80 MPa.
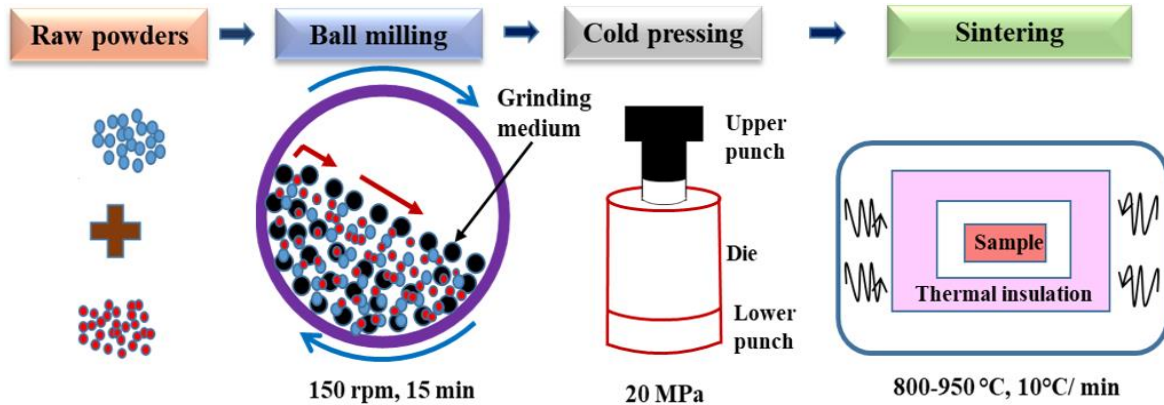
Figure 5. Schematic illustration for the preparation of foam glass [118]

An idea explored in this research is the addition of a small amount of water to the powder mixture to create a cohesive mass, thereby eliminating the need for powder pressing. Although a few studies have been found in the literature where water and sodium silicate (waterglass) were added to the precursor powder for foam glass, these studies primarily focused on the foaming effects of the mixture of water and waterglass [121-119]. Therefore, this is the first study to investigate the impact of adding just water to the precursor powder for foam glass to eliminate the dry pressing step from the foam production process. This part of the research was also conducted using the Taguchi design of experiments method.

Knowledge gap and research question:

What is the effect of adding only water to the precursor powder for foam glass, without using water glass, to eliminate the dry pressing step from the production process? Sections 2.2.3 and 4.4 focus on the analysis of this subject.

1.7. Application of foam glass as aggregate in concrete

Although foam glass has been produced and utilized in various industries for nearly 50 years, its lightweight structure, high resistance to heat transfer, and high mechanical properties make it a candidate for use in the construction of lightweight concrete.

In none of the previous studies available in the literature has the possibility of producing structural lightweight concrete using foam glass granules been explored. Although a few articles have been written on concrete made with foam glass, all of them have either used crushed foam glass or focused on non-structural concrete [44, 122-126]. The difference between crushed and granulated foam glass is shown in Figure 6.
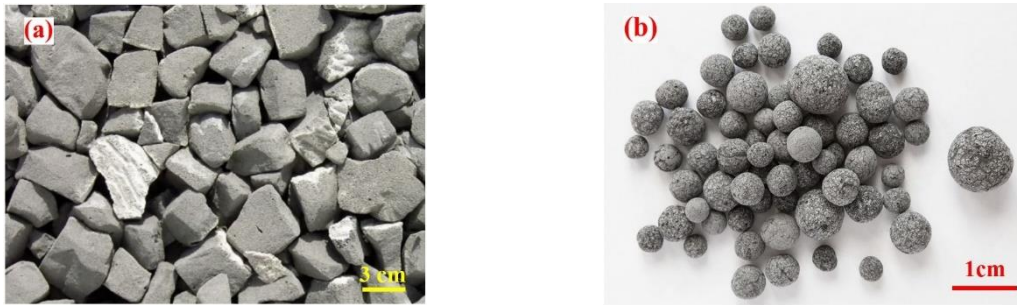
Figure 6. Foam glass shapes a) crushed, b) granules [41]

One study [127] examined the use of crushed foam glass in the production of structural lightweight concrete in the form of beams. In this study, foam glass was used to replace 0, 25, 50, 75, and 100 vol% of natural aggregates to create lightweight concrete, and a four-point bending test was employed for evaluation. The test results indicated that as the amount of foam glass increased, the flexural strength decreased linearly, and the concrete's strength significantly reduced with the formation of the first crack. In this study, the effect of using granulated foam glass was missing. Kumar et al. [37] reviewed the properties of expanded glass aggregate, including its thermal insulation and durability. The findings are promising for using expanded glass in non-structural concrete as a sustainable and potentially beneficial alternative to natural aggregate. The other research focused on developing a super lightweight non-structural concrete with a density of rage from 400 to 550 kg/m³, and compressive strength ranging from 0.9 to 2.1 MPa [128]. In another research, the optimization of foam glass aggregate usage was investigated by testing different sizes and replacement volume ratios (0% to 100%) of natural fine aggregate. The findings suggest that foam glass aggregate size plays a crucial role, with smaller aggregates resulting in higher concrete strength. It was observed that replacing natural aggregate with foam glass, even up to 100% for coarse aggregate, can increase compressive strength due to the smaller, smoother foam glass creating a better bond with the cement and improving the semi-structural concrete's microstructure [129]. A study has shown that increasing the compaction of foam glass aggregate in concrete (from 10% to 40%) significantly reduces the time required for the concrete to fail under constant compressive load. This indicates that the foam glass aggregate acts as the limiting factor in the compressive strength of the concrete [130]. Although density is generally of greater importance than thermal

conductivity in the production of lightweight concrete using foam glass, one study demonstrated that increasing the compaction ratio from 0% to 40% leads to a linear rise in the thermal conductivity (λ) of FGA at both 50% and 95% relative humidity levels [131].

The other research explored the use of recycled waste glass processed into foam glass aggregate (in the form of crushed foam glass) as a partial replacement for natural aggregate in concrete. The feasibility of using up to 60% foam glass aggregate (both coarse and fine) was tested, and it was found to be a viable substitute for natural aggregate. In terms of compressive strength, up to 30% coarse foam glass aggregate or 5% fine aggregate had minimal impact, while higher coarse aggregate content led to some strength loss, and fine aggregate improved early strength. A replacement of up to 60% aggregate achieved the required 28-day design strength and showed satisfactory durability performance, comparable to natural aggregate concrete, with an appropriate water-to-cement ratio. For ASR, foam glass aggregate replacements up to 50% exhibited minimal expansion, suggesting no adverse ASR effects. The study suggests using 30-40% coarse foam glass aggregate and 15% fine aggregate as could be the optimal balance of aggregates to use [132].

The aforementioned summary provides an overview of past studies on the use of foam glass as an aggregate in concrete. In all the cited research, crushed foam glass was used as the aggregate. Due to the porous nature of foam glass, if it breaks, the pores open up for water penetration, which can cause cracks during the freeze-thaw process in aggregates. On the other hand, the contact surface of foam glass with cement pastes increases, which can lead to increased ASR in concrete. Therefore, the use of spherical foam glass granules can be a solution to this problem. In other words, the construction of structural concrete using foam glass made from granular foam glass is feasible, and this is a further knowledge gap that this research aims to address.

Knowledge gap and research question:

Can the use of spherical foam glass granules, instead of crushed foam glass, address the issues of water penetration and freeze-thaw damage, as well as mitigate alkali-silica reaction (ASR) in cement matrix composites, thereby enabling the construction of structural material with granular foam glass? In sections 2.5 and 5.4 this matter is investigated.

1.8. Production method of granular foam glass

As mentioned, it is preferable to use foam glass in granule form for concrete applications. However, producing foam glass in granular form requires large and expensive equipment. Typically, foam glass industries produce it in bulk, which is then cut into blocks or crushed and used as gravel.

However, creating foam glass granules presents a significant challenge in small-scale settings due to the intricacies of controlling the foaming process [133, 134]. In recent years, researchers have actively pursued novel methods for producing foam glass granules in laboratory settings [135]. The manufacturing process for foam glass granules typically unfolds in three stages: glass preparation, foaming, and granulation. In the glass preparation stage, molten glass is created by melting diverse glass compositions like soda-lime glass or borosilicate glass. The foaming stage introduces bubbles into the molten glass, forming the characteristic porous structure of foam glass [136]. To achieve the desired cell size and distribution, various foaming agents, such as steam, chemical agents, and mechanical agitation are employed [90]. The granulation stage is more challenging stage that involves some of the studies conducted to develop new methods for producing foam glass granules with improved properties. One method involves utilizing microwave heating to expedite the foaming process, resulting in the creation of granules with a finer cell structure and enhanced mechanical properties [74, 137]. The choice of foaming method significantly influences the characteristics of foam glass granules [138]. Chemical foaming introduces a foaming agent into the softened glass, creating smaller particles with the need for precise chemical control [139]. Mechanical foaming uses mechanical agitation for bubble formation, providing enhanced control over particle size and morphology [97]. The granulation process is crucial in determining the properties of foam glass granules. Widely used techniques like fluidized bed granulation and spray granulation promote the breakage of foamed glass particles into smaller ones. Extrusion granulation employs extruders to shape foamed glass into pellets or granules. The properties of foam glass granules depend not only on foaming and granulation processes but also on glass composition [140]. The glass network structure influencing strength, thermal conductivity, and chemical resistance is significantly affected by the glass composition [141]. For example, borosilicate glass granules with high silica content exhibit excellent thermal insulation and chemical resistance [75, 119, 142, 143]. The conventional procedure of granulated foam glass production is illustrated in Figure 7.

Figure 7. Fabrication process of granular foam glass aggregates, a) electric rotary furnace, b) rotation in alumina tube, and c) foam glass granules processed at 900°C [144]

As the demand for foam glass granules continues to rise, ongoing research will focus on optimizing manufacturing processes, exploring new glass compositions, and expanding the range of applications for these unique materials [145]. Therefore, researchers need the capability to produce foam glass granules in their desired dimensions and specifications, subjecting them to examination. To address this, none of the previous studies have presented a comprehensive and practical laboratory method for manufacturing foam glass granules. In a part of this investigation a new approach to crafting foam glass granules with a uniform cellular structure and a smooth surface, minimizing open porosity is introduced.

Knowledge gap and research question:

How can a comprehensive and practical laboratory method be developed to produce foam glass granules with variety of sizes, a uniform cellular structure, and a smooth surface while minimizing open porosity, given the lack of such methods in previous researches? A novel laboratory method is designed and presented in sections 2.2.6 and 4.7.

1.9. Structural foam glass–cement matrix mixture

As mentioned before, so far, a limited number of studies have been conducted on the use of foam glass in cement matrix composites. This is because, in industry, foam glass is made in bulk and then divided into smaller pieces. This will increase the open pores of the foam on the surface. Additionally, the angularity of crushed foam glass reduces the workability of the concrete. Out of a few numbers of studies in the field of foam glass concretes, all of them have focused on basic mechanical properties, and none of them discussed the cement matrix composites made from foam glass as a structural application [52, 146-150]. So, in this study, the main goal was to investigate the feasibility of creating structural cement matrix composites from granulated foam glass, and this is another innovation which obtained through this research.

Structural lightweight concrete is essentially concrete with a compressive strength of at least 17 MPa after 28 days, and its dry density is a maximum of 2000 kg/m^3. In the concrete industry,

the initial step is to develop a comprehensive concrete mix plan. In the studies conducted, the overall process of the mix plan for lightweight concrete is similar to ordinary concrete, with the key difference that, in addition to parameters considered for normal-density concrete mix design, such as strength, workability, and durability, density is also of significant importance [151]. Therefore, when creating a mix plan for lightweight concrete, mix proportions, such as the amount of cement, coarse aggregate, fine aggregate, water-to-cement ratio, and particle sizes, must be adjusted in a way that design parameters fall within an acceptable range [151]. The major challenge in designing a mix plan for lightweight concrete lies in the highly variable density of structural lightweight concrete, ranging from 1400 to 2000 kg/m^3 [152]. This is in contrast to the relatively constant density of ordinary concrete, typically falling within the range of 2250 to 2450 kg/m^3. The variability in lightweight concrete density significantly affects its properties, putting mix proportions under considerable influence [151].

In the study by Wattanasiriwech et al. [153], a 1:1 water-to-cement ratio was used to create mortar, and foam glass made from CRT glass and calcium carbonate (4% by weight) was used to replace 0 to 60 vol% of cement mortar. Finally, thermal conductivity and compressive strength tests were tested on the samples. The compressive strength test results from this study produced graphs that allow for the estimation of the compressive strength of granulated foam glass made from CRT, based on the volume percentage used in the cement mortar. This study does not provide any explanation for the choice of the 1:1 water-to-cement ratio or the method used for developing the mix plan. Smirnov et al. [154] introduced a method called the Energetic Metrics in their study. This method presents two metrics: strength and thermal conductivity. Through analytical relationships, they demonstrated that using ground glass instead of foam glass could result in higher-quality concrete. The study only referenced the cement grade, and although the concrete mix plan is crucial, no details regarding it were provided.

Jurga Šeputyt et al. [155] investigated the impact of foam glass composition on the flammability of concrete made with foam glass. In their research, ordinary Portland cement and metakaolin waste were used to create the mortar. They tested six different mixtures based on the raw materials, with the water-to-cement ratio ranging from 34% to 66%, and calculated the concrete density according to EN 1097-6. Although their results successfully produced lightweight concrete with a density between 225 and 375 kg/m³, and they presented the optimal concrete, the mix plan they used was not fully based on standards, scientific, and precise method.

Martin Sedlmajer et al. [150] focused on producing concrete using crushed foam glass. Ordinary Portland cement was employed, with a water-to-cement ratio of 0.4 for the sample

preparations. The foam glass content was varied between 50 and 70 vol%, resulting in concrete with a density ranging from 470 to 600 kg/m³ and compressive strength between 0.85 to 1.81 MPa. However, their study only mentions that the mix plan was based on the ordinary concrete mix plan. It is important to note that when using an ordinary mix plan for concrete, all constituent materials must have similar density, compressive strength, and water absorption characteristics as those in ordinary concrete. From a scientific perspective, applying an ordinary mix plan is inappropriate when using foam glass to produce lightweight concrete, given that foam glass has a different characteristics compared to natural aggregates.

The number of studies conducted on cement-based concrete made from foam glass is limited [26, 37, 127, 129, 132, 146, 150, 155-157]. Furthermore, no research was found that precisely followed a standardized mix plan for the preparation of the samples. The reason for this is that no specific standard has been defined for concrete made from foam glass. However, there are methods for designing lightweight concrete mix plans mentioned in the literature, which can be utilized as guidelines.

In the design of lightweight concrete mixes, three methods are commonly utilized: the ACI (American Concrete Institute) method, the two-phase mix design method, and the mix design method based on strength capacity [158-160]. The ACI weight method for lightweight concrete mix design is an empirical approach that establishes approximate relationships between various parameters based on previous experiences. These relationships are summarized in tables used as a guide for the initial mix design of concrete. The ACI weight method is suitable for lightweight aggregate concretes with lightweight coarse and natural fine aggregates. This method considers various parameters in concrete mix design, and these parameters must be selected to provide the desired characteristics and workability of the concrete. The key parameters considered in the lightweight concrete mix design using the ACI method include: minimum cement content, concrete slump, nominal maximum aggregate size, air-entraining admixtures, compressive strength, weight, and unit volume. Another method commonly used for lightweight concrete mix design is the two-phase method [161, 162]. In this approach, to simplify the mix design process, concrete components are divided into two parts: the binder materials and the aggregates, or, in other words, the lightweight coarse aggregates are limited. It is also assumed that these two components are in complete contact. Unlike the ACI mix design method, primarily based on empirical relationships, the two-phase method is founded on solid theoretical principles. In calculating the mix design using this method, it is assumed that the volumetric ratio of cement paste to the total concrete volume is between 0.28 and 0.35,

and the volumetric ratio of lightweight aggregates with particle sizes of 2 to 12 mm should fall within the range of 35 to 45 Vol%. Given that foam glass, among the lightweight aggregates, typically has lower compressive strength, filling 35 to 45 percent of the concrete volume with foam glass may result in reduced compressive strength of the concrete to less than 17 MPa, and may not allow for the creation of structural lightweight concrete.

The last method among the three conventional methods for lightweight concrete mix design is the strength capacity-based method [163, 164]. This method utilizes the strength capacity diagram of lightweight aggregates. Similar to the two-phase method, in this approach, concrete components are divided into two parts: the binder materials and the aggregates, or, in other words, the cement mortar and lightweight coarse aggregates. However, instead of expressing the concrete strength theoretically based on mortar and aggregate strength, it uses experimental strength capacity diagrams obtained through testing to establish the relationship between concrete strength and the constituents forming it. Therefore, if these strength capacity diagrams are available, this method provides a more accurate mix design compared to the previous methods. In past research, it seems that no diagram based on the strength capacity of cement mortar reinforced with foam glass has been presented. Therefore, this method may not be suitable for foam glass concrete mix design.

With this interpretation, the ACI mix design method emerges as the most suitable approach for designing lightweight concrete mixes incorporating foam glass. What has been discussed is a summary of findings from past research. Until now, no research has been conducted on the use of foam glass granules in structural cement matrix composite materials incorporating foam glass. Moreover, none of the previous studies have utilized a precisely designed mix plan for constructing their samples, which represents one of the key knowledge gaps in this field.

Knowledge gap and research question:

Can the American Concrete Institute (ACI) method be effectively applied to develop a mix design for structural lightweight cement matrix composites using foam glass? In sections 2.4.1 and 5.2, the usage of ACI in cement matrix composites is discussed.

1.10. The alkali-silica reaction in foam glass in a cementitious environment

While it's possible to create lightweight concrete using foam glass as proposed, the durability of concrete against chemical aggressors should be evaluated due to the siliceous structure of foam glass aggregates. Research has shown that even small amounts of harmful components in aggregates can have detrimental effects on the concrete. One of the most important harmful materials is amorphous silica in aggregates [165]. Since foam glass has an amorphous silica

structure, the reaction of silica with the alkaline environment is one of the potential reactions [166]. This reaction can lead to undesirable cracking of concrete [167]. In general, two types of alkali reactions occur in concrete: the alkali-carbonate reaction involving carbonate minerals, and the ASR involving reactive silica components in aggregates. More than 99% of the alkali reactions form ASR reactions. [167, 168].

The presence of alkalis in concrete is due to the use of Portland cement (which contains potassium and sodium oxides) [169-171]. If the aggregates in the concrete contain unstable silica, these alkalis can react with it, leading to the alkali-silica reaction [172]. The product of the reaction is an alkali silicate gel (Figure 8) [173]. The ASR gel then absorbs water and expands, which can cause swelling and lead to the formation of cracks in the concrete [174].
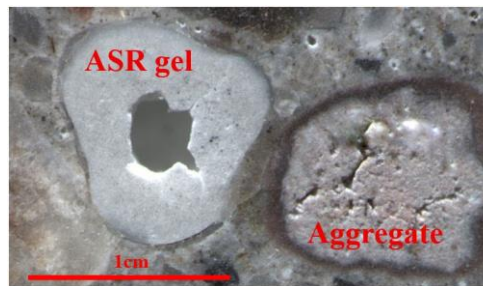
Figure 8. The silica gel in concrete due to the presence of reactive aggregate [175]

It has been claimed that ASR, according to chemical equation 1, occurs due to the attack of hydroxide ions present in the pore solution on the hydrated silica [176]. Alongside this reaction, sodium and potassium cations also attack the silica in the aggregates [177].

Equation 1. Hydroxylation of silanol group with hydroxide ion, resulting in the formation of a siloxide ion and water.

$$\equiv Si - OH + OH^- \rightarrow \equiv Si - O^- + H_2O$$
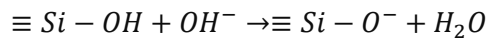
The bond between the negatively charged O bond and the Na and K cations is formed due to their presence [178]. This process leads to the formation of ASR gel [179-181].

However, many aggregates contain silica [182]. Researches show that amorphous silica is unstable, while crystalline silica is categorized as stable (Figure 9) [182, 183].
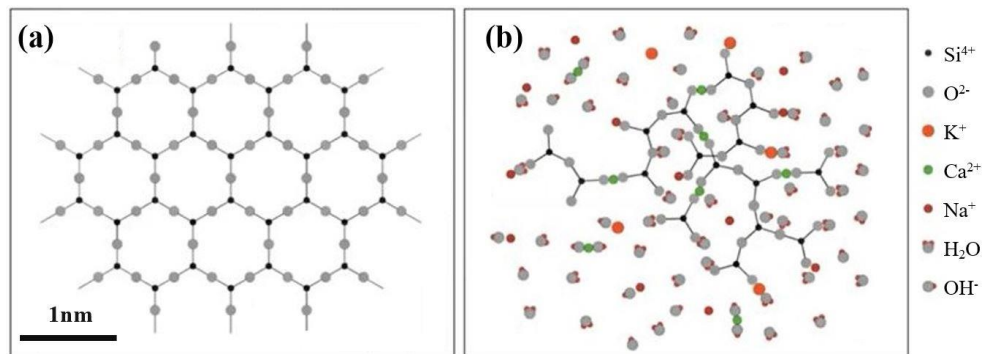
Figure 9. Different structures of SiO$_2$ in aggregates a) quartz b) amorphous *[184]*

For ASR to occur, four conditions must be met. The existing calcium sources are needed, the need for existing sufficient alkalis, the need for existing sufficient moisture, and the need for reactive silica [185]. Calcium generally comes from cement or supplementary cementitious materials. Reactive silica can come from foam glass aggregates. Also, it is necessary for the alkalis to be present, which is more in cement paste, and then sufficient moisture is required. Research has shown that for ASR to occur, moisture above 60% is required [186]. Therefore, structures like dams, bridges, bridge decks, columns, and other structures where concrete is exposed to external moisture consider its properties against ASR [187-189]. The natural ASR reaction may take decades to deteriorate concrete [190]. Thus, various tests and standards have been designed to accelerate this reaction for assessing the susceptibility of concrete [191-193].

In the United States ASTM C1260 or 1567 standards are commonly used [194]. These standards involve the use of prismatic specimens with dimensions of 25 mm by 25 mm by 285 mm. The specimens are then immersed in a sodium hydroxide solution at 80 °C for 14 days (Figure 10). The change in length of these bars after 14 days is examined [194, 195].
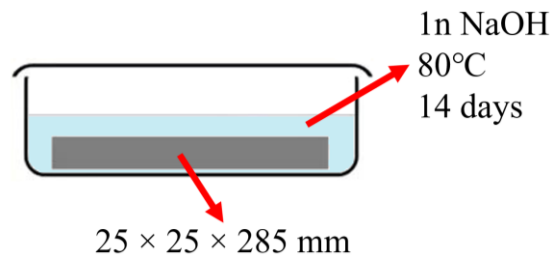
Figure 10. Accelerated mortar bar test (AMBT)/ ASTM C1260 and C1567

Another ASR testing method, known as the concrete prism test (ASTM C1293), requires a larger cross-section, with specimen dimensions of 75 by 75 mm millimeters and a length of 285 mm. According to the intention of the test, this test is conducted at 38 °C in relative humidity (RH) of more than 95% for one or two years (Figure 11) [194, 195].
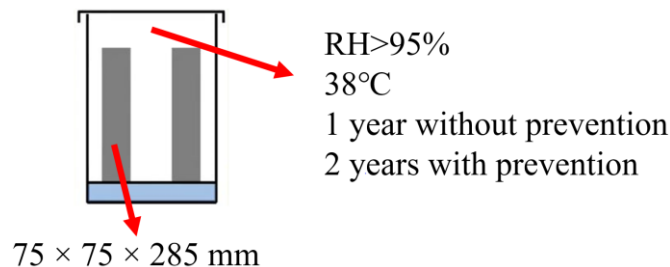
Figure 11. Concrete prism test (CPT)/ ASTM C1293

To benchmark the accelerated methods, the outdoor exposure method is employed. In this approach, a large block with dimensions of $380 \times 380 \times 710$ mm is fabricated and exposed to the environment. Over the years, the expansion of this block is monitored to determine the efficacy

22

of the accelerated methods [196]. With the increase in dimensions of the specimens under investigation, the reliability of the test improves, but the test duration also increases [197-199]. In all the mentioned testing methods, attention is paid to changes in the length of specimens.
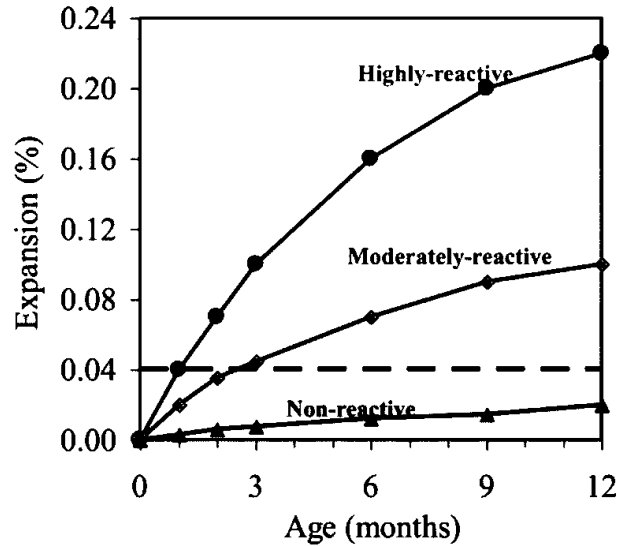
Figure 12. The expansion–age diagram for concrete for highly, moderately, and non-reactive aggregate [200]

In Figure 12, the horizontal axis represents months, indicating the lifespan of the concrete prism under the environmental conditions relevant to the test being conducted, while the vertical axis indicates expansion along the length of the specimen. It is evident from the diagram that for non-reactive aggregates, the expansion value is below 0.04%. For moderately reactive aggregates, this value should be below 0.22% [183, 191, 193, 195, 198]. If the test results indicate that the examined concrete prisms are non-reactive, their aggregates can be used for making concrete in external moist conditions, although if the aggregates are reactive, methods are proposed to control the ASR reaction [201, 202].

In a study conducted by Mukesh Limbachiya et al. [203], concrete made with foam glass granules was examined, and ASTM C1260 was used to assess ASR , with the research taking 14 days to complete. The results showed that using foam glass up to 50% by volume could produce concrete with an acceptable level of expansion. Another study [204] examined the impact of foam glass crystallization on reducing ASR in concrete. In this investigation, the samples were stored at 60°C in the 1 molar NaOH solution for three months to test for ASR. The results of their study showed that the binary glass ceramic composition of foam glass has a significant ASR decrease. Mladenovič et al. [205] also investigated ASR in common lightweight aggregates. Although their study did not utilize synthetic foam glass, they employed expanded glass, which is essentially foam glass derived from natural volcanic rock deposits. In their research, they used the ASTM C1260 standard over a 16-day period and demonstrated that expanded glass, due to its amorphous nature, is unstable against alkaline attack.

23

Another study [206] examined the impact of different types of glass aggregates on the shrinkage and expansion of concrete. In part of the research, both expanded glass granules and crushed expanded glass were used as aggregates. The results indicated that the ASR (which was tested according to ASTM C1260 for 14 days) was less pronounced when granules were used compared to when crushed expanded glass was employed.

In summary, there is a potential for the occurrence of ASR in cement-based concrete containing foam glass, and only a limited number of previous studies have examined this issue. In all of these studies, long-term methods requiring the field. To achieve this, the reactivity of the aggregate must be assessed. Upon reviewing the literature, it was observed that ASR is less common in concretes made from Alkali alkali-activated slag[1] (AAS) compared to Ordinary Portland Cement (OPC) [207]. Al-Otaibi noted that most alkalis are bound in hydration products, reducing the likelihood of ASR in AAS [208]. This leads to a lower expansion in concrete [209]. However, Shi et al. [210] in their study stated that this phenomenon is due to the lower concentration of hydroxide in the pore solution of AAS.

In addition to the mentioned reasons, the low amount of calcium hydroxide in the pore solution of AAS should also be considered. Various studies have shown that the presence of calcium hydroxide in ordinary Portland cement due to the hydration of calcium silicate increases the ASR in this type of mortar compared to AAS mortar [184, 210-218].

However, the effect of calcium on ASR expansion is inconsistent, with some studies reporting increased expansion [219, 220], while others report decreased or negligible effects [216, 218]. Some research suggests calcium is essential for ASR expansion [193, 214, 221], though ASR gel can form without calcium, and the consumption of $Ca(OH)_2$ by ASR is minimal [222]. So, as is evident, the pore solution of Portland cement is saturated with calcium hydroxide.

To determine the reactivity level of the ASR, the reactivity of foam glass as aggregate can be measured in conjunction with $Ca(OH)_2$. In some novel research, they went through assessing ASR in aggregates according to a Thermogravimetric Analysis TGA method which suggests that the aggregate is ground into powder and combined with calcium hydroxide powder. After a specified period, the mixture is subjected to TGA. Calcium hydroxide is expected to decompose at around 500°C, and if no sharp peak is observed in the TGA graph at this temperature, it indicates that the aggregates have reacted with calcium hydroxide. The extent of this reactivity determines the aggregate's reactivity.

---

[1] Alkali-Activated Slag (AAS) composites are materials produced by activating Ground Granulated Blast Furnace Slag (GGBFS) using a suitable alkaline solution. Common activators include water glass and sodium hydroxide, with potassium hydroxide occasionally used as well. The primary binding phases in these composites are various forms of CSH gel, which play a critical role in the material's properties [191].

Knowledge gap and research question:

The thermogravimetry analysis (TGA)-*based alkali-silica reactivity assessment analysis has been recently applied to other aggregates [223-226], but it has not been conducted for foam glass before. This part of the research was carried out in collaboration with Professor Marco Valenta's scientific team at Sapienza University of Italy and presented in sections 2.3.4 and 5.6.*

1.11. Knowledge gap – summaries

Based on the information we have obtained, there has been no research conducted so far on the construction of structural lightweight cement matrix composite material using foam glass granules and natural aggregates. To create concrete, a mix design must be established, and according to the literature, none of the previous studies have utilized a standardized method for their mix design. Additionally, in past research focusing on lightweight concrete made from foam glass, there has been no comparison regarding the effects of using crushed foam glass versus granular foam glass in cement matrix. In cementitious environment that use aggregates containing amorphous silica, there is a risk of deterioration due to alkali-silica reaction (ASR). A limited number of past studies have examined ASR in concrete made from foam glass, and their investigations were based on standards that are very time-consuming. In contrast, the reactivity of aggregates can be assessed using simpler and less costly methods that also take less time to perform. The most well-known of these methods, which has recently been applied to various aggregates, is the thermogravimetry analysis (TGA) test. However, no studies have been conducted to examine the reactivity of the aggregates based on the TGA test. Moreover, in studies that have utilized granular foam glass, the granules have either been purchased from industry or hand-crafted in large sizes, highlighting a significant knowledge gap regarding a laboratory technique for producing foam glass granules in various sizes. All the experiments previously conducted on foam glass have been based on factorial design methods, and so far, there has been no investigation aimed at reducing the number of required experiments and accurately predicting results using statistical design methods. One of these methods is the Taguchi design of experiments. To create foam glass, it is essential to identify the optimal composition and manufacturing method for use in structural lightweight concrete. The literature lacks research on the optimal sintering temperature, holding time in the furnace, the optimal particle size of raw materials, raw material content, and type of materials required for producing foam glass granules intended for structural lightweight cement matrix composites. Furthermore, previous studies on foam glass have not employed any mathematical decision-making methods to identify the best sample for a specific performance. This is crucial because the various properties of foam glass have different values depending on their applications, and scientific decision-making methods are necessary for

determining the suitability of foam glass. Due to its waste nature and various oxides, cement factory soot has the potential to serve as a new foaming agent in foam glass production; however, there has been no research examining this possibility to date.

1.12. Research questions and objectives

This study aims to address critical knowledge gaps in the use of foam glass as an aggregate in structural lightweight concrete by investigating a series of pivotal research questions.

1. Is the Taguchi design of experiments and Taguchi analysis applicable in foam glass research? Can it reduce the number of required experiments and accurately predict results?

2. What is the effect of changing the composition, sintering temperatures, and using different particle sizes of glass powder on the final properties of foam glass?

3. Can cement factory soot be used as a new foaming agent, given its waste material nature, for the production of foam glass? If so, what properties will this foam glass exhibit?

4. Considering that there is no technique available for laboratory production of foam glass granules in various sizes, what innovative techniques can be employed to produce foam glass granules with intact shells and different sizes?

5. Is there a difference in the properties of foam glass granules made from virgin glass powder compared to waste glass?

6. Given that foam glass has different properties and a specific type must be selected for use as an aggregate in CMFGC, what scientific and mathematical methods, specifically decision-making methods, should be employed to select the optimal production conditions and composition of foam glass?

7. What standardized mix design should be used for constructing structural lightweight concrete that incorporates foam glass as an aggregate, and how can it be developed?

8. Is there a difference in the properties of lightweight CMFGC when using granular foam glass versus crushed foam glass?

9. Is CMFGC made from foam glass (both granular and crushed) resistant to ASR and Can a rapid method based on TGA be used to assess ASR in foam glass? If so, what would the results indicate?

This work aims to address critical knowledge gaps in the use of foam glass as an aggregate in structural lightweight CMFGC by investigating a series of pivotal research questions.

2. Materials and methods

The exploration of the potential use of new lightweight aggregates in the construction of lightweight concrete requires a comprehensive investigation in this field. This research focuses on the development of a novel class of composite materials consisting of foam glass and a cementitious binder. The material system is composed of cement paste as the matrix phase and foam glass particles, either in granulated or crushed form, as the dispersed phase. Foam glass serves not only as a lightweight aggregate substitute but also actively influences the physical, mechanical, and thermal properties of the composite due to its porous structure, low density, and specific surface chemistry.

This section of the thesis is dedicated to the experimental method and the materials employed in the construction of lightweight aggregates, specifically foam glass granules, to assess their performance in structural lightweight concrete. The discussion spans from an in-depth examination of foam glass to the optimization of concrete mix designs and manufacturing methods, culminating in the presentation of a method for producing structural CMFGC. The section delves into the analysis of compositions, particle size, weight percentages of mixtures' components, the manufacturing process of foam glass, the optimization of its sintering parameters, and the method for mixing the CMFGC. Through a combination of theoretical study and practical experiments, this research methodology seeks to unravel the complexities of foam glass granular materials, paving the way for innovative and sustainable applications in lightweight structural CMFGC. This section begins with explanations on the characterization of raw materials and progresses through the methods of investigating and optimizing foam glass for use in CMFGCs. It concludes with an explanation of a CMFGC mix plan, as well as the methods for evaluating and testing the CMFGC.

2.1. Exploring the properties of raw materials

Throughout this research, various materials have been used, which are introduced and subsequently characterized. In the production of foam glass, silicon carbide, recycled glass, virgin glass powder, soot, and alumina were used. To produce lightweight CMFGC, granulated foam glass, natural coarse aggregate, natural fine aggregate, ordinary Portland cement, and distilled water were employed.

2.1.1 Foam glass: raw materials and their characterization methods

Figure 13 shows the primary raw material utilized for making foam glass was waste window glass, and virgin glass powder, supplied by Qazvin Farsjin Float Glass Company. These two types of glass were used to produce foam glass in this research. Additionally, as an integral

part of the investigation, SiC (Silicon Carbide) was sourced from Ibiden Ltd. (Hungary), with a particle size of less than 1 micron. Cement factory soot, a byproduct of the firing process, was provided by Firouzkuh Cement Company (Iran), and alumina was sourced from Merck (Germany) were used.

Figure 13. foam glass raw material a) Waste glass particles, b) virgin glass powder, c) SiC, d) Soot, e) Al_2O_3, photos are taken by mobile phone camera (iphone 13 pro max)

To characterize the raw material, a comprehensive range of instruments was employed to assess the physicochemical properties of the initial powders. Virgin glass powder, waste glass powder (which was sieved to obtain powder less than 90 microns), alumina, and soot were analyzed in the ceramics laboratory of Miskolc University using a QUANTACHROME laser particle size analyzer (model CILAS715), which investigated the distribution of particle sizes. However, the SiC particle size, being smaller than 1 micron, could not be accurately measured by the instrument. The mineral phase composition of the powders was evaluated using a Rigaku Miniflex II X-ray diffractometer, operating in Bragg-Brentano geometry with CuKα radiation, k = 1.54184 Å. Analysis was carried out in the 0–90°range of 2h intervals with a scanning rate of 1°/min and a step size of 0.01015°. The diffractometer run in Bragg-Brentano geometry. X'Pert HighScore Plus program was used for the computer-based examination using PDF (Powder Diffraction File Database) of the ICDD (International Center for Diffraction Data). An X-ray fluorescence spectrometer (XRF) was used to determine the chemical composition of oxides in glass powders, and soot.

To examine the morphological and microstructural characteristics, an EVO MA10 model Carl Zeiss scanning electron microscope (SEM) was utilized. The SEM, coupled with energy dispersive spectroscopy (EDS), facilitated the analysis of elemental composition. All the optical observations were photographed using a Canon EF-S 60mm f/2.8 Macro USM.

The thermal behavior of the soot was studied using a 1750 SETARAM Sestys evolution instrument through thermogravimetric analysis (TGA) and differential thermal analysis (DTA). Changes in the physical state of the glass powder and foam glass preform powders at different temperatures were investigated with a heating microscopy test (MicrOVis, Camar Elettronica), conducted at a heating rate of 10 °C/min up to a maximum temperature of 1000 °C (Figure 14). In this test, the

sample was prepared then placed on an alumina plate and put into a thermal chamber. One side of the chamber had a light source, and the other side had a camera. The camera took photos of the sample's shadow every 5 seconds or every 5°C increase. The heating microscopy software recorded the sample's height, the angle between the sample and the alumina plate, and the temperature for each photo. Using this data, the changes in the sample with increasing temperature were analyzed. This heating microscopy method was used for all the sets aimed at investigating foam glass.

Figure 14. Heating microscopy equipment

The images captured from heating microscopy show the samples in silhouette form. One of the analyses conducted involved comparing the trend of height changes in the sample shadows with changes in the area of these shadows. This investigation was carried out on three foam glass compositions, mixed with 1, 2, or 3 wt% SiC.

2.1.2. Raw material for cement matrix composite material

For the production of CMFGC paste, in addition to foam glass, Portland cement from the Danucem Magyarország Kft, natural coarse crushed aggregates with a maximum diameter of 19 millimeters, and natural fine aggregates were used. An X-ray fluorescence spectrometer (Rigaku Supermini 200 WDXRF machine, Japan) was used to determine the chemical composition of oxides in cement powder.To formulate the mix design, in addition to the properties of foam glass granules, the physical properties of natural fine and coarse aggregates, and cement needed to be measured and specified.

The main investigation carried out on the fine sand involved the test to determine the sand fineness modulus. This test was conducted according to ASTM C848-136 standards. For this purpose, a quantity of 400 grams of sand was selected and sieved through sieves No. 4, 10, 16, 30, 40, 60, and 100 (the numbers represent the mesh size in openings per inch). The sieving process was conducted for 10 minutes for each 50 grams. The remaining amount on each sieve was weighed, and the fineness was calculated using the equation 2.

Equation 2. The remaining percentage accumulated on sieve number k [227]

$$C_K = \frac{\sum_{i=1}^{K} m_i}{\sum_{i=1}^{n} m_i} * 100$$

In this equation, where i represents the sieve number, n denotes the total number of sieves, C_K signifies the cumulative amount on sieve K, and m_i denotes the remaining weight of sand on each sieve. It should be noted that as i increases, the size of the sieve openings becomes smaller, with i=1 corresponding to a sieve with the largest opening size. Finally, the sand fineness modulus was calculated based on equation 3.

Equation 3. The fineness modulus of sand [227]

$$FM = \frac{\sum_{i=1}^{n} C_i}{100}$$

In this equation, FM stands for Fineness Modulus, a parameter that provides a single value representing the average particle size of the aggregate. A higher FM indicates a coarser aggregate, whereas a lower FM suggests a finer aggregate.

The next characterization required for utilizing the ACI method to develop the CMFGC mix plan is determining the density of natural aggregates (both coarse and fine). It was measured based on the Archimedes method. For this purpose, the aggregates were first boiled in water for 4 hours to saturate the pores with water. Then, their volume was measured using a graduated cylinder and distilled water. With their dry mass known, their density was calculated. This method ensured accurate measurement of the natural aggregates' density, essential for precise CMFGC mix design and quality control.

2.2. Foam glass: design of experiments, and sample preparation

As mentioned, this is the first time the Taguchi method has been used in research related to foam glass. The Taguchi method is a statistical approach that significantly reduces the number of experiments needed to achieve the desired results. In the experiments related to foam glass in this study, the Taguchi Design of Experiments (DOE) was utilized. Depending on the number of parameters being tested and their levels of variation, different orthogonal arrays were used. These orthogonal arrays are standard tables used for DOE and are denoted by a number in front of the letter "L" to indicate the number of experiments required. The results of these experiments allowed us to accurately predict the outcomes for other conditions. The

Taguchi experimental design method was employed in this study to investigate various aspects of foam glass.

2.2.1. Influence of particle size and foaming agent content.

As mentioned, one of the costly stages in the production of foam glass is grinding recycled glass. Therefore, finding the optimal particle size for producing high-quality foam glass can reduce the costs associated with the grinding process. Additionally, the amount of foaming agent used is another influential parameter. This part of the research examines the properties of foam glass produced from different particle sizes and varying ratios of foaming agents.

For the experiments, three levels of particle size and three levels of foaming agent percentage were considered, and the tests were designed according to the orthogonal array L9. Waste glass was used to create the glass powder, with 100 grams placed in a ball milling jar and milled for 20 minutes at a speed of 250 RPM (ball mill machine: Retsch PM 400). The resulting glass powder was then sieved using standard sieves to obtain powders with particle sizes between 125 µm and 160 µm, and less than 90 µm. For simplicity, powders with particle sizes between 125 µm and 160 µm will be referred to as D_1, and powders with particle sizes less than 90 µm will be referred to as D_2. The three levels of particle size considered in the study are combinations of D_1 and D_2 (table 1). The foaming agent used in this study was silicon carbide, with levels of 1%, 1.5%, and 2% being tested (table 1). The specimens were coded as P_{n-m}, where "n" represented the level of particle sizes (1, 2, or 3), and "m" denoted the level of foaming agent ratio (1, 2, or 3). The particle size levels are defined as follows: n=1 represents 66 wt% D_1 and 34 wt% D_2, n=2 represents 50 wt% D_1 and 50 wt% D_2, and n=3 represents 34 wt% D_1 and 66 wt% D_2.

Table 1. Specimen compositions (in wt%) along with the sintering temperature determined by heating microscopy

Code	Glass particle size	Foaming agent ratio (wt%)	Sintering temperature (℃)
P_{1-1}	66 wt% D_1 – 34 wt% D_2	1	986
P_{1-2}	66 wt% D_1 – 34 wt% D_2	1.5	940
P_{1-3}	66 wt% D_1 – 34 wt% D_2	2	930
P_{2-1}	50 wt% D_1 – 50 wt% D_2	1	959
P_{2-2}	50 wt% D_1 - 50 wt% D_2	1.5	941
P_{2-3}	50 wt% D_1 - wt% 50 D_2	2	951
P_{3-1}	34 wt% D_1 - 66 wt% D_2	1	946
P_{3-2}	34 wt% D_1 - 66 wt% D_2	1.5	953
P_{3-3}	34 wt% D_1 - 66 wt% D_2	2	928

To prepare the samples, the powder mixtures were prepared according to the specified Table 1 based on Dry powder method (see detailed description in chapter 2.2.3). The samples were then sintered for 30 min in a furnace to the maximum height temperature extracted from the heating microscopy test. The temperature was adjusted to the level at which the sample exhibited the

highest increase in height due to the foaming agent decomposition. Since each composition reached its maximum volume increase at a specific temperature, this temperature was designated as the maximum sintering temperature. To enhance the accuracy of the experiments, five repetitions were made for each group. Finally, the fabricated samples underwent tests for density, water absorption, open porosity percentage, and thermal conductivity. And finally, the test results were analyzed using Minitab software (downloaded from https://www.minitab.com).

2.2.2. Sintering parameters

As previously mentioned, one of the key investigations in this study was the impact of sintering temperature and holding time in the furnace on the properties of foam glass. Thus, holding time was examined at three levels: 10 minutes, 30 minutes, and 50 minutes. The results of previous experiments showed that the maximum height temperature and maximum area temperature obtained from the heating microscopy machine do not necessarily coincide. Therefore, two main temperature levels were employed: the maximum height temperature (T_{MH}) and the maximum area temperature (T_{MA}).

In addition, four more levels were derived based on the average of three repeated heating microscopy measurements:

1. The sintering temperature of expansion: (T_{Ex})
2. The average of maximum height and maximum area temperature (T_{Avg})
3. Temperature $T_A = T_{Avg} - (T_{MA} - T_{MH})$
4. Temperature $T_B = 2T_{MH} - T_{MA}$
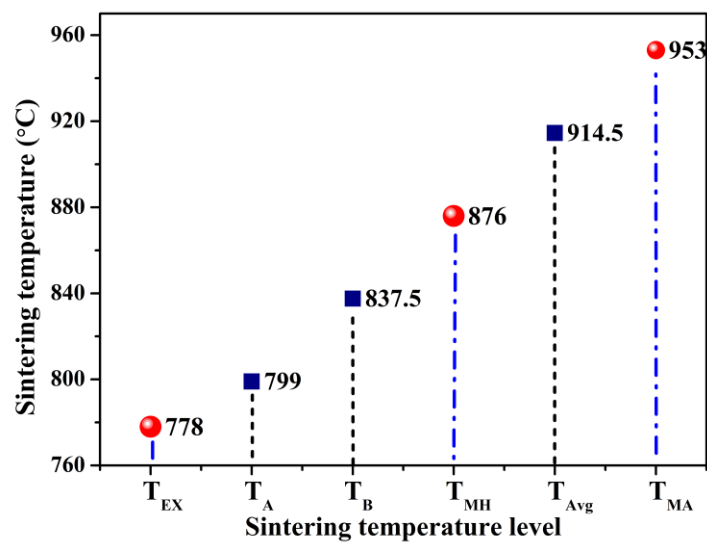
Figure 15. The sintering temperature levels

By investigating these parameters, the study aims to optimize the firing conditions for foam glass production, ensuring the best possible balance between material properties and energy efficiency. The L18 Taguchi design of experiments was chosen due to the limitation of a maximum of 18 treatment combinations allowed by the number of levels for each parameter. This method offered an efficient approach to investigating the influence of multiple factors while minimizing the number of experiments required. The specific design layout is presented in Table 2. Waste glass powder (mesh size < 90 micrometers) with 1wt% SiC addition was dry-pressed to fabricate the specimens.

Table 2. Design of experiments to test the effect of sintering parameters on foam glass behavior

Treatment number	Holding time (minute)	Sintering temperature (℃)
1	10	778
2	30	778
3	50	778
4	10	799
5	30	799
6	50	799
7	10	837
8	30	837
9	50	837
10	10	876
11	30	876
12	50	876
13	10	914
14	30	914
15	50	914
16	10	953
17	30	953
18	50	953

After the samples were fabricated, their water absorption capacity and density were initially tested. The volume of the samples was calculated based on their density and dry weight. With the known preform volume before the sintering stage, the expansion rate was also determined. Finally, the samples were prepared for thermal conductivity testing, and after this, their compressive strength was measured, and then the Taguchi analysis was employed to analyze the experimental data.

The next part of the research focuses on examining the effect of adding water as a binder to the foam glass preform on the final properties of the foam glass. The experimental method used for this analysis is explained in detail in the following sections.

2.2.3. Fabrication methods.

In this research, two methods—referred to as the Dry Powder Method and the Wet Powder Method—were used to produce foam glass. In the Dry Powder Method, the foam glass preform powder is first prepared, and then 5 grams of it is placed in a mold with a diameter of 2.5 cm. This powder is then subjected to a pressure of 80 MPa for two minutes. Subsequently, the cylindrical foam glass preform is unmolded, placed on a refractory tray covered with a layer of alumina powder, and then sintered in a furnace.

One of the challenges encountered through the fabrication of foam glass samples was molding and unmolding the preform. So, an alternative method for the dry pressing method was proposed where a small amount of water was added to the powder mixture instead of subjecting the sample to a 80 MPa pressure. This method significantly reduced the sample fabrication time. Figure 16 shows the fabrication method of the samples.
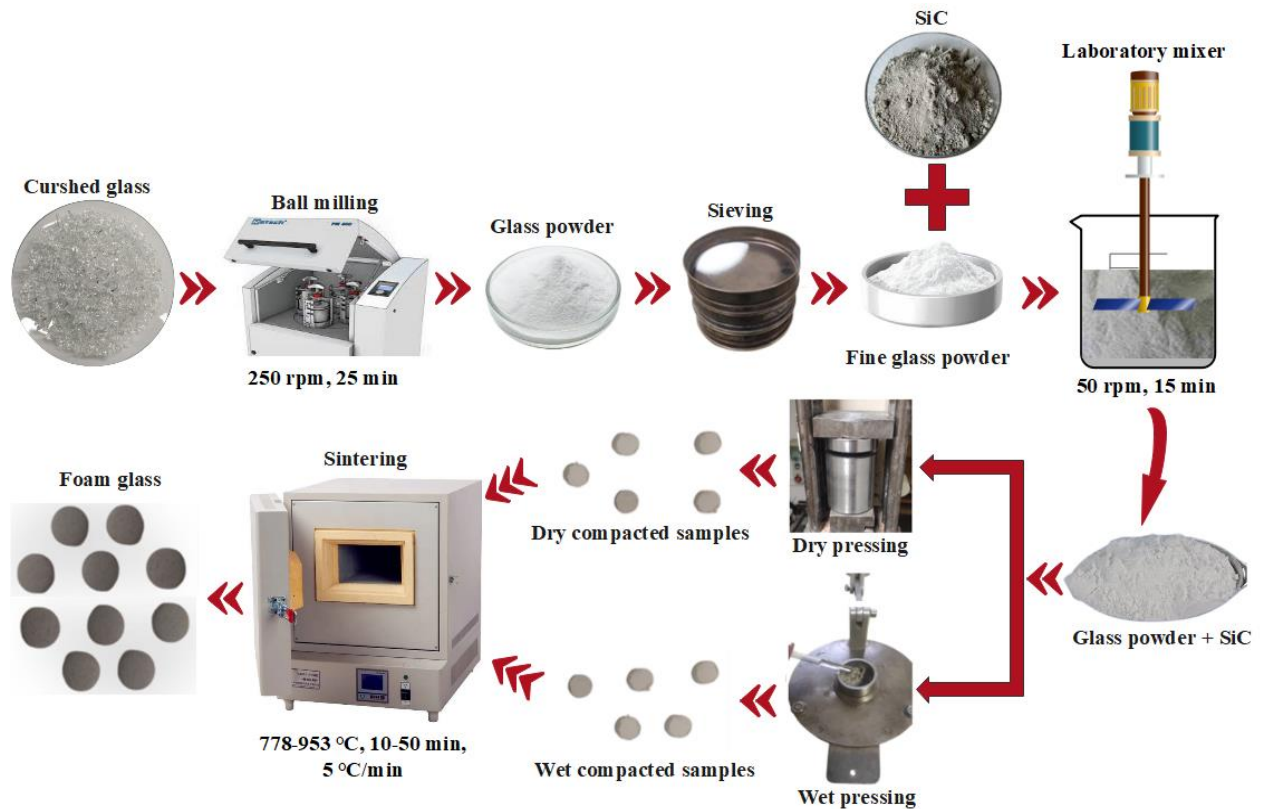
Figure 16. The procedure of dry powder molding for producing foam glass

A simultaneous examination of three parameters—molding method (dry powder pressing or wet powder method), sintering temperature (maximum height temperature (T_{MH}), maximum area temperature (T_{MA}), expansion start temperature (T_{Ex}), and the average of maximum height and maximum area temperature (T_{Avg})), and holding time (10 and 30 minutes)—was designed based on Taguchi design of experiments and using an orthogonal array L8, as detailed in Table

3. Waste glass powder with particle sizes below 90 microns and 1% SiC as a foaming agent was used to prepare the samples. Samples designated in Table 3 with a mention of "dry" were fabricated using the dry powder pressing method, with each sample subjected to 5 repetitions. Samples defined as "wet" are prepared by injecting 1 milliliter of distilled water into 5 grams of the prepared powder in a mold cavity, mixing it thoroughly with a needle, and compressing the mixture manually with the other part of the mold.

Table 3. The fabrication characteristics for testing the dry-powder and wet-powder method effects on foam glass

Number	Temperature (°C)	Holding Time (min)	Fabrication Method
1	(T_{Ex}) 778	10	dry
2	(T_{Ex}) 778	30	wet
3	(T_{MH}) 876	10	dry
4	(T_{MH}) 876	30	wet
5	(T_{Avg}) 914	10	wet
6	(T_{Avg}) 914	30	dry
7	(T_{MA})953	10	wet
8	(T_{MA}) 953	30	dry

After the fabrication of the samples, tests related to water absorption, density, thermal conductivity, compressive strength, expansion, and open porosity were conducted on the samples. The results of this analysis were processed using Minitab software, and the effectiveness ratio of each parameter was extracted.

2.2.4. Using cement factory soot and alumina in foam glass

In this section of the research, virgin glass powder, a mixture of soot and silicon carbide as a foaming agent, and alumina as a mechanical strength enhancer were used. All the raw materials were sieved to achieve a particle size below 90 microns. The Taguchi experimental design with an orthogonal array L9 was selected for this part of the study, as shown in Table 4.

These nine powder compositions were subjected to heating microscopy to determine the temperatures at which maximum expansion (considered as the maximum area) occurred. The minimum and maximum temperatures among the nine were identified.

Several considerations were taken into account after determining the minimum and maximum temperatures. Firstly, larger preforms require more time to achieve uniform heating. Therefore, higher sintering temperatures can cause the outer layers of the preform to reach the furnace temperature more quickly, resulting in non-uniform sintering [228]. To ensure uniform heating, lower sintering temperatures are recommended for bigger preforms (the samples were sintered in the furnace in comparison to the samples of heating microscopy). Additionally, higher sintering temperatures in bigger samples increase the likelihood of defects [88], while lower

temperatures can help reduce thermal stress and create a more cohesive structure. Given these factors, the furnace temperature was set at 30°C below the maximum expansion temperature obtained from the heating microscopy. Each of the nine different compositions was investigated at two temperatures, 842°C (group A) and 890°C (group B). All 18 groups (with 5 repetitions for each) of samples were fabricated using the wet pressing method. The holding time at the peak temperature was set for 10 min.

Table 4. The weight percentage of additives in each experimental group according to the L9 design of the experiment

Group	SiC (wt%)	Soot (wt%)	AL_2O_3 (wt%)
1	1	1	0
2	2	2	0
3	3	3	0
4	1	2	4
5	2	3	4
6	3	1	4
7	1	3	8
8	2	1	8
9	3	2	8

After the sintering step, the specimens were pulled out from the furnace and they were weighed. Subsequently, tests were conducted to evaluate water absorption, calculate open porosity, measure density, thermal conductivity, optical imaging, SEM imaging, and compressive strength of the samples. The extracted data was analyzed, using Taguchi analysis method and the ranking of effective parameters and signal-to-noise ratio diagrams were drawn.

The results of the investigations carried out so far in this research have led to a deeper understanding of the effect of material composition and sintering conditions on the physical and mechanical properties of foam glass. Since the main goal of this investigation is to use foam glass in CMFGC production, the production of granular foam glass was one of the concerns of this research. We could not find a method to produce foam glass granules in laboratory scale so, a new idea proposed for the laboratory production of granular foam glass. The feasibility and applicability of this idea were investigated in the next part of the study.

2.2.5. Selection the optimal foam glass (multi criteria decision making)

Up to this point in the research, various experiments have been conducted on foam glass, and different samples have been produced using the methods previously outlined. Several tests were performed to extract the characteristics of these foam glasses. The next phase of the study involves producing foam glass granules to be used as aggregate in CMFGC. However, before proceeding, it is crucial to determine the optimal composition and production method that will provide the best properties for use in CMFGC. Each tested group has advantages and

disadvantages in different criteria. This decision-making process for selecting the optimal composition and fabrication method is a multi-criteria decision-making (MCDM) problem. The simplest method for solving multi-criteria decision-making problems is introduced by Fishburn in 1967 [229]. The weighted sum model (WSM) is probably the most commonly used approach, especially in single-dimensional problems. This method is used in this project and it is detailed in Appendix A. Based on Appendix A, it is necessary to assign a value to each physical and mechanical property of the foam glass. Based on the experimental results obtained so far, additional 8 tests were conducted using only SiC and alumina, with varying proportions of 2wt% and 3wt%, utilizing both waste glass and virgin glass. In total, the number of successfully foamed sample groups that have been examined up to this point in the project reached 61 groups. Out of the tests conducted, the optimal choice will be made from among these 61 groups. For foam glass to be used in lightweight CMFGC, it is preferable that it has lower density, lower thermal conductivity, lower water absorption, higher compressive strength, and higher expansion. However, depending on the geographical region where the CMFGC will be used, and the type of CMFGC being designed based on this, the value weighting of these properties can vary. For example, in regions with extreme temperature fluctuations between winter and summer, the water absorption factor will have a higher weight. Similarly, for structural CMFGC, mechanical strength will carry more importance.

Table 5. The importance value for multi-criteria decision making

Criteria	Water absorption	Density	Expansion	Thermal conductivity	Compressive strength
Unit	wt%	g/mm^3	Vol%	W/m·K	MPa
Weight	0.25	0.15	0.05	0.15	0.4

The value assignments, as seen in Table 5, are based on expert judgment for the design of foam glass for getting used as aggregate in structural lightweight CMFGC. Using these values and the method outlined in Appendix A, the best composition and manufacturing method for the foam glass was selected.

2.2.6. The laboratory method for making foam glass granules

As mentioned in all previous sections of this research, the general method for producing foam glass is to mix powdered glass with a foaming agent, mold it, and sinter it in a furnace. The behavior of this powdered mixture is such that with increasing temperature, the glass powder first starts to soften and after a certain temperature, the foaming agent decomposes and causes foaming. This behavior led to the idea of a method for producing foam glass granules. For the

experimental investigation of this idea, both waste and virgin glass powder, silicon carbide, and alumina were used.

However, since soot is an industrial waste product with variable oxide compositions depending on its origin and production conditions, preliminary compositional analysis is essential prior to large-scale application.

Based on previous experiments, it was determined that the optimal range for using silicon carbide in foam glass production is 1-3 wt%. Given that alumina was added as an additive in this study, which can increase the viscosity of the softened sample at high temperatures, the addition of 2% and 3% silicon carbide was examined. For each group, five replicates were produced. All four powders were analyzed using heating microscopy to determine their Tg temperatures. The temperature obtained from heating microscopy is not the softening point but the Tg temperature. The Tg temperature is the point at which the sample deforms under its own weight. Below this temperature, the glass structure is softened but still requires an external load to deform. Therefore, the Tg temperature ensures that the glass particles have softened and bonded together, while the foaming agent has not yet been activated. For each composition, the Tg temperature was used for first level of sintering. The holding time was set to 50 minutes to ensure the complete sintering of the samples. After the samples hardened and became brittle, they were crushed using a mortar, and the crushed particles were refired in the furnace at a temperature 20°C below the maximum expansion temperature (Table 6). Figure 17 shows the procedure of making foam glass granules.
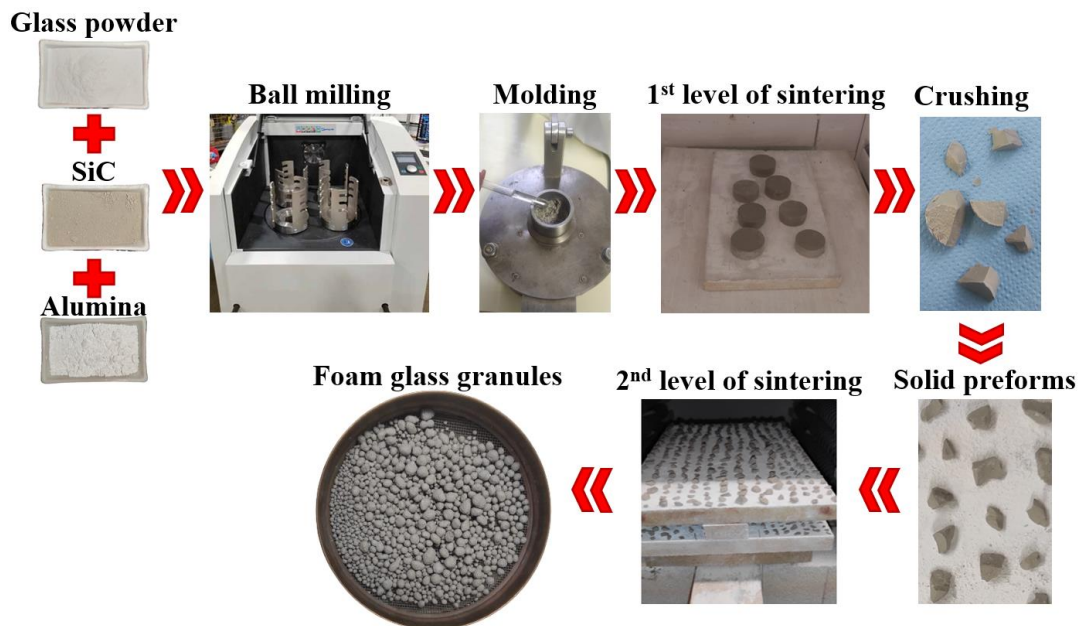
Figure 17. The process of making foam glass granules

Table 6. The composition and sintering conditions of the foaming process

Sample number	Sintering temperatures			Composition (wt%)			
	Alumina	SiC	Glass	Tg (°C)	Average of Tg and the start of expansion (°C)	Start temperature of expansion (°C)	Maximum height temperature - 20 (°C)
1	2	2	96 (virgin)	652	716	780	833
2	3	3	94 (virgin)	638	691	744	825
3	3	2	95 (virgin)	647	721	794	830
4	2	3	95 (virgin)	631	708	784	843
5	2	2	96 (waste)	630	669	708	864
6	3	3	94 (waste)	615	660	705	848
7	3	2	95 (waste)	609	661	710	875
8	2	3	95 (waste)	590	653	715	855

This step produced granulated particles with minimal open porosity and a nearly spherical shape. Finally, the density, water absorption, and compressive strength of the aggregates were tested according to ASTM C330/C330M, and XRD and SEM tests were performed on samples. The optimal granulated foam glass was then used to produce lightweight aggregate CMFGC.

2.2.7. Crystallization of foam glass granules

Part of the research aimed at determining the crystallization temperature of foam glass made from waste glass and virgin glass was conducted using DSC (Differential Scanning Calorimetry) at the University of São Carlos in Brazil, under the supervision of Professor Edgar Zanotto. For this purpose, as shown in Figure 18, a small foam glass sample was placed in the DSC crucible, and the sample's temperature was increased to 1000°C at a rate of 10°C/min. Finally, the graphs were drawn and analyzed.
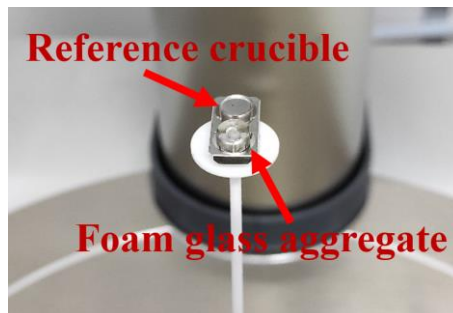
Figure 18. Foam glass aggregate sample in a Differential Scanning Calorimetry (DSC) testing machine

2.3. Foam glass properties

2.3.1. Density, water absorption, and open porosity

In the initial experiments of this project, the density of foam glass was measured using the buoyant force exerted by a fluid on a solid. A specialized device was designed and constructed for this purpose (Figure 19). The principle of density measurement via buoyancy is based on the fact that the force exerted on a submerged object is equal to the weight of the fluid displaced by that object. Therefore, by knowing the dry weight of the foam glass, then saturating it with

water and submerging it, the reduction in the weight of the foam glass in water relative to its weight in the air can be measured. This upward force on the foam glass is equal to the weight of the displaced water [138].
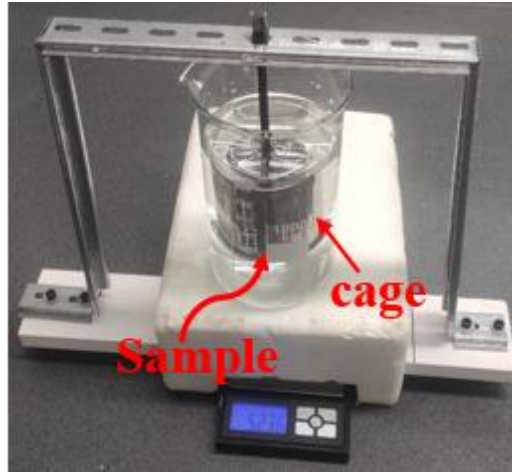
Figure 19. Handmade density measurement device based on buoyancy force

Thus, using the equations related to buoyancy force, the apparent volume of foam glass is calculated through the equation 4.

Equation 4. Apparent volume (volume of the solid skeleton and close pores [138]

$$V = \frac{m_{dry} + m_{cage} - m_b}{\rho}$$

Additionally, knowing the density of the absorbed water, the weight of the saturated foam glass, and the weight of the dry foam glass, the open porosity volume can be determined using the equation 5.

Equation 5. The volume of open porosity

$$V_{open\,porosity} = \frac{W_{saturated} - W_{dry}}{\rho_w}$$

2.3.2. Thermal conductivity

For the thermal conductivity test on foam glass, the top and bottom surfaces of the foam glass were first sanded to ensure the sample had two parallel surfaces. The foam glass sample was then placed on the sensor of the C-therm TCI instrument (Figure 20), and its thermal conductivity was measured. To minimize device error, each test was repeated five times, and the average of the results was reported as the thermal conductivity of the foam glass sample.
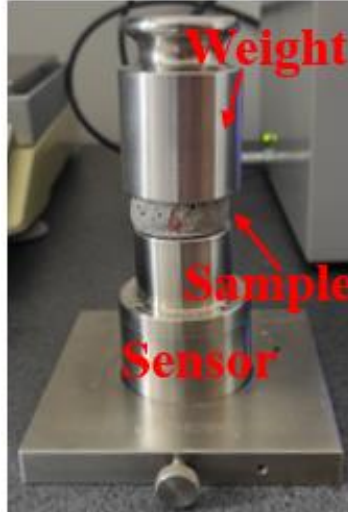
Figure 20. The thermal conductivity instrument loaded with a foam glass sample

2.3.3. Compressive strength

The next test conducted on both the foam glass and the foam glass CMFGC was the compressive strength test. This test was performed using different devices for the foam glass samples and the CMFGC samples.

For the foam glass samples, the surface area of the top face, which had been sanded to ensure parallel surfaces, was measured first. So, the photographs of the sample were analyzed with ImageJ software to extract the surface area. The samples were then placed in the INSTRON 5566 universal tensile machine, and compressed at the speed of 5mm/min. The maximum stress was extracted from this test. For the foam glass granules, the same device and loading rate were used, but the compressive strength was calculated based on the maximum force sustained (F_{max}) and the diameter of the granule (D), using the equation 6 [230].

Equation 6. The compressive strength calculation of spherical aggregate

$$\sigma = \frac{2.8 * F_{max}}{\pi D^2}$$

2.3.4. Foam glass reactivity (Thermo gravimetry analysis-based test)

This part of the project, which was carried out at Sapienza University in Rome, under the supervision of Professor Marco Valente and Dr. Matteo Sambucci, focuses on evaluating a new rapid method for identifying the reactivity of foam glass. In this method, firstly foam glass was crushed and milled to find foam glass powder, then foam glass powder-$Ca(OH)_2$ paste (10 g) was prepared by dry mixing reagent grade calcium hydroxide (> 95%, Alfa Aesar, Haverhill, MA, USA) and the analyte powder in 1:1 mass ratio. Then, water (10 g) was added, achieving a solid-to-liquid ratio of 1. For each composition of foam glass, the resulting paste was sampled into 3 batches for performing the reactivity analysis at 1, 7, and 28-day hydration times. The

samples were stored in plastic containers and left in an oven at 40°C to ensure a high-humidity environment and minimize the effect of carbonation. Once the day of testing was reached, the blend was manually pulverized using a porcelain mortar. Acetone (purity 99.5%), purchased from Honeywell (Charlotte, NC, USA), was added during the milling operation to block the hydration. The excess solvent was removed using a vacuum pump filtering system by collecting the powder on a Whatman540 qualitative filter paper (Whatman, Maidstone, UK) with pore sized diameter of 8μm. Then for TGA testing, the sample was pre-dried at 60 °C for 3h, and then the samples were tested in a TGA device. The steps related to the sample preparation are shown in Figure 21.

Figure 21. The procedure of testing ASR using a TGA device

Changes in sample weight are monitored concerning temperature. At approximately 500°C, $Ca(OH)_2$ undergoes phase transformation. If the foam glass aggregates are alkali-reactive, it is expected to react with $Ca(OH)_2$, resulting in a very smooth change in the TGA curve. Conversely, for non-reactive aggregates, $Ca(OH)_2$ decomposition dominates, leading to weight loss and a sharp peak in the TGA curve. This rapid TGA method offers a promising alternative to conventional ASR testing, enabling quick identification of alkali-reactive aggregates and assessment of ASR potential in foam glass.

2.4. Preparation of cement matrix composite material with foam glass additive

The section on the development of lightweight CMFGC using foam glass is divided into two major parts. The first part focuses on the production and analysis of lightweight CMFGC made with foam glass granules derived from virgin glass, with a composition of 2 wt% of SiC and 2wt% alumina. In the second part, lightweight CMFGC made from granules produced from both waste glass and virgin glass, as well as crushed foam glass gravel made from waste and virgin glass, is examined. In this section of the research, the same composition was used to produce the foam glass.

As previously explained, the ACI (American Concrete Institute) method was used for the mix design. In this method, we employed empirical tables developed by earlier researchers. During the mix design process, which is explained in detail, the coarse aggregates were sieved, and coarse aggregates with a maximum diameter of 19 mm were considered.

2.4.1. Concrete mix design

The mix design process, according to ACI, involved considering the type of CMFGC used, the desired slump, and the maximum nominal size of lightweight aggregates. The fineness modulus of sand and the density of aggregates were also included as input data. The specific gravity of coarse natural aggregates, sand, lightweight foam glass aggregates, and cement was used to estimate the density of the produced CMFGC. The mix design process was carried out according to the following steps:

- Determining the slump: The required slump was defined based on the structural application of CMFGC. In this study, a slump of 7.5 cm was selected [231].

- Determining the amount of water: Based on Table 7 and considering the specified slump and the absence of any additives in the CMFGC, the water content was set at 202 kg/m³ of CMFGC.

Table 7. The recommended required water for concrete based on the coarse aggregate maximum size and slump [231]

	Maximum nominal size of coarse aggregates (mm)		
	9.5	12	19
Slump (cm)	Water requirement for concrete with air-entraining agents (kg/m³)		
2.5 - 5	181	175	166
7.5 - 10	202	193	181
12.5 - 15	211	199	187
Slump (cm)	Water requirement for concrete without air-entraining agents (kg/m³)		
2.5 - 5	208	199	188
7.5 - 10	228	216	202
12.5 - 15	237	222	208

- Determining the water-to-cement ratio: The water-to-cement (W/C) ratio, which is the most critical parameter in mix design, was determined by extrapolating from Table 8, prepared for Portland Type 1 Cement. The W/C ratio was set at 0.67, considering a target compressive strength of 17 MPa for concrete.

Table 8. Approximate water-to-cement ratio vs. 28-day compressive strength (MPa) [231]

28-day compressive strength (MPa)	Approximate water-to-cement ratio	
	Cement without bubble-forming agents	Cement with bubble-forming agents
41.3	0.41	-
34.4	0.48	0.4
27.5	0.57	0.48
20.6	0.68	0.59
13.7	0.82	0.74

- Calculating the amount of cement: Given the water content and the water-to-cement ratio, the cement content was calculated to be 348 kg/m³ of CMFGC.

- Estimating the amount of coarse aggregate: The amount of coarse aggregate was estimated using Table 9. taking into account the fineness modulus of the sand, which had been previously calculated.

Table 9. The volumetric ratio of coarse aggregates based on the maximum size and the coefficient of sand porosity [231]

	Coarse aggregates (Vol%)			
	Fineness modulus			
Maximum size of aggregates (mm)	2.4	2.6	2.8	3
9.5	0.58	0.56	0.54	0.52
12	0.67	0.65	0.63	0.61
19	0.74	0.72	0.7	0.68

- Calculating the fine aggregate and air content: The lightweight CMFGC density was estimated using Table 10, assuming an air content of 6%.

Table 10. Specific weight of natural coarse aggregates vs. initial density of concrete (kg/m³) based on concrete air content [231]

Specific weight of natural coarse aggregates (kg/m3)	Initial estimate of concrete density, kg/m³, based on concrete air content		
	4v%	6 v%	8 v%
1.0	1595	1560	1518
1.2	1678	1643	1607
1.4	1767	1726	1690
1.6	1850	1809	1773
1.8	1933	1898	1856
2	2022	1981	1939

The quantity of fine aggregate was calculated using equation 7.

Equation 7. Calculation of fine aggregate amount in concrete

$$S = \rho - (C - W - NCA)$$

Where S is the quantity of fine aggregates in one cubic meter, ρ is the concrete density, and C, W, and NCA represent the weights of cement, water, and natural coarse aggregates in one cubic meter of concrete, respectively. These steps ensured a systematic approach to optimizing the CMFGC mix for the desired properties, focusing on achieving the required slump, compressive strength, and density.

2.5. Replacing natural coarse aggregate with foamed virgin glass in cement matrix composite material

To explore the feasibility of producing lightweight CMFGC using granular foam glass made from virgin glass, the mix design plan, as explained in detail, was utilized. Given the known density of the coarse aggregates and the foam glass granules, the natural coarse aggregates were replaced with foam glass granules in 20%, 40%, and 60% by volume. A reference group with no foam glass added was also prepared for comparison.

For each group, five replicates were produced. The CMFGC mix was first prepared, and after air removal using a vibrator, it was placed into silicone molds with dimensions of 5×5×5 cm. The samples were then cured in a humid environment for one day. After demolding, the density was measured, and the samples were submerged in a water bath for 24 days. Following

the water bath, the samples were dried at room temperature for three days, after which their density was re-measured. In the next phase, the samples underwent a compressive strength test, and the results of the tests were recorded for analysis.

2.5.1. Characterization of cement matrix composite material with foam glass

- Compressive strength

An Instron 1121 Canton, Massachusetts, USA was used to determine the maximum compressive strength of the CMFGC samples. In these tests, the cross-sectional area of the CMFGC samples was measured using a caliper. The speed rate was 2mm/min according to ASTM C39/C39M or EN 12390-3. This process allowed for the plotting of the stress-strain curve until the sample failed. The maximum compressive stress sustained was recorded as the compressive strength of the CMFGC.

- Comparison of compressive strength and ASR in CMFGCs made from waste and virgin foam glass aggregates (granulated and crushed)

After extracting the results from the previous experiment, four categories of samples were created to compare the properties of CMFGC made from waste foam glass and virgin foam glass in both crushed and granular forms. 20% by volume of foam glass was used in each group. Table 11 shows the type of foam glass tested groups.

Table 11. The type of foam glass used to make a lightweight cement matrix composite

	Foam glass aggregates	
Sample code	**Type of glass**	**Type of foam**
VL$_1$	Virgin glass	Crushed
VL$_2$	Virgin glass	Granule
WL$_1$	Waste glass	Crushed
WL$_2$	Waste glass	Granule

These sample groups were prepared based on the standard dimensions for the ASR test. A plexiglass mold with dimensions $25 \times 25 \times 285$ mm was made, and the CMFGC mix was poured into the mold. As with the previous experiment, after one day, the samples were removed from the mold and followed the same hydration process, with density measurements taken afterward. The samples were then subjected to the ASR test.

For the ASR test, the initial length of the samples was measured, and they were submerged in a 1N NaOH solution for 14 days. After this period, the expansion of the samples was measured again. Following that, 4 cm pieces were cut from the samples and subjected to a compressive strength test to determine their compressive strength. This portion of the experiment was also conducted at Sapienza University in Italy. The compression tests have been conducted following the ASTM C 109/109 M standard method on a Zwick-Roell Z150 (150 kN load cell) testing system (Zwick-Roell, Ulm, Germany). The preload was 100 N and the loading rate was 1 mm/min. The test parameter selection and the acquisition of the load–strain data were carried out by TestXpert computer-controlled testing software (Zwick-Roell, Ulm, Germany). The compression plates were equipped with iron blocks measuring 40×40 mm to consider a test surface of 40×25 mm. Three replicates for each formulation were tested. After the compressive strength test, SEM analysis was performed to examine the presence of silica gel at the interface between the foam glass and the cement paste.

3. Raw materials characterization results

This sub-chapter investigates the properties of the raw materials used in the production of foam glass in structural lightweight CMFGC. The primary focus is on the characterization of virgin and waste glass powders, soot, alumina, and silicon carbide (SiC), as well as their suitability for use in foam glass production. Several analytical techniques were employed to assess the raw materials.

3.1. Particle size

The laser particle size analyzer was employed to examine the variation in particle size among virgin glass powder, soot, and alumina, with the findings graphically depicted in Figure 22. The analysis revealed distinct differences in the mean particle size, denoted as D50, for each material. Specifically, the D50 value for glass powder was determined to be 29.9, contrasting with 2.2 μm for alumina and 4.7 μm for soot. Notably, the distributions of particle size of the raw samples reveal significant differences, with glass powder characterized by larger particles compared to the finer particles of alumina and soot. This difference is important because smaller particles have a greater ability to penetrate deeply into a mixture, efficiently filling gaps and making a more integrated, homogenous structure inside the substance. The high variation in particle sizes spectrum facilitates superior packing, leading to compacted structures and sustaining the material's overall strength.
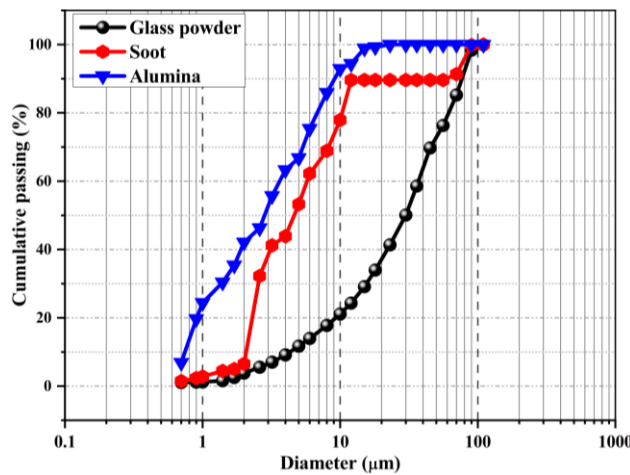
Figure 22. Raw materials' particle size distribution

Since the SiC powder particles were previously identified as being smaller than 1 μm [232], the particle size analyzer was not suitable for measuring their distribution, so it is not measured and considered to be less than 1 μm. Also, we used sieving to determine the particle size of the waste glass because there was a possibility that particles larger than the permissible size for measurement might be present. To prevent potential damage to the equipment, we relied on the sieving results.

3.2. Chemical composition (XRD and XRF analysis)

The X-ray diffraction (XRD) analysis (Figure 23) conducted on the raw materials, namely waste and virgin glass powders, SiC, soot, and alumina, provided valuable insights into their crystalline structures, aiding in understanding their properties and potential applications. The investigation of the glass powders revealed a characteristic feature of an entirely amorphous structure. This finding confirms the basic nature of glass, which lacks long-range atomic order, thereby exhibiting an X-ray diffraction pattern devoid of distinct peaks. The absence of identifiable peaks in the XRD spectrum confirms the non-crystalline, disordered arrangement of atoms within both waste and virgin glass. This result underscores the suitability of glass powder as a raw material for foam glass manufacturing.

Contrary to the amorphous structure observed in the glass powder, the XRD analysis of soot exhibited the presence of calcite as the main phase together with a minor amount of dolomite (Table 12). The emergence of sharp diffraction peaks corresponding to the crystalline structure of calcite indicates the ordered arrangement of atoms within the soot particles. The identification of calcite in the soot suggests its potential as a foaming agent for the synthesis of foam glasses. The X-ray diffraction pattern obtained from the received silicon carbide particles exhibits peaks that correspond to known silicon carbide crystal structures. The XRD analysis of alumina showcased the presence of a single-phase corundum structure. Corundum, characterized by its hexagonal crystal lattice arrangement, is the most thermodynamically stable phase of alumina. The identification of corundum in the alumina sample highlights its suitability for applications as reinforcement in the foam glass, contributing to the higher compressive strength.

Table 12. Phase composition of raw materials powder (XRD analysis)

Raw materials	Phase composition (wt%)				
	Calcite	Dolomite	Corundum	SiC	Amorphous
Virgin glass powder	-	-	-	-	100
Waste glass powder	-	-	-	-	100
Soot	86.61	6.39	-	-	7
Alumina	-	-	100	-	0
SiC	-	-	-	100	0
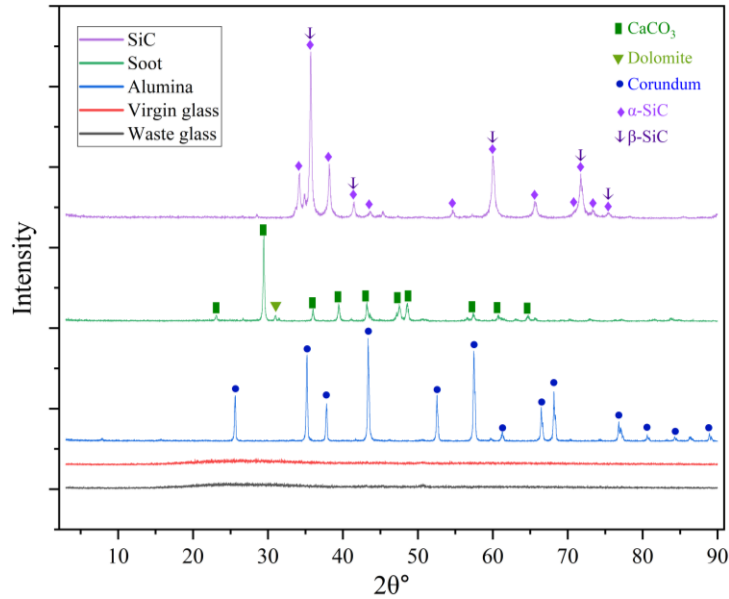
Figure 23. XRD diffraction graph of Virgin glass powder, Waste glass powder, soot, SiC, and alumina

Table 13 shows the composition of virgin glass, waste glass, and soot obtained from XRF evaluation. As indicated, glass powders consist of high percentage of the silicon oxide (72.7 and 70.6 for virgin and waste glass, respectively) and low content of other oxides (Na_2O, CaO, etc.), The soot consists of mainly (49.35 wt%) calcium oxide with a small amount of SiO_2 and MgO (3.6 and 1.5 wt%, respectively). However, the LOI (Loss on Ignition) for soot indicates the decomposition of one of its oxides and the evaporation of some of the decomposition products. Given that calcium carbonate decomposes into calcium oxide and CO_2, this is the primary mechanism by which soot acts as a foaming agent. Thus, the LOI corresponds to the following chemical equation. To calculate the amount of calcium carbonate, we consider that in a completely stoichiometric scenario, the molar mass of calcium carbonate is 100.09 grams per mole, the molar mass of calcium oxide is 56.08 grams per mole, and the molar mass of carbon dioxide is 44.01 grams per mole.

Therefore, with the known mass percentage of calcium oxide in the material, the mass percentage of calcium carbonate can be derived using a simple mathematical proportion. By substituting the mass percentage of calcium oxide into this equation, the mass percentage of calcium carbonate was calculated to be 87.84 percent.

Table 13. Chemical composition of raw materials (XRF analysis)

Component (wt%)	Raw Materials		
	Virgin glass	Waste glass	Soot
SiO_2	72.67	70.58	3.59
Al_2O_3	0.97	0.62	0.45
MgO	3.55	2.98	1.53
CaO	8.84	9.13	49.35
Na_2O	14.37	11.65	0.36
K_2O	0.31	0.28	0.23
Fe_2O_3	0.52	0.07	0.28
MnO	0.007	0.008	0.009
TiO_2	0.065	0.032	0.032
P_2O_5	0.016	0.012	0.117
S	0.24	0.14	1.91
F	<0,3	<0,3	<0,3
Loss On Ignition (LOI)	-	-	38.61
Total	101.6	95.5	57.9

3.3. Morphology and elemental compositions

Understanding the raw materials' morphological characteristics is crucial to comprehend how well they perform during the production process. Microscopical analysis of the raw materials reveals irregular and angular particles with a variety of morphologies, as Figure 24 illustrates. Please note that the waste glass was analyzed using Scanning Electron Microscopy (SEM) and Energy Dispersive Spectroscopy (EDS) after being ground and sieved through a 90-micron sieve. The raw materials' broad range of particle sizes is seen in the micrographs. Interestingly, glass powder particles tend to be bigger in size, followed by soot, alumina, and SiC, in that order. This reinforces the pattern of particle size distribution seen in Figure 22.
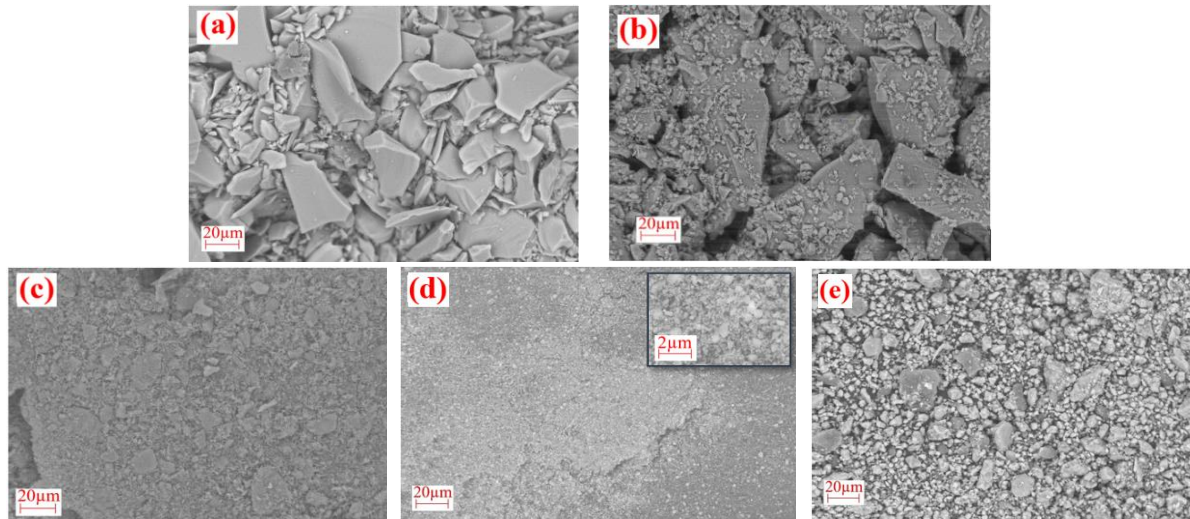
Figure 24. SEM micrographs of a) Virgin glass, b) Waste glass, c) Al_2O_3, d) SiC, e) Soot

The EDS analysis of the raw materials is depicted in Figure 25. The EDS analysis of the glass powders (Figure 25a and Figure 25b) reveals silicon as the primary constituent, alongside detectable amounts of sodium, calcium, and minor percentages of carbon and magnesium.

Conversely, Figure 25c presents the EDS analysis outcomes for soot, highlighting calcium as the basic component, followed by oxygen, carbon, and trace levels of magnesium and silicon (1.49 and 1.81 wt%). Figure 25d displays the EDS analysis results of SiC, indicating a high concentration of silicon and carbon, with minimal oxygen content. Furthermore, Figure 25e exhibits the EDS analysis findings for alumina, confirming the exclusive presence of aluminum and oxygen.
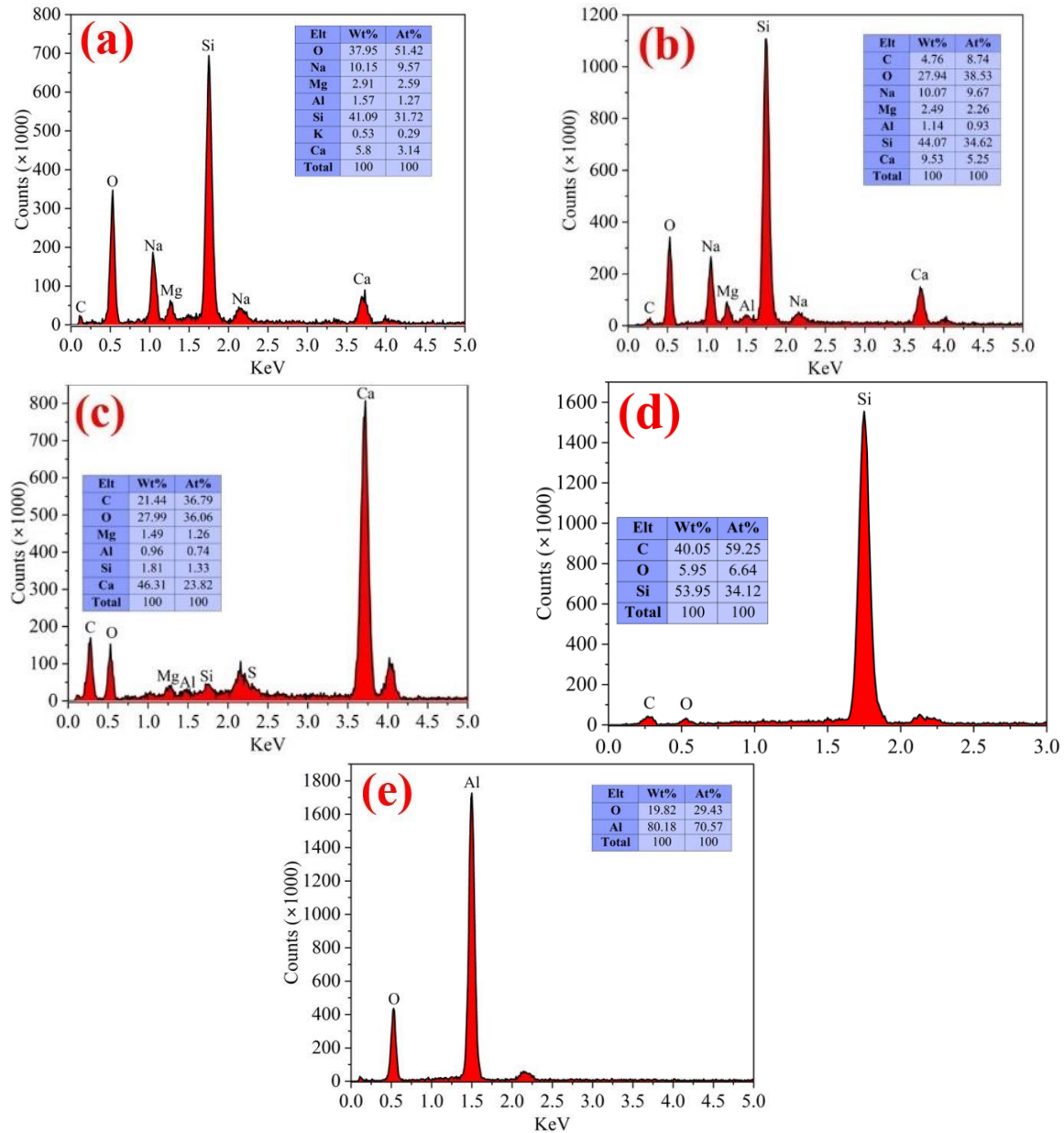
Figure 25. EDS examination of a) Virgin glass powder, b) Waste glass powder, c) soot, d) SiC, and e) alumina

These EDS findings align with the elemental composition determined from X-ray Diffraction (XRD) measurements showcased in Figure 23. Further proof of the elemental composition of the materials under evaluation is supplied by the supplemental information obtained through EDS analysis.

3.4. Thermal behavior of soot at high temperature (TGA/DTA analysis)

Figure 26 shows the TG-DTA curve for cement factory soot. It can be observed that with increasing temperature up to approximately 310°C, water and other absorbed substances in the powder evaporate and volatilize. Following this stage, between 310°C and 474°C, there is an approximate 1.3% weight loss in the sample. The fluctuations in the DTA curve within this temperature range indicate the chemical decomposition of certain materials present in the soot. As the temperature increases from 474°C to 814°C, a significant amount of volatile and decomposable materials breaks down, and the sample mass continues to decrease. From 814°C to 947°C, which overlaps well with the softening point of the glass powder, the sample mass further decreases as the entire soot undergoes decomposition.
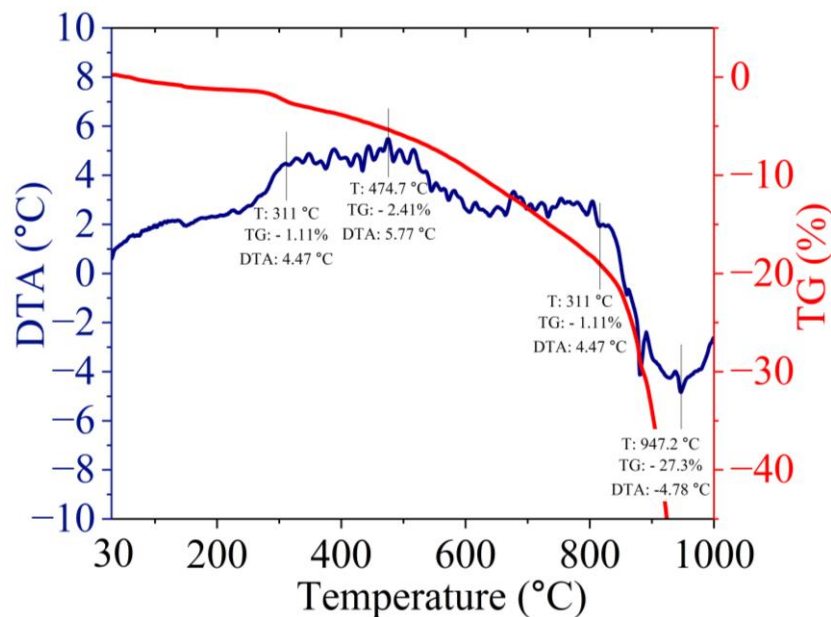
Figure 26. The DTA-TG curve of cement factory soot

The fact that soot undergoes various decompositions over a wide temperature range can be analyzed from two perspectives. Firstly, soot can be used as a foaming agent for producing foam glass from glass powders that soften at lower temperatures. For example, borosilicate glasses soften at around 500°C to 600°C, while lead-containing glasses have even lower softening points, around 450°C. Secondly, the use of soot may result in interconnected cells in the foam glass, as these cells form throughout the entire heating process.

Summary: *Glass powders have larger particles compared to soot, alumina, and SiC, which have finer particles that improve packing density and homogeneity in the final product. X-Ray Diffraction (XRD) analysis revealed that glass powders are amorphous, while soot exhibited a crystalline phase of calcite ($CaCO_3$), and alumina was primarily corundum (Al_2O_3). This makes soot a suitable foaming agent due to its decomposition into calcium oxide at higher temperatures. X-ray Fluorescence (XRF) analysis showed that virgin glass contains mostly*

SiO_2 (72.67 %) with trace amounts of other oxides. Soot has a high content of CaO, which can break down to form CO_2 and calcium oxide, promoting the foaming process. Scanning electron microscope (SEM) and energy dispersive X-ray spectroscopy (EDS) analysis revealed that glass powders have a broad range of particle sizes (D50= 29.9 µm), while soot contains mostly calcium (46.31wt%) and carbon (21.44 wt%), SiC has high silicon content (53.95 wt%), and alumina is predominantly aluminum (80.18 wt%) and oxygen (19.82 wt%). Thermogravimetry (TGA) analysis indicated that soot decomposes over a broad temperature range, making it suitable for use as a foaming agent in foam glass production. Its decomposition is accompanied by weight loss (38.61 wt%) due to the release of CO_2 from calcium carbonate decomposition, which aids in the formation of foam structure.

4. Foam glass characterization results

4.1. Influence of particle size and foaming agent content

As it mentioned in the last section one part of this study explored how the ratio of the foaming agent (SiC) and the particle size of glass powder affect the density and thermal conductivity of foam glass. The experiment utilized three particle size categories (coarse, equal, and fine) alongside varying foaming agent ratios (1 wt%, 1.5 wt %, 2 wt %).

As it can be seen from Figure 27, the density analysis revealed that for samples with coarser particles (levels 1 and 2), increasing the foaming agent ratio initially led to a rise in density due to trapped gas. However, at the highest ratio, the density decreased. Conversely, finer particles (level 3) exhibited a consistent increase in density with a higher foaming agent ratio. In terms of thermal conductivity, it generally increased with a higher foaming agent ratio, with the size of the particles having minimal influence. Based on these findings, the study opted for the lowest foaming agent ratio (1%) and the finest particle size (level 3) for further testing, aiming to achieve optimal foam glass properties.

a　　　　　　　**b**　　　　　　　**c**
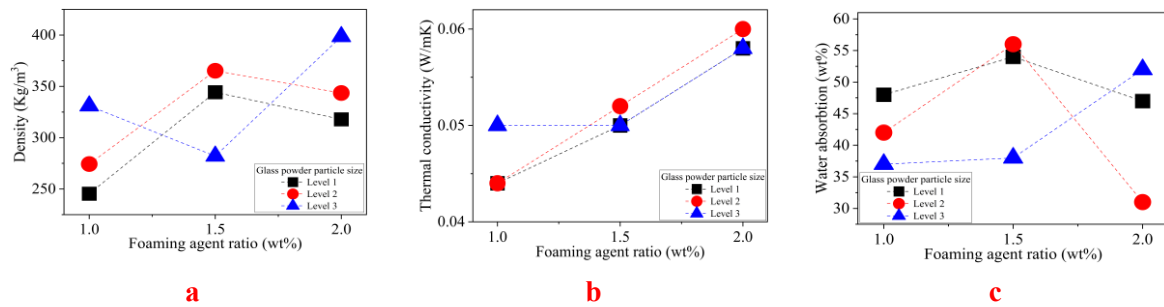
Figure 27. Three-dimensional plots illustrating the effects of particle size and foaming agent ratio on various properties of foam glass. a) Density, b) Thermal conductivity, c) Water absorption. Notice that particle size levels are defined as level 1: 66 wt% D1–34 wt% D2, level 2: 50 wt% D1–50 wt% D2, and level3: 34 wt% D1–66 wt% D2, were 125 μm < D1 < 160 μm and D2 < 90 μm

Figure 28 shows the sanded cross-sections of the samples. When using glass powder with smaller particle sizes (Level 3), better packing occurs during the preform making. As a result, when 1wt% silicon carbide is used, the pores are more uniform and smaller, leading to less water absorption due to the good packing of foam preform, resulting in more closed porosity. With an increase in the foaming agent, the pore sizes initially enlarge. However, with further increases in the foaming agent, the structure deteriorates, forming interconnected open pores. The water absorption percentage of this group was also higher than the others. Therefore, if the goal is to use foam glass as a drainer, the group containing 2% silicon carbide, with finer glass powder particles, represents the optimal composition. Additionally, it will exhibit high resistance as a sound insulator, where it can be used as an acoustic insulator.

Particle size level	Foaming agent ratio (wt%)		
	1	1.5	2
1			
2			
3			

1: 66 wt% D1 + 34 wt% D2

2: 50 wt% D1 + 50 wt% D2

3: 34 wt% D1 + 66 wt% D2

and

125 µm < D1 < 160 µm
D2 < 90 µm
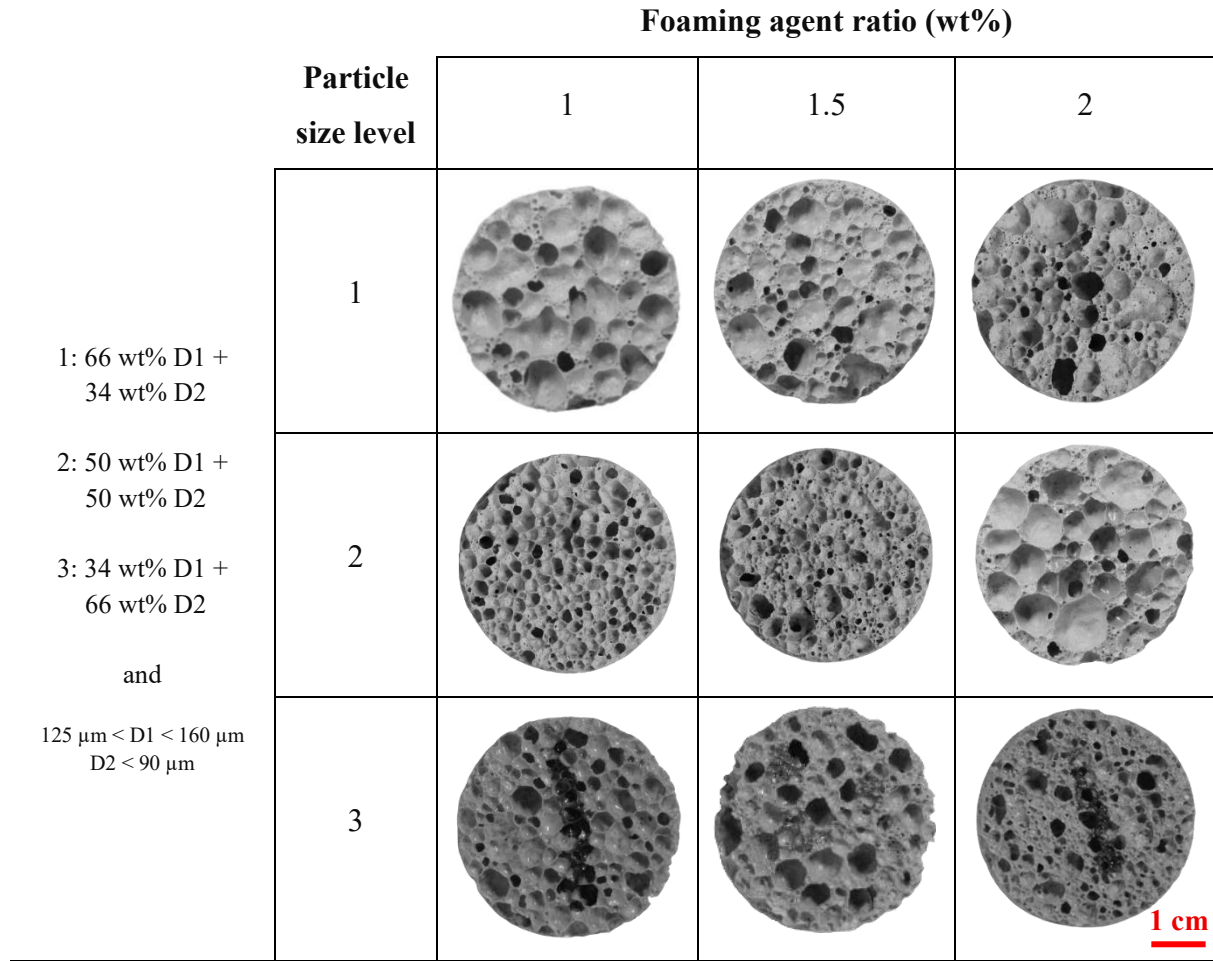
Figure 28. Images of foam glass cross-sections prepared with different particle sizes and foaming agent ratios

The water absorption data shown in Figure 27 directly correlates with open porosity: higher open porosity leads to higher water absorption. As observed, water absorption is higher in samples with particle sizes at Levels 1 and 2 when the foaming agent is 1.5wt%. However, for samples with particle sizes at Level 3, the highest water absorption occurs in the sample with 2 wt% of SiC. This is because the 2 wt% of the foaming agent disrupts the uniform matrix structure of the sample.

Summary: For coarser particles (Levels 1 and 2), increasing the foaming agent ratio initially raised the density (Figure 27) due to gas trapping. However, at the highest foaming agent ratio (2 wt%), the density decreased. Finer particles (Level 3) showed a consistent increase in density as the foaming agent ratio increased, indicating more compact structures. Generally, the thermal conductivity increased with a higher foaming agent ratio, with particle size having minimal impact on the conductivity. The water absorption increased with higher foaming agent content, particularly when the particles were finer (Level 3). This was due to the disruption of the matrix structure, which led to higher open porosity and greater water absorption. The cross-sectional images (Figure 28) of the foam glass samples revealed that smaller particles

(Level 3) resulted in better packing during the preform stage, leading to more uniform, smaller pores, and lower water absorption. As the foaming agent content increased, the pore size enlarged, and at higher ratios (2 wt%), the structure became more open and interconnected, resulting in higher water absorption. This suggests that for applications where foam glass needs to resist water absorption, a balance between particle size and foaming agent content is essential. The combination of the finest particle size (Level 3) and the lowest foaming agent ratio (1 wt%) provided the best overall foam glass properties, with a well-packed structure that minimized water absorption and enhanced density.

4.2. Investigation of maximum height and area on heating microscopy images

This sub-chapter explores the relationship between the changes in the area and height of foam glass samples during the heating microscopy test. The goal is to understand how variations in area and height correlate with temperature changes and to determine the most accurate way to assess the maximum expansion of foam glass during the sintering process.

Heating microscopy was used to monitor and analyze the changes in both the area and height of foam glass samples as they were heated. The experiments were conducted at various temperatures, and the data were used to investigate the point of maximum expansion. The results were analyzed by comparing graphs of height change versus area change across three datasets of foam glass compositions.

The results of these analyses are presented in Figure 29. The behavior of the graphs demonstrates that variations in height and area are not perfectly aligned. Additionally, the temperature at which maximum expansion occurs in the area-based curve does not coincide with the maximum expansion point in the height-based curve. This discrepancy suggests that determining the maximum expansion temperature based entirely on the point of maximum height increase is not accurate. A more precise approach is to define the temperature of maximum expansion based on the peak in the area-based curve. The findings reveal that the maximum area is reached at a temperature of 18 to 60 °C higher than the temperature at which the maximum height is attained.
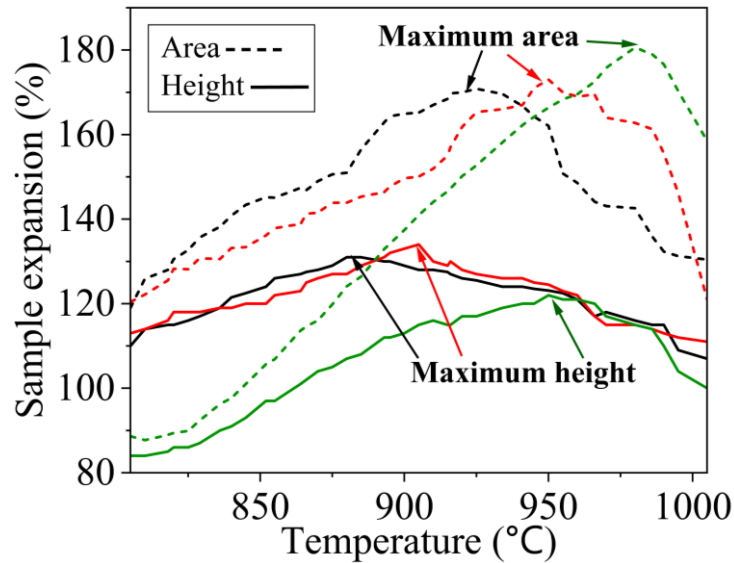
Figure 29. The difference in area and height change graphs for samples made from waste glass powder and, 1 wt% (green lines), 2 wt% (red lines) and 3 wt% (black lines) of SiC

Four samples with a composition of 99 wt% waste glass and 1 wt% SiC were sintered at both the maximum area and maximum height temperatures. The results, presented in Figure 30, show that the volume of the samples sintered at the maximum area temperature is larger than those sintered at the maximum height temperature. This supports the conclusion that surface area changes, derived from heating microscopy data, provide a more accurate approximation of volume changes in the samples than height variations.

Sintering temperature	Foam glass
940 °C (Maximum height)	
962 °C (Maximum Area)	
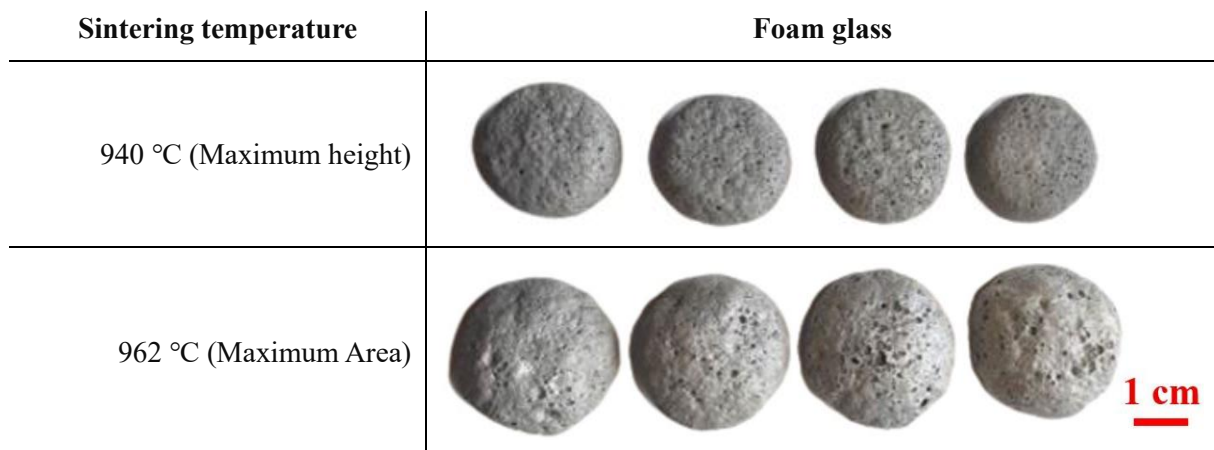
Figure 30. Comparison of foam glass compositions which are sintered in maximum height and maximum area temperatures

Moreover, this phenomenon is clearly illustrated in Figure 31, which highlights the differences in data extracted from the heating microscopy experiment, specifically comparing maximum height and maximum area. These results were crucial in identifying the temperatures used to assess the effect of sintering parameters on the properties of foam glass.
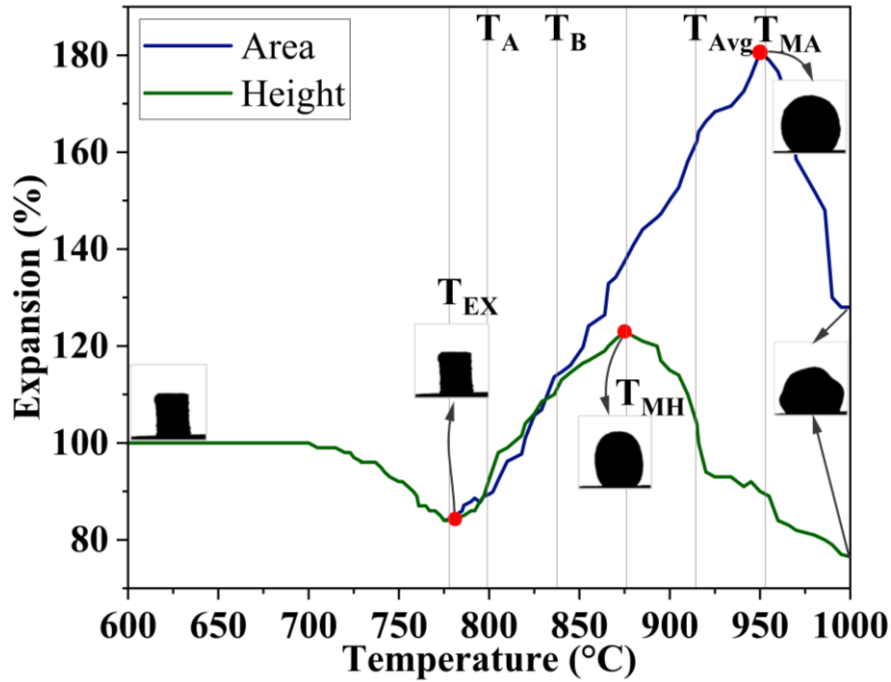
Figure 31. The sintering temperatures of the sample and correspondence heating microscope photos. T_{Ex}, T_{MA}, T_{MH}, T_{Avg}, T_A, and T_B represent the temperatures of the start of the expansion, maximum area, maximum height, average of maximum height and maximum area, The average of maximum height and maximum area temperature (T_{Avg}), $T_A = T_{Avg} - (T_{MA} - T_{MH})$, and $T_B = 2T_{MH} - T_{MA}$.

Summary: The results from the heating microscopy images revealed that the maximum expansion in height did not coincide with the maximum expansion in area. Specifically, the temperature at which the maximum area expansion occurred was 18 to 60°C higher than the temperature for the maximum height increase. The maximum volume derived from area changes was larger when the foam glass samples were sintered at the temperature of maximum area expansion compared to the temperature of maximum height expansion. The findings suggest that, instead of height changes, surface area changes should be the key parameter used to assess the maximum expansion of foam glass during heating to improving the precision of the sintering process and to controlling better over foam glass production.

4.3. Effect of the sintering parameters

The influence of sintering parameters (temperature and holding time) on the microstructure, crystalline phases, and technical properties of foam glass, with an emphasis on achieving optimal density, compressive strength, porosity, and thermal conductivity were investigated in this sub-chapter. Foam glass samples were prepared using soda-lime glass as the base material and silicon carbide as the foaming agent according to Table 2. The sintering temperature (778°C–953°C) and holding time (10–60 minutes) were systematically varied using the L18 Taguchi orthogonal array design of experiments.

4.3.1. Microstructural characterization

Cross-sections of the samples are shown in Figure 32. The size of the cells does not change significantly with increased holding time in the furnace, indicating that holding the sample at the sintering temperature for 10 minutes is sufficient for forming the desired cells, and further increasing the holding time is unnecessary. Furthermore, as observed in the cell size (Figure 32), increasing the sintering temperature results in larger cell sizes. This occurs because higher sintering temperatures enhance the decomposition intensity of the foaming agent and decrease the viscosity of the foam matrix, allowing the formation of larger cells. When the sintering temperature is 876°C (T_{MH}, which means the temperature where the sample reaches the maximum height) and lower, the cell structure is more uniform. However, as the temperature increases, cell size dispersion becomes more pronounced. It is also observable in Figure 32. that the average cell diameter in samples sintered at 876°C and lower temperatures is smaller than in those sintered above this temperature and sintering in higher temperatures result in the formation of a seamless and impermeable glassy crust on the foam glass, reducing the water absorption of these samples. Another observation from the appearance of the samples is that at lower temperatures (below T_{MH}), the cells are more interconnected. This interconnection leads to higher water absorption in these samples.

The microstructure of the samples (that were fabricated regarding Table 2) was characterized by SEM as well. The SEM analysis in Figure 33a reveals that the sample sintered at 837.5°C for 10 minutes exhibits uniform cells with small pores, formed due to the release of CO_2 gas from the partial decomposition of SiC. Due to the high viscosity of the foam matrix at this lower sintering temperature, these pores remain open during the sintering process. A small number of pores are distributed throughout the thickness of the cell walls. At higher magnification, large flower-shaped crystals, measuring approximately 30 to 40 µm in length, are visible on the sample surface, while smaller crystals, about 5 to 10 µm long, are observed within the matrix. The morphology of the crystals indicates that they are prismatic and fibrous, respectively, which could contribute to enhanced mechanical strength in the foam. When the holding time is increased to 50 minutes, as shown in Figure 33b, the cell uniformity remains high, and the quantity of crystals increases. The crystals, ranging from 10 to 20 µm in length, become thinner, while larger and thicker crystals are observed on the sample surface.

Figure 33c presents the SEM image of a sample sintered at 876°C for 10 minutes, where uniformly sized cells are observed, along with small pores inside the cells that contribute to higher water absorption. Crystals within the sample measure about 15 µm in length, with

narrow widths. Increasing the sintering time to 50 min, as seen in Figure 33d, reduces both the number and size of the crystals, with lengths decreasing to around 10 µm. These crystals appear as needle-like structures within the matrix.

Sintering temperature	Holding time		
	10 Minutes	30 Minutes	50 Minutes
778 ℃			
799 ℃			
837.5 ℃			
876 ℃			
914.5 ℃			
953 ℃			
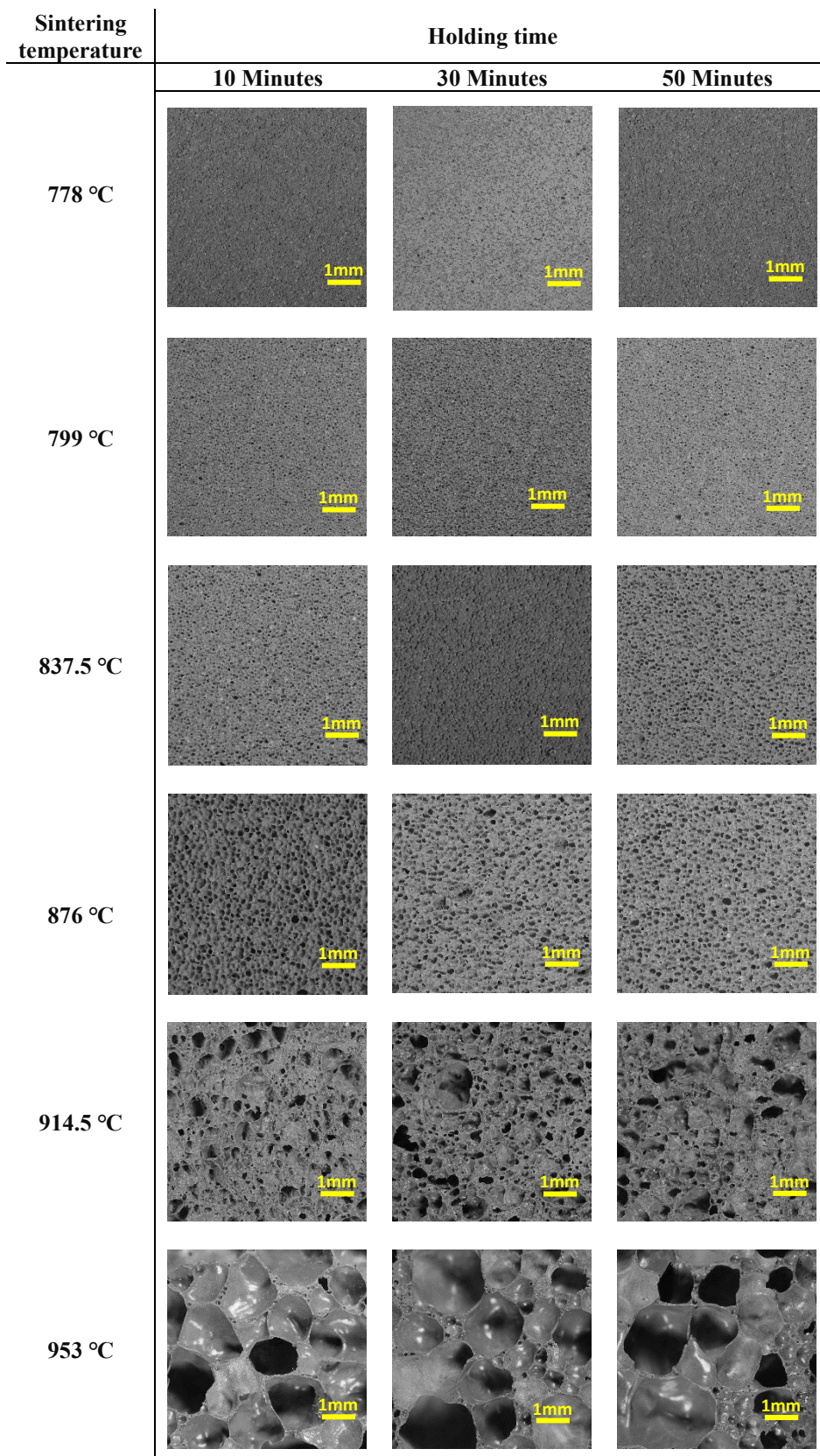
Figure 32. Microstructural changes of foam glass by sintering temperature and sintering time

60

The SEM micrographs of the sample sintered at 914.5°C for 10 min (Figure 33e) show a notable reduction in the amount of crystalline material. Large, flower-shaped crystals, up to 40 μm in size, are present on the surface. Extending the holding time to 30 min results in the continued formation of pores within the cell walls and the appearance of fibrous crystals (Figure 33f). Further increasing the holding time to 50min does not significantly change the overall morphology, but the fibrous crystals remain present, while the needle-like crystals show a clear decrease in both thickness and length, measuring approximately 10 μm (Figure 33g).

Additionally, samples sintered at 914.5°C and 953°C exhibit a glassy surface, indicating partial melting of the crystals and an increase in the amorphous phase of the foam. The melting of crystals at higher sintering temperatures causes the foam matrix to lose its complex structure, leading to larger cell sizes [233, 234]. The SEM micrograph of the sample sintered at 953°C for 30 min (Figure 33h) shows the accumulation of pores along the edges of the cell walls. In these samples, the crystals become smaller and fewer in number, embedded within the matrix. Increasing the holding time to 50 min at this temperature results in a further reduction in crystallinity, rendering the foam almost entirely amorphous (Figure 33i). Despite the reduction in crystallinity, flower-shaped crystals, approximately 40 μm in length, are still observed on the surface of samples sintered at both 914.5°C and 953°C.
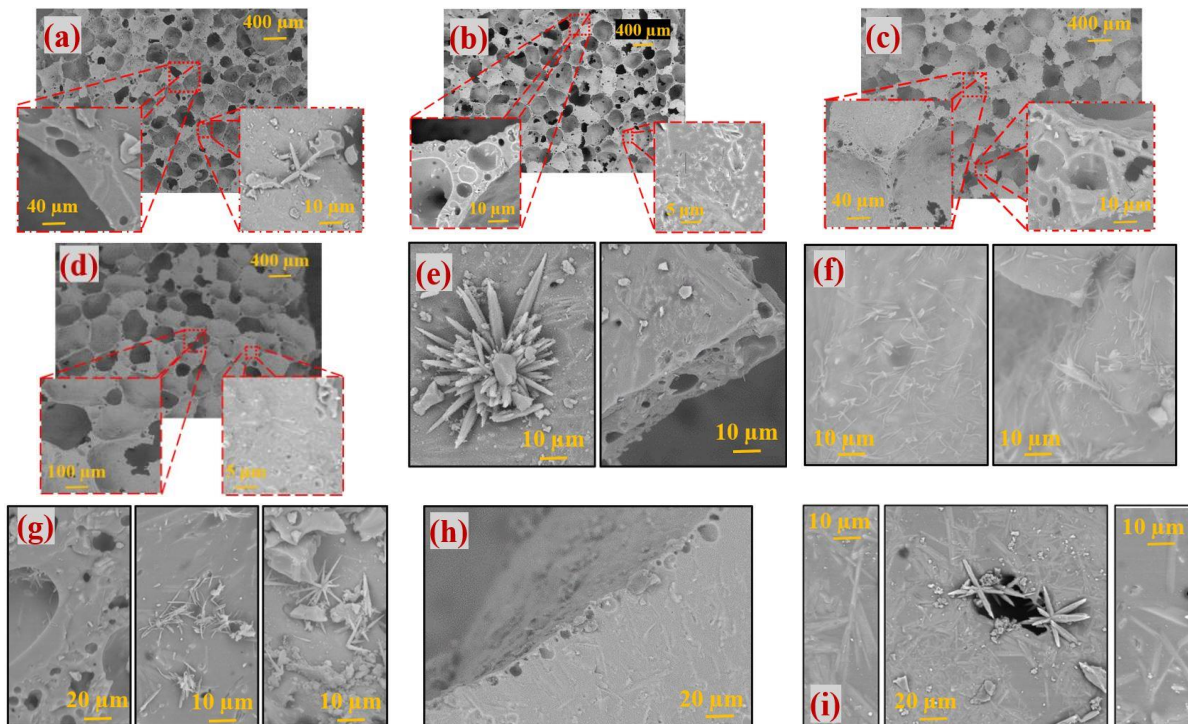
Figure 33. The SEM micrographs of foam glass samples, sintered at a) 837.5°C for 10 min, b) 837.5°C for 50 min, c) 876°C for 10 min, d) 876°C for 50 min, e) 914.5°C for 10 min, f) 914.5°C for 30 min, g) 914.5°C for 50 min, h) 953°C for 30 min

XRD analysis of the samples (the experiments are detailed in Section 2.2.2. revealed further insights into their properties. Figure 34 presents 12 diffractograms of samples sintered at four different temperatures and held in three different holding times. The trends in the patterns indicate that at a sintering temperature of 837.5°C, crystallization increases with longer sintering times, leading to a higher amount of wollastonite and diopside crystals in the foam. This temperature appears to be the crystal formation temperature point for this type of foam glass. When the temperature is increased to 876°C, the trend changes slightly, as some of the crystals begin to melt [234]. From 876°C to 953°C, with increasing sintering time, the peak heights in the XRD patterns decrease, indicating that the crystals start to melt. At 953°C and 50 minutes of sintering, the structure becomes almost amorphous [234].
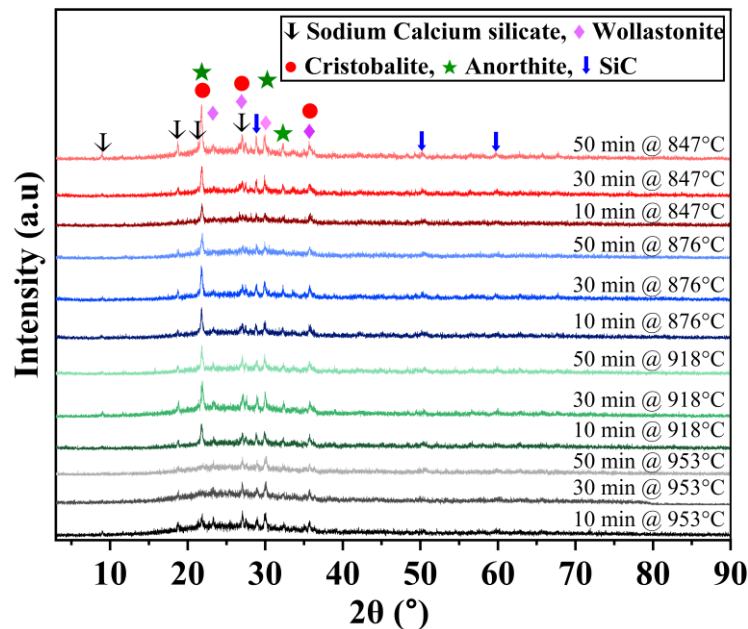
Figure 34. X-ray diffraction patterns of samples sintered at different temperatures and a holding time of 10 minutes

4.3.2. Technical properties of foam glass samples

The Taguchi signal-to-noise (S/N) ratio analysis conducted on the data extracted from various experiments (DOE: Table 2, detailed experiments: section 2.2.2) has provided some insightful findings. To explain the S/N ratio charts, consider that each chart is associated with a term such as "smaller is better" or "larger is better." An increasing trend in the S/N ratio indicates that the characteristic being tested is approaching the optimal level defined by the selected term.

- Density

Figure 35a depicts the signal-to-noise (S/N) ratio for density. As seen in the graph, the "smaller is better" term has been selected, indicating that a lower density is preferred for the foam glass. The S/N ratio increases from 778 °C to 876 °C, corresponding to a decrease in density. This is

expected, as larger pores form at these temperatures. However, moving to 914.5 °C results in some crystal melting, which leads to a loss of matrix integrity and the coalescence of cells. This cell coalescence increases water absorption and density since open porosity is not accounted for in the density measurement. At 953 °C, some cells collapse and close the open porosity, thus reducing the foam's density again. Although holding time has a lesser impact on density compared to sintering temperature, it is evident that increasing the holding time also reduces the sample density. This trend suggests that prolonged exposure at the sintering temperature allows more extensive pore formation and stabilization within the foam glass structure. The trend of density changing (3D plot) which is shown in Figure 35b confirms the Taguchi analysis for signal-to-noise ratio.
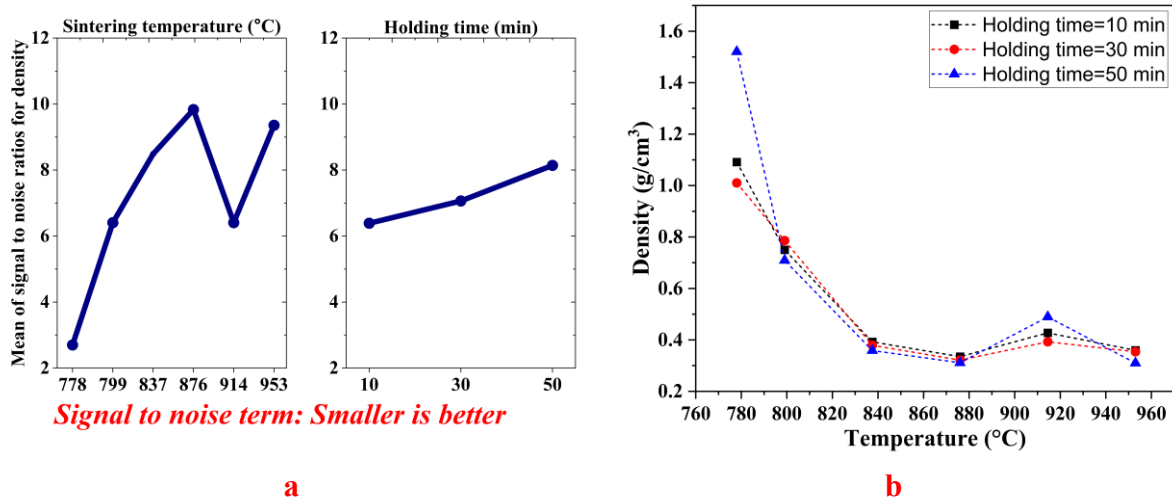
Figure 35. a) The S/N graphs, and b) The 3D plot of density vs sintering temperature and holding time

- Compressive strength

Figure 36a illustrates the signal-to-noise (S/N) ratio for compressive strength, utilizing the "larger is better" term. The graph shows a decrease in the S/N ratio from 799°C to 953°C, indicating a corresponding decrease in compressive strength. This observation is attributed to the enlargement of pores as the sintering temperature increases. It is important to note that at 778°C and 799°C, the foam structure is not fully developed. Therefore, the increase in temperature within this range promotes the formation of a more robust and interconnected matrix, leading to improved compressive strength. Figure 36b. The maximum compressive strength takes place in the sample which is sintered at the T_{EX} (778 °C) for 30 min confirms the signal-to-noise ratios as well.

63
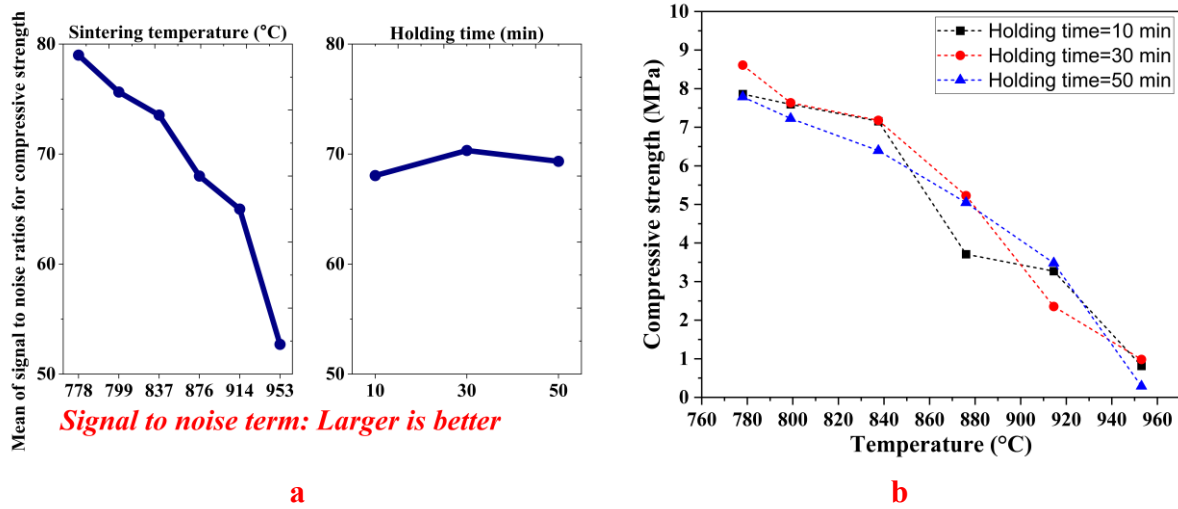
Figure 36. a) The S/N graphs, and b) The 3D plot of compressive strength vs sintering temperature and holding time

- Porosity and water absorption

For the analysis of open porosity and water absorption, the "smaller is better" criterion was applied, as shown in Figure 37. This is because, when foam glass is used as aggregate, lower water absorption is desirable—higher absorption can reduce strength under freeze–thaw conditions. Additionally, high water absorption reflects greater open porosity, which is unfavorable for thermal insulation. Closed porosity is preferred to enhance both moisture resistance and thermal performance.

The graphs show that increasing the foaming temperature from 876 °C to 914 °C raises open porosity. Similarly, longer holding times also increase it due to extended gas expansion. However, at 953 °C, as seen in the density results, some pores close, reducing both open porosity and water absorption.

This trend agrees with findings by Maria Laura Ligabue et al. [235], who observed a rise in open porosity with temperature up to a point, followed by a slight decrease. They also found minimal changes in water absorption with increased holding time. These results support the trends observed in this study.
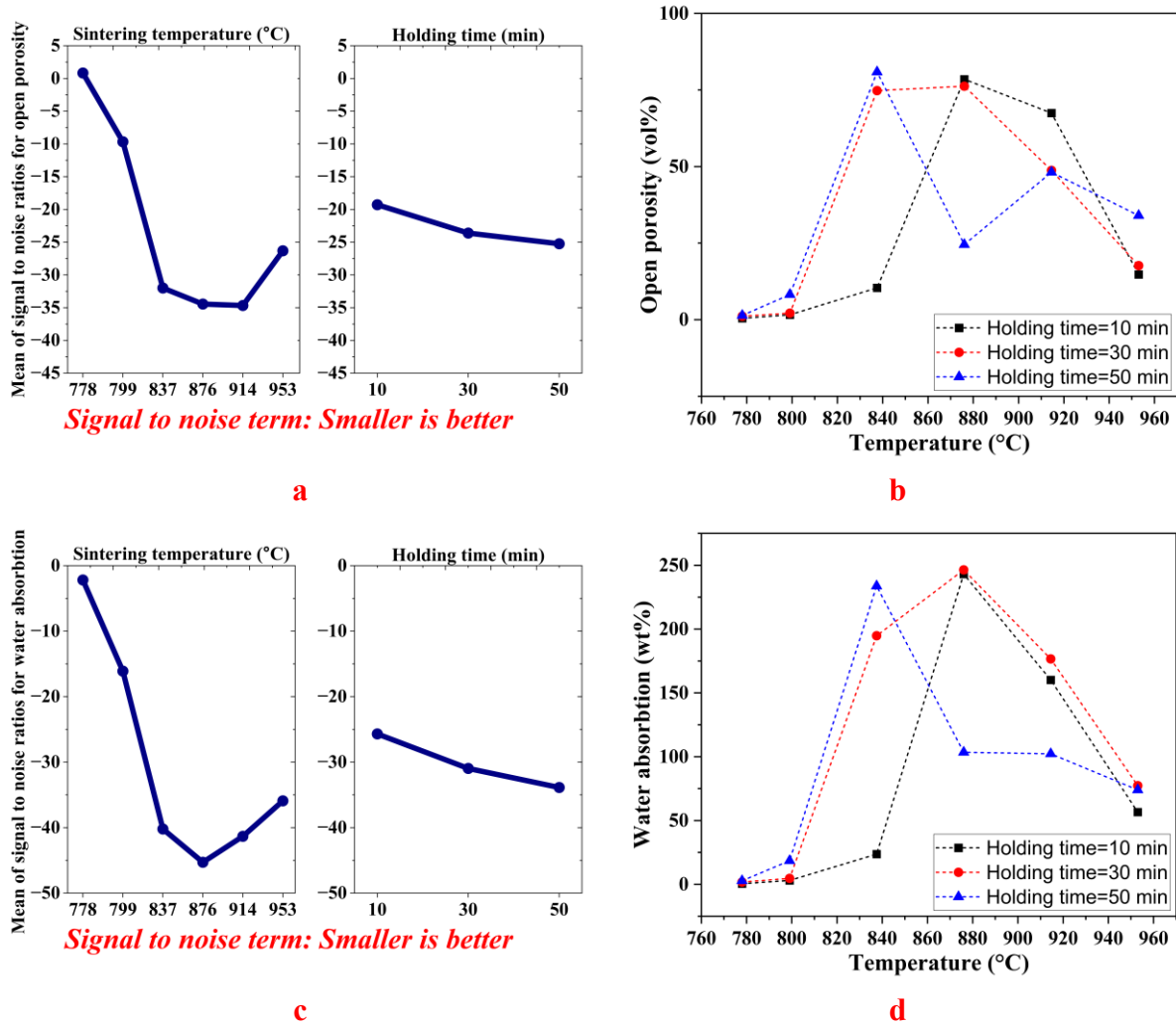
Figure 37. a) The S/N graphs, and b) The open porosity vs sintering temperature and holding time 3D plot, c) The S/N graphs, and d) The 3D plot of water absorption vs sintering temperature and holding time

- Volume expansion

The term "larger is better" was chosen for expansion, which is derived from the buoyancy test used to determine sample volume. The rationale behind this is the desirability of producing foam glass with a specific volume from a minimal amount of raw material. The overall trend is similar to the density analysis (Figure 35). Since the preforms before sintering had approximately the same volume and mass, the volume expansion percentage is linearly related to the decrease in sample density, so the trend of volume expansion S/N diagrams is somehow similar to S/N of density. The results of analyzing this graph are crucial, as it shows that the maximum signal-to-noise ratio for sintering temperature occurs at 953°C (T_{MA}). However, this is just a statistical analysis and modeling based on the experimental results, the graph of which is shown in Figure 38b. The sample sintered at T_{MA} for 50 minutes exhibited the highest volume expansion compared to all other samples. This observation strongly corroborates the findings from the heating microscopy analysis (chapter 4.2).
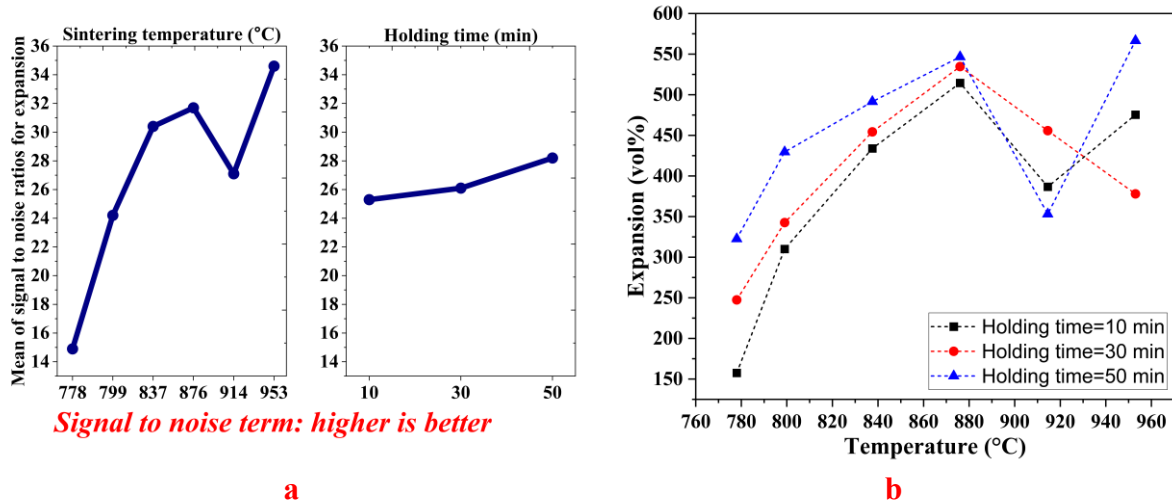
Figure 38. a) The S/N graphs, and b) The 3D plot of volume expansion vs sintering temperature and holding time

The thermal conductivity (Figure 39) decreases with an increase in sintering temperature up to 876°C, due to the increase in pore size. At 914.5°C, thermal conductivity slightly increases due to the collapse of some pores, resulting in the walls coming into closer contact and enhancing the connection between the walls and the thermal conductivity sensor. The "smaller is better" term was used for analyzing this graph, indicating that as the holding time in the furnace increases, thermal conductivity shows a slight decrease, suggesting an increase in pore size.
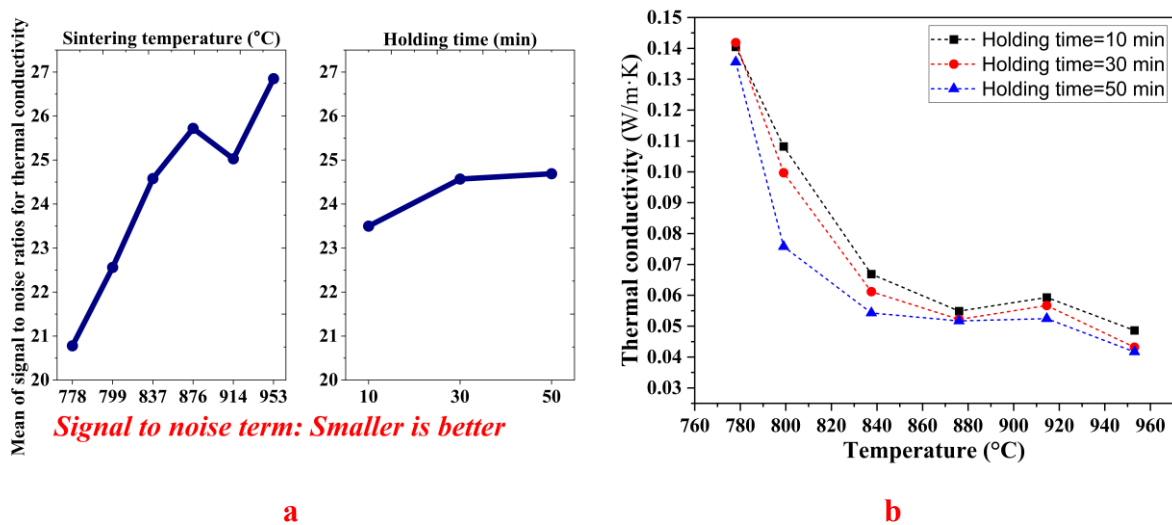
Figure 39. a) The S/N graphs, and b) The 3D plot thermal conductivity vs sintering temperature and holding time

Summary: *As the sintering temperature increases, up to around 876°C, the cell size enlarges, and water absorption decreases due to the formation of a glassy crust. Although holding time (ranging from 10 to 50 minutes) has a lesser impact, it affects the uniformity of the cell structure and the formation of crystalline phases. Scanning electron microscope (SEM) analysis reveals that at higher temperatures, the cells become larger and more dispersed, while at lower temperatures, the cells are smaller and more interconnected, which influences both water absorption and density. In terms of technical properties, lower sintering temperatures (876°C) produce foam glass with a lower density, while higher temperatures lead to cell coalescence and an increase in density. Compressive strength is higher at lower sintering temperatures (778°C to 799°C), as higher temperatures cause the cells to enlarge, reducing the structural integrity. Higher sintering temperatures also result in increased open porosity and water*

absorption, but at very high temperatures (953°C), pore collapse reduces these properties. This part of the study highlights the significant influence of sintering parameters on the structural and thermal properties of foam glass, underlining the importance of optimizing these parameters for desired performance characteristics.

4.4. Effect of molding type on foam glass samples

The focus is on studying the effects of different molding methods, holding time in the furnace, and sintering temperature on the properties of foam glass. The Taguchi design of experiments (DOE) method, using an L8 orthogonal array, was applied to analyze and predict these effects. The Taguchi approach allowed predictions for untested samples, confirming the accuracy of the results. 2 different fabrication methods (wet and dry powder) were used to fabricate samples. Foam glass powder used in two molding types: dry-powder and wet-powder methods. Samples were subjected to different sintering temperatures (778 °C, 876 °C, 914.5 °C, and 953 °C) and holding times (10 minutes and 30 minutes).

4.4.1. Taguchi prediction and experimental results

As detailed earlier (see section 2.2.3 and Table 3), L8 orthogonal array was used to investigate the effects of the molding method (at two levels), holding time in the furnace (at two levels), and sintering temperature (at four levels). To provide a clearer perspective of the tested and predicted samples, Table 14 including all 16 possible groups for conducting experiments was created. As previously mentioned, 8 out of these 16 groups were tested according to the L8 orthogonal array.

Table 14. The design of experiments of groups that were fabricated and then tested (T) and the groups that just predicted (P)

Grupe number	Sintering temperature	Fabrication type	Holding time	Status
1	778	Dry-powder	10	P and T
2	778	Dry-powder	30	P
3	778	Wet-powder	10	P
4	778	Wet-powder	30	P and T
5	876	Dry-powder	10	P and T
6	876	Dry-powder	30	P
7	876	Wet-powder	10	P
8	876	Wet-powder	30	P and T
9	914	Dry-powder	10	P
10	914	Dry-powder	30	P and T
11	914	Wet-powder	10	P and T
12	914	Wet-powder	30	P
13	953	Dry-powder	10	P
14	953	Dry-powder	30	P and T
15	953	Wet-powder	10	P and T
16	953	Wet-powder	30	P

4.4.2. Microstructure characterization

SEM imaging of the samples made using the wet powder method shows that the crystals are clearer and more luminous. Additionally, the number of crystal particles in SEM micrographs is significantly higher in the foams produced by the wet powder method compared to those made by the dry powder method (e.g. Figure 40a and b). In the sample prepared at 914°C for 10 minutes using the wet powder method (Figure 40c), fiber-shaped crystals are clearly visible. These crystals were also observed in the dry powder method samples, as previously described. In the sample prepared at 953 °C for 10 min using the wet powder method, SEM imaging (Figure 40d) revealed a network-like structure in which this morphology closely resembles calcium aluminum silicate [236], likely formed during the foaming process due to the presence of water. This phase is highly resistant to acid and base attacks and enhances the mechanical strength of the foam's skeleton [237].
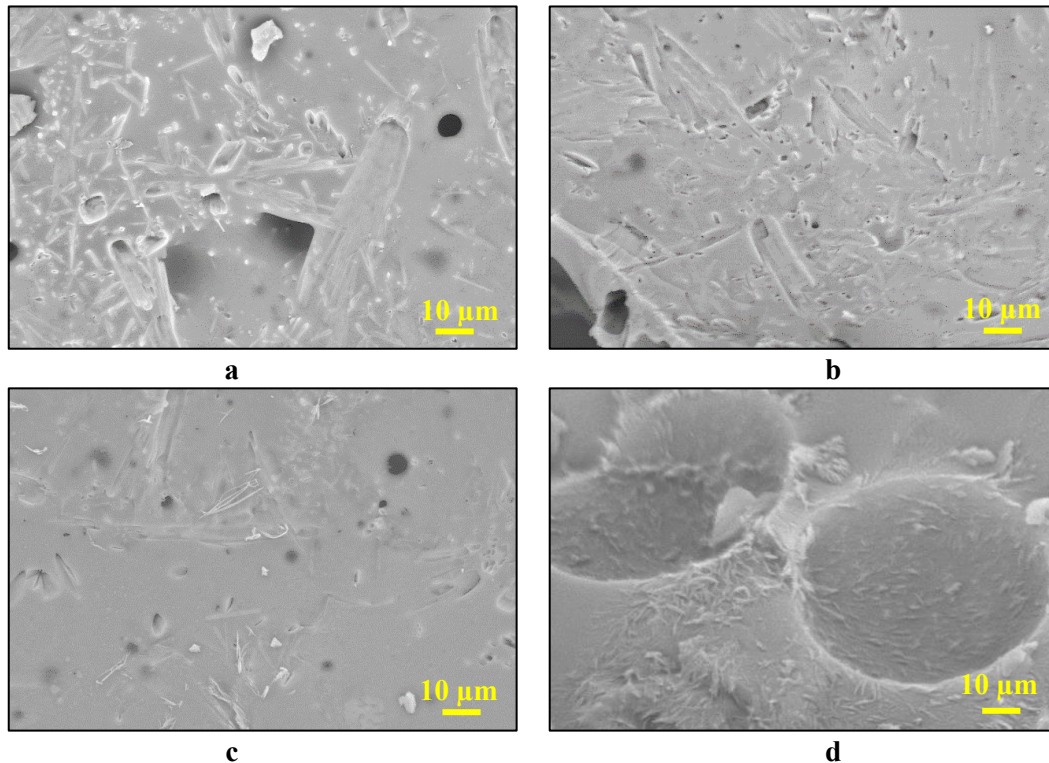
Figure 40. a) The SEM picture shows bright crystals of the sample made using the wet powder method and sintered in 876 for 10 min, b) The SEM picture shows not bright crystals of the sample made using the dry powder method and sintered in 876 for 10 minutes. c) fibers in the sample made using the wet powder method and sintered in 914 for 10 min. d) the network-like crystals in the sample were made using the wet powder method and sintered in 953 for 10 min

Comparing the XRD diffractograms of samples made by the dry powder and wet powder methods at the same sintering temperature and holding time, as shown in Figure 41, reveals new insights into the crystalline structure of the foams. The intensity and sharpness of the XRD peaks are generally higher in samples produced by the wet powder method compared to those

made by the dry powder method. Higher intensity and sharper peaks in the XRD diffractogram typically indicate more crystallinity or larger crystal size.

Upon closer examination of the diffractograms in Figure 41, the higher crystallinity is evident in the samples made using the wet powder method (higher peaks).

It appears that with increasing furnace temperature, the difference in crystallinity between samples produced via the wet powder and dry powder methods diminishes. As evidenced by the intensity of the peaks in Figure 41, the samples produced using the wet powder method exhibit higher crystallinity compared to those fabricated using the dry powder method. This observation can be attributed to several factors. First, the addition of water facilitates the partial dissolution of certain free oxides, such as calcium oxide, leading to enhanced chemical reactivity and subsequent crystal formation at elevated temperatures. Moreover, water can improve the homogeneity of the mixture before sintering, promoting more uniform phase development and increasing the likelihood of crystallization. Additionally, residual moisture trapped within the samples may influence the sintering dynamics, potentially altering the oxidation behavior of silicon carbide and affecting the formation of mineral phases. Furthermore, the presence of water may contribute to a slower cooling rate after thermal treatment, as trapped moisture delays heat transfer. This extended cooling period provides more time for nucleation and crystal growth, further enhancing the crystallinity of the foam glass. Another key observation is that the wollastonite content in the foam glass structure decreases with increasing temperature. Therefore, at higher sintering temperatures, the reduction in compressive strength can be attributed to both the decline in wollastonite crystallites and the increase in porosity.
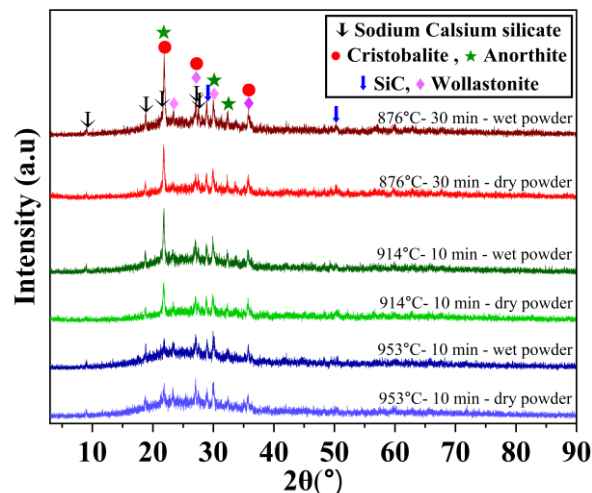
Figure 41. XRD diffractograms comparing foam glass samples made with dry powder and wet powder techniques at identical sintering temperatures and holding times

4.4.3. Technical properties

- Density

In Figure 42a, the signal-to-noise (S/N) ratio for density indicates that, as the temperature increases to 876 °C, density decreases (higher S/N represents a "smaller is better" effect).

With an increase in sintering temperature (from 876 °C to 914 °C), a rise in density is observed, primarily due to the collapse of certain cells caused by the melting of crystals within the matrix. The collapse of these cells leads to the closure of some open pores, thereby reducing the overall open porosity. Moreover, at this temperature, density exhibits a direct correlation with thermal conductivity. As illustrated in Figure 46, thermal conductivity also increases with the rise in sintering temperature.

Subsequently, cell growth up to 953 °C reduces density again. The prediction and experimental data (Figure 42b) align closely, confirming the accuracy of the model.
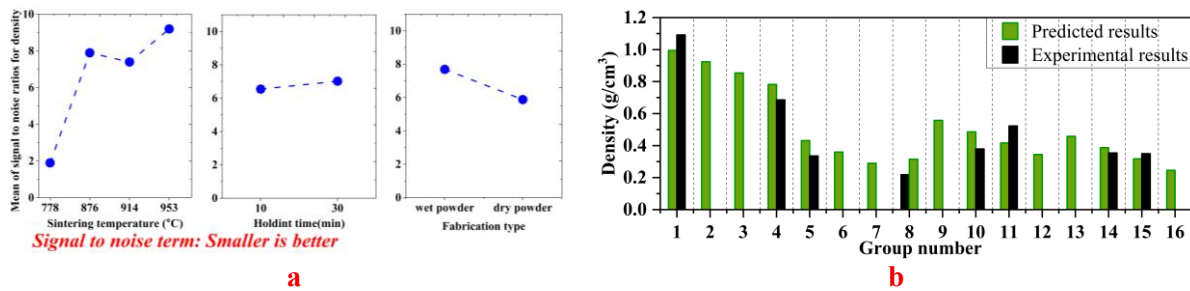
Figure 42. The results of the molding method's effect. a) S/N for density, and b) The Taguchi predicted and examined values for density

- Compressive strength

Similarly, Figure 43a displays the S/N ratio for compressive strength, where mechanical strength logically decreases with temperature as foaming progresses. Notably, samples incorporating wet powder exhibit higher mechanical strength. Here, results from experiments on foamed samples (Group 5 onwards) correlate strongly with predictions, as shown in Figure 43b. With an increase in sintering temperature to 914°C, the slope of the curve undergoes a noticeable change. At this temperature, although the collapse of some cells has occurred, resulting in slightly thicker cell walls due to the remnants of the previously collapsed structures adhering to the newly formed walls, the compressive strength of these walls has slightly decreased due to the melting of crystals. Consequently, despite the increase in foam glass density, the overall compressive strength has declined.
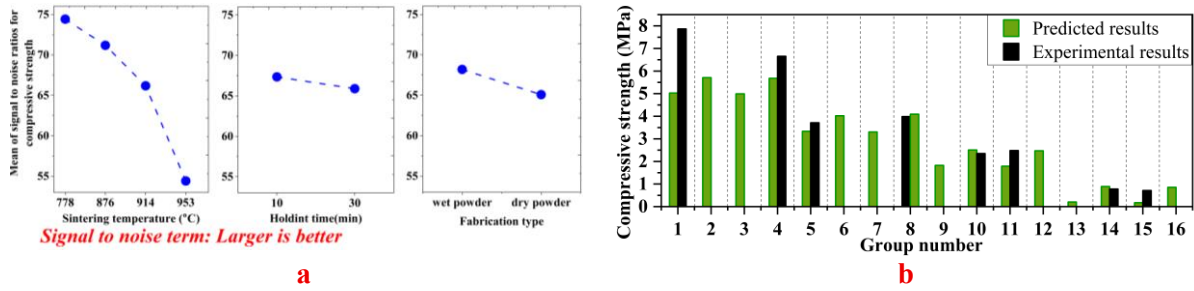
Figure 43. The results of the molding method's effect. a) S/N for compressive strength, and b) The Taguchi predicted and examined values for compressive strength

- Open porosity and water absorption

The S/N and predicted values for open porosity and water absorption, shown in Figure 44, reveal an increase in open porosity up to 876 °C, followed by a decrease due to the formation of a denser, seamless surface. Experimental results in Figure 44b strongly validate the S/N analysis, and open porosity is directly related to water absorption. Figure 44c illustrates similar behavior for water absorption, although water absorption S/N (Figure 44d) slightly diverges from open porosity due to sample shrinkage at 914 °C. Nonetheless, experimental data and Taguchi predictions consistently support the S/N analysis. A comparison between Figure 44a and Figure 46a reveals that as the sintering temperature increases from 776°C to 876°C, thermal conductivity decreases while open porosity increases. Given that a structure with predominantly closed porosity is preferable for reducing thermal conductivity, this observation suggests that at 878°C, the fraction of closed porosity has significantly increased. Consequently, the enhancement of closed porosity has led to a reduction in thermal conductivity. This phenomenon is clearly observable when comparing the first and fourth rows of images in Figure 32.

However, with a further increase in sintering temperature to 876°C, the amount of open porosity decreases due to the collapse of some cells onto each other, an effect that has also been discussed in relation to density. This reduction in open porosity is accompanied by a decrease in closed porosity, leading to an overall reduction in total porosity. As a result, thermal conductivity increases.
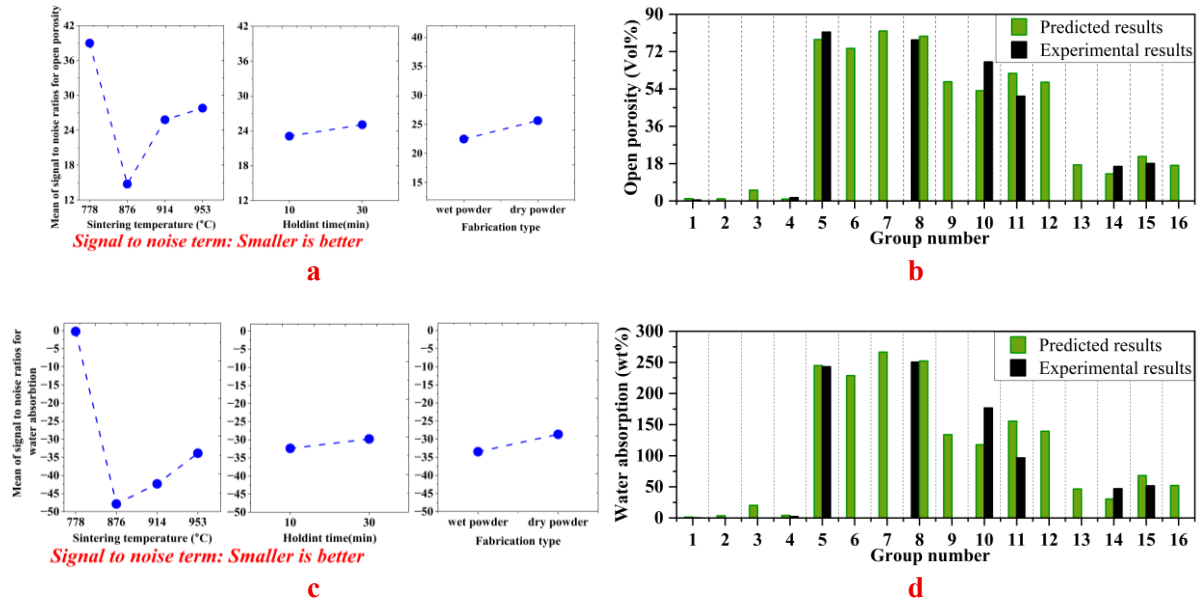
Figure 44. The results of the molding method's effect. a) S/N for open porosity, and b) The Taguchi predicted and examined values for open porosity. c) S/N for water absorption, and d) The Taguchi predicted and examined values for water absorption

- Volume expansion

Figure 45 shows maximum expansion at 953 °C, affirming previous findings that the expansion at maximum area exceeds maximum height. Prediction and test results here confirm the S/N outcomes. Finally, the highest volume expansion is observed in the sample sintered at 953 °C. The signal-to-noise ratio (S/N) trend for expansion closely follows that of the S/N ratio for density (Figure 42). This is because, as the sample volume increases while maintaining a constant mass, its density decreases. Similarly, the S/N trend for expansion exhibits a strong resemblance to that of thermal conductivity. The underlying reason is that expansion in foam occurs due to porosity formation; greater porosity leads to increased expansion, and higher porosity results in lower thermal conductivity.
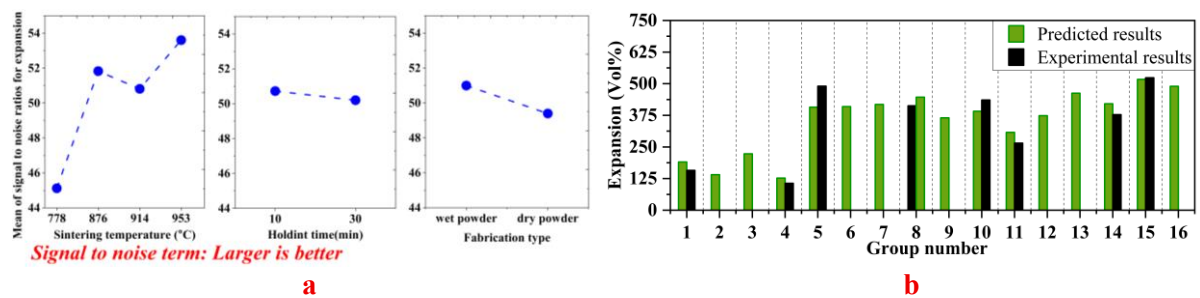
Figure 45. The results of the molding method's effect. a) S/N for expansion, and b) The Taguchi predicted and examined values for expansion

- Thermal conductivity

For thermal conductivity (Figure 46), the trend is inversely related to open porosity. As open porosity increases, thermal conductivity decreases. The S/N ratio chart shows an increase in

thermal conductivity from 876 °C to 914.5 °C due to cell collapse and melting of internal crystals, but a subsequent decrease at 953 °C due to larger cell sizes. A comprehensive explanation of the relationship between thermal conductivity, expansion, and density has been provided in the previous subsections.
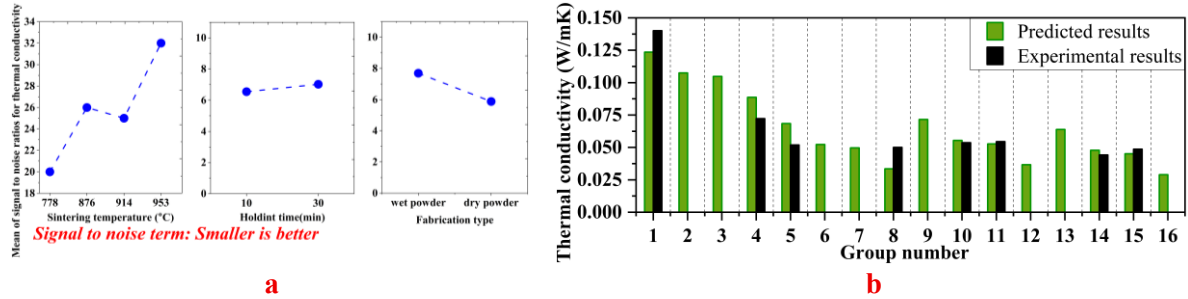
Figure 46. The results of the molding method's effect. a) S/N of thermal conductivity, and b) The Taguchi predicted and examined values for thermal conductivity

- Determination of the parameters' effectiveness

This is clearly indicated in the S/N ratio charts where the holding time shows negligible influence across all experiments. The manufacturing method also shows minimal impact on foam properties. However, generally, the wet powder method seems to slightly improve the properties.

In all S/N ratio charts, a parameter named "delta" represents the difference between the maximum and minimum S/N ratio. By dividing the delta of each parameter by the total deltas for each test, the influence of each parameter on the foam properties can be determined. As shown in Table **15**, the sintering temperature has the highest impact, ranging from 69% to 92% on the properties of foam and an average of 86%. The manufacturing method's impact ranges from 3% to 18% and an average of 8.56%, and the holding time's impact ranges from 4% to 13% and an average of 5.51%.

As it is clear the predictions have good coincidence with the real test results. It confirms using Taguchi design of experiments. Based on the accurate results of Taguchi's predictions, it can be claimed that a full-factorial design of experiments is not required to perform costly and time-consuming experiments in the field of detecting mechanical and thermal properties of foam glass material, and by following Taguchi design of experiments the number of required tests can be reduced. Also, by following this method, the ranking of effective parameters and the percentage of effectiveness of different parameters on the desired output can be extracted.

Table 15. The effectiveness of each variable and the delta values for experiments

Output variable	Term	Input variables		
		Sintering temperature	Holding time	Molding type
Thermal conductivity	Delta	6.720	1.280	1.76
	Effectiveness ratio (%)	68.85	13.11	18.038
Density	Delta	8.512	0.475	1.813
	Effectiveness ratio (%)	78.81	4.39	16.78
Water absorption	Delta	47.637	2.613	4.819
	Effectiveness ratio (%)	86.50	4.74	8.75
Open pores	Delta	39.194	1.974	1.317
	Effectiveness ratio (%)	92.253	4.646	3.101
Expansion	Delta	8.50	0.76	1.31
	Effectiveness ratio (%)	80.416	7.190	12.393
Compressive strength	Delta	21.00	3.20	5.40
	Effectiveness ratio (%)	70.95	10.81	18.24
Total	Delta	110.563	7.102	11.02
	Effectiveness ratio (%)	85.91	5.51	8.56

Summary: *In this part of the study, only 8 out of 16 possible experiments were conducted, with the remaining results predicted using the Taguchi model. The strong alignment between experimental and predicted values validated the accuracy of the model, confirming that a full-factorial design of experiments (DOE) was unnecessary, effectively reducing both cost and time.*

Microstructural analysis revealed distinct differences between wet and dry powder samples. Wet-powder specimens exhibited more numerous and well-defined crystals, as confirmed by SEM micrographs. X-Ray Diffraction (XRD) analysis further confirmed higher crystallinity in wet-powder samples, indicated by sharper and more intense peaks. These findings underscore the critical role of sintering conditions and molding techniques in tailoring foam glass properties, with implications for optimizing production efficiency and material performance in structural and thermal applications. The findings of this research indicate that using a hydraulic press is not necessary for preparing foam glass precursors. Instead, adding 20 wt% water to the powder allows for the formation of cylindrical samples with significantly lower pressure. Moreover, the properties of the samples produced using this method show no significant difference compared to those made with hydraulic pressing.

The results demonstrated that density decreased up to 876°C due to expansion, followed by an increase as cell collapse and melting occurred, with another decline at 953°C. Strength decreased with increased foaming at higher temperatures, while wet-powder samples consistently exhibited higher mechanical strength. Open porosity increased until 876°C, then declined as a denser structure formed, a trend also observed in water absorption, though slight deviations occurred due to shrinkage at 914°C. Maximum volume expansion was recorded at 953 °C, with lateral expansion exceeding height growth. Thermal conductivity was inversely related to porosity, increasing between 876°C and 914.5°C due to cell collapse, then decreasing at 953 °C as cell size expanded. Sintering temperature had the most significant influence on foam glass properties (69%–92%, avg. 86%), followed by the molding method (3%–18%, avg. 8.56%) and holding time (4%–13%, avg. 5.51%).

4.5. Effect of using virgin glass and alternate additives (alumina, cement factory soot)

The next experiment conducted in this research explored the possibility of using cement factory soot as a foaming agent, with the detailed methodology outlined in the previous chapter (section 2.2.4 and Table 4).

4.5.1. Microstructural characterization

- Visual inspection

Figure 47 shows the samples containing 8 wt% of alumina (groups 7, 8, and 9). The expansion of these groups is lower than that of groups 4, 5, and 6 containing 4 wt% of alumina. These groups have lower expansion in comparison with the first 3 groups which do not contain alumina. It is because the presence of alumina in the composition results in softened glass becoming more viscous [238, 239] and prevent bubbles from forming facilitative. On the other hand, increasing the foaming agent content leads to more intensive decomposition and gas production in the specimens.

Figure 47. Nine groups of foam glass specimens – the compositions are according to Table 4. Sintered at 842 ℃, heating rate of 5 ℃/min, and holding time of 10 min

For the morphology of foam glass cells, it is necessary to revisit the DTA results of soot, as shown in Figure 26. This graph indicates the intensive decomposition of soot at 890°C. It causes the destructive effect of increasing the soot content on the integrity of cells. By increasing the intensity of foaming agent decomposition, the probability of cells collapsing increases. This is attributed to the formation of a eutectic point in the mixture. In any case, the decomposition of SiC and its CO_2 production occur with less intensity compared to soot at 890°C. So, the effect of changing the SiC content on the final properties of foam glass is less than the effect of changing in soot weight percentage.

Figure 48 shows the porosity of all 9 groups which sintered in 890 ℃. It can be seen that when the SiC is 2 wt% (groups number 3, 6, and 9), the porosity is more uniform. In these groups, numerous crystals were formed within the foam matrix, and these crystals acted like fibers embedded in a composite, reinforcing the foam and preventing the collapse of cell walls and their coalescence. As a result, in samples containing 2 wt% SiC, the uniformity of the cells was higher. The higher cell wall connection with the thermal conductivity sensor causes higher thermal conductivity. By increasing from 2 to 3 wt% of SiC the amount and size of pores increase and the thermal conductivity decreases. Increasing the soot content from 2wt% to

75

3wt% causes increasing the thermal conductivity (in the groups that sintered at 890 ℃), because in that temperature, the intensity of decomposition of soot destroys the pores, and subsequently the thermal conductivity increases.
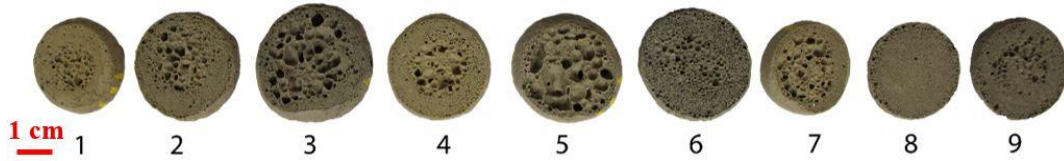
Figure 48. The pore structure of nine groups of specimens

- Microstructure

In samples having 3 wt% soot, 3 wt% SiC, and 0 wt% alumina from group A (sintered at 842°C), it was observed that a network-like structure was created (Figure 49a). This network could resist mechanical loads and increase the destruction energy. It is expected that this network-like structure tolerates dynamic loads better than static loads. The reason for this expectation is that when dynamic loads like impact or cyclic loads come in, lots of energy should be absorbed to break this network down and after the failure of this network, the matrix will be started to fail. It damps energy and if the foam glass needs to be used as CMFGC aggregates in the geographical locations where earthquakes are very common (e.g. Croatia), it could be more useful. The result of compressive strength is a force-displacement plot, and the area under this plot represents the energy absorption so it is expected that the area for this sample be higher than that for the samples without this network-like structure.In samples having 3 wt% soot, 3 wt% SiC, and 0 wt% alumina from group A (sintered at 842°C), it was observed that a network-like structure was created (Figure 49a). This network could resist mechanical loads and increase the destruction energy. It is expected that this network-like structure tolerates dynamic loads better than static loads. The reason for this expectation is that when dynamic loads like impact or cyclic loads come in, lots of energy should be absorbed to break this network down and after the failure of this network, the matrix will be started to fail. It damps energy and if the foam glass needs to be used as CMFGC aggregates in the geographical locations where earthquakes are very common (e.g. Croatia), it could be more useful. The result of compressive strength is a force-displacement plot, and the area under this plot represents the energy absorption so it is expected that the area for this sample be higher than that for the samples without this network-like structure.

Figure 49. a) The network structure in the sample having 3 wt% soot, 3 wt% SiC, and 0 wt% alumina, sintered at 842°C.
b) Whisker structure in sample having 1 wt% soot, 3 wt% SiC, and 4 wt% alumina, sintered at 842 °C

In a sample having 1 wt% soot, 3 wt% SiC, and 4 wt% alumina, sintered at 842 °C the whisker structure (Figure 49b) was the major morphology observed. The whiskers were dispersed inside the matrix, and they could enhance the mechanical properties of the material but not as much as the network structure. This structure works as reinforcements like chopped fibers in polymer matrix composites (PMC). The EDS analysis showed that the main elements of these whiskers were Ca and O, so they could be united into $CaCO_3$ in the form of calcite [240]. The presence of alumina in the material resulted in increasing the mechanical properties but in some parts, it caused the stress concentration and guided the crack growth.

Figure 50 shows the pore structure of the sample having 2 wt% soot, 3 wt% SiC, and 8 wt% alumina, sintered at 842 °C (group A). The closed pores formed the major porosity of this specimen. The pores are spherical, and they are not connected together, and the maze-shaped porosity was not formed. It will be seen in the signal-to-noise ratio graph as well. When the soot content is lower the water absorption is lower. The reason is that in this treatment the close porosity (vol%) is at maximum. Also, it is obvious from Figure 47 that the uniformity of the porosity is higher than others.
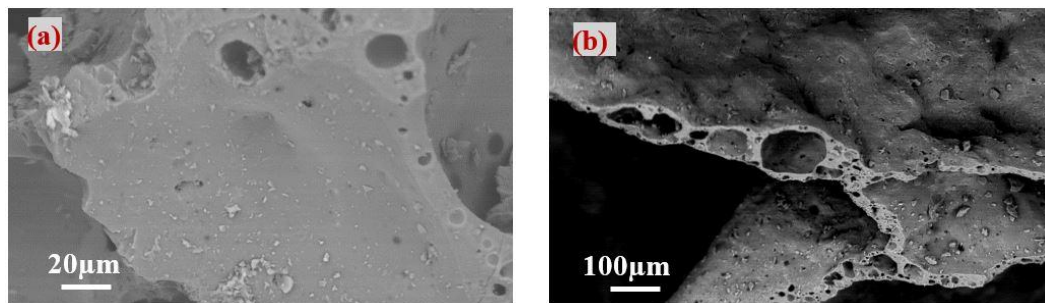
Figure 50. SEM micrograph of sample having 2 wt% soot, 3 wt% SiC, and 8 wt% alumina, sintered at 842 °C - the closed pores form the majority of porosity

By increasing the sintering temperature (group B, 890 °C) some crystal grains were observed. In sample having 1 wt% soot, 1 wt% SiC, and 0 wt% alumina from the group B (890 °C), we observed a network-like structure made of SiO_2 and also $CaCO_3$ crystal grains (calcite). These structures , were observed in other research [241, 242]. Increasing the soot amount to 2 wt% in

the presence of sufficient sintering temperature caused the formation of aragonite inside the foam matrix (Figure 51). The presence of these needle-like aragonite structures has been presented in literatures as well [243]. Aragonite structure made some specific characteristics in the foam glass, since there are a lot of voids between the aragonite crystals, the produced gas from the foaming agent decomposition can flee into other cells and form connected pores leading to open porosity and maze-shaped pores. In Figure 47, the sample having 3 wt% soot, 2 wt% SiC, and 4wt% alumina contains larger pores in the microstructure.

The other characteristic that aragonite can induce to the cell walls is decreasing the thermal conductivity. Since in the structure of walls there are lots of unintegrated grains, heat convection is the principal heat transfer way through the cell walls. As the heat transfer from the convection in solids is lower in comparison to conduction [244], in the cell walls of this sample, heat transfer capacity is lower than others. The other characteristic that the aragonite structure caused to this sample was its toughness, since during mechanical loading by failing aragonite needles, others resist the load and the whole component does not tend to fail at once. Thus, the toughness of this specimen is higher than other specimens.

However, to use CMFGC reinforcement there is a need to use the aggregate with higher yield stiffness. So, if there is a need to use foam glass material as a drainer in the fundamentals of sport stadiums or roads' soft shoulders, the composition of specimen having 3 wt% soot, 2 wt% SiC, and 4 wt% alumina, sintered at 890 °C (group B) could be one optimal candidate.
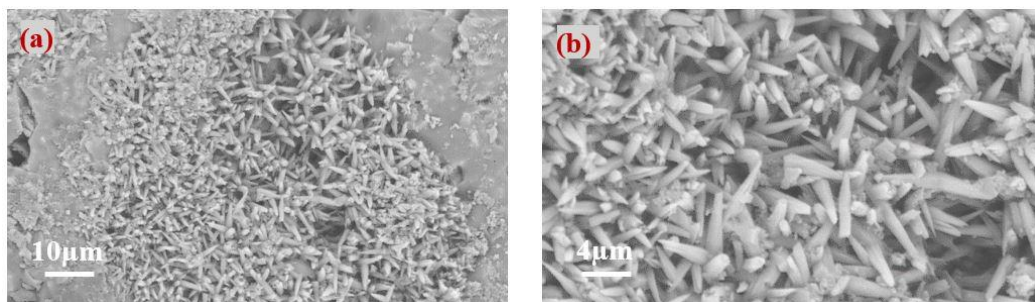
Figure 51. SEM micrographs of sample having 3 wt% soot, 2 wt% SiC, and 4 wt% alumina, sintered at 890 °C - The aragonite structure under a) magnification of 10μm and b) magnification of 4μm.

Figure 52 shows the SEM micrographs of specimens having 2 wt% soot, 3 wt% SiC, and 8 wt% alumina, sintered at 890°C. It is seen in Figure 52b that lots of individual micropores exist in this sample. According to Taguchi analysis, it can be concluded that the integration of cell walls takes place because of the presence of a high amount of alumina. Alumina additive causes increasing the viscosity of softened glass, since the higher is the viscosity, the higher is

the Tg^2 [245], the time needs for vitreous to become relaxed increases. So, fewer crystals are produced in these conditions and no needle-like aragonite was found in this sample.
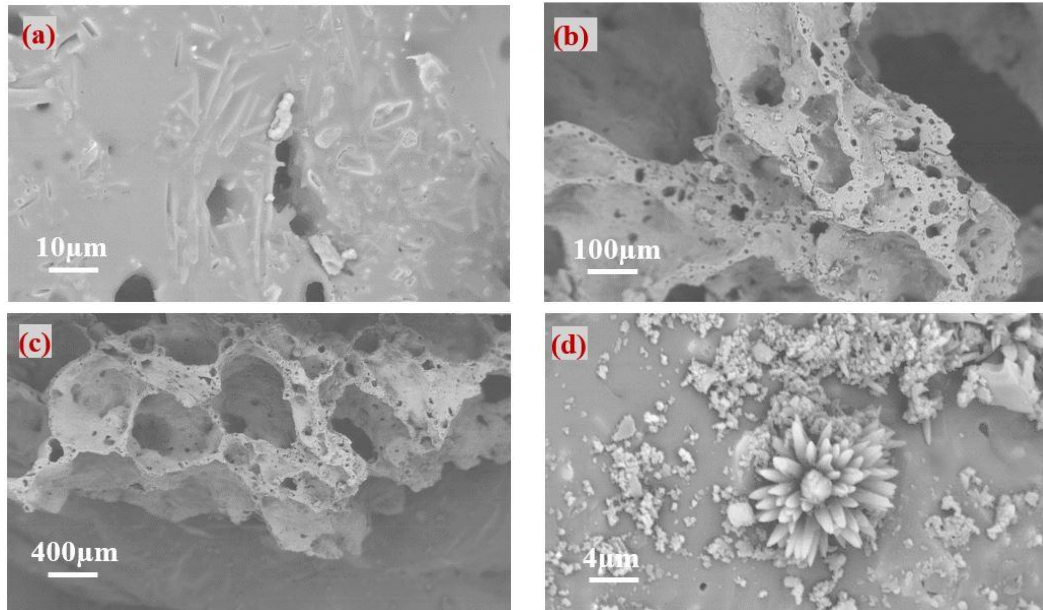
Figure 52. micrographs of having 2 wt% soot, 3 wt% SiC, and 8 wt% alumina, sintered at 890 °C a) The whiskers structure in the matrix b) and c) the connected pores and collapsing of the porosity d) the flower-like structure of aragonite

SEM micrographs also revealed some flower-like structures in this sample (Figure 52d). According to the EDS analysis, the major element of this structure is Ca. However, throughout the literature, pure calcium has no flower-like structure. This structure is probably a flower-like aragonite [246, 247] and it is not crystallite of pure calcium.

4.5.2. Technical properties

Similar to the previous sections, which were based on Taguchi design of experiments, in this part as well, after extracting the test results, the signal-to-noise ratios plot was drawn for the characteristics obtained for each group of samples. Considering 3 factors and 3 levels, there are 2 available orthogonal arrays that could be chosen to use, L9 and L27. The difference between L9 and L27 is in considering 3 repetitions. In L27 the design of experiments is like the one in L9 but with 3 repetitions. So, in order to analyze the results, we went through the L9 (the average of repetitions was used), and L27 simultaneously. The Taguchi analysis shows a good coincidence between the L9 and L27 design of experiments. It means that the statistical method behind the Taguchi analysis method can eliminate the noise of data precisely. Figure 53 to Figure 56 show the results of Taguchi analysis according to L9 and L27 for group A (sintered at 842 °C) and group B (sintered at 892 °C). L9 could be used instead of L27 in this method. On the other hand, there is a difference between lines representing groups A and B

---

[2] Tg is the threshold temperature where the supercooled glass liquid starts to freeze, and by getting close to that temperature the relaxing time of frozen glass decreases, from 100,000 years in room temperature to 15 seconds in Tg temperature.

which differ in sintering temperature. As it is concluded in sections 4.3 and 4.4, the sintering temperature significantly affects the final properties of foam glass.

-Density

The density is the first important factor. Figure 53 shows the signal-to-noise ratios for the density of foam glass. By increasing the alumina content, the signal-to-noise ratio decreases, and since the required term is lower is better, it means the density increases. But with increasing the foaming agent content the density decreases because more foaming agent causes more expansion. And since the mass of preforms were equal in all the samples so more expansion causes lower density.
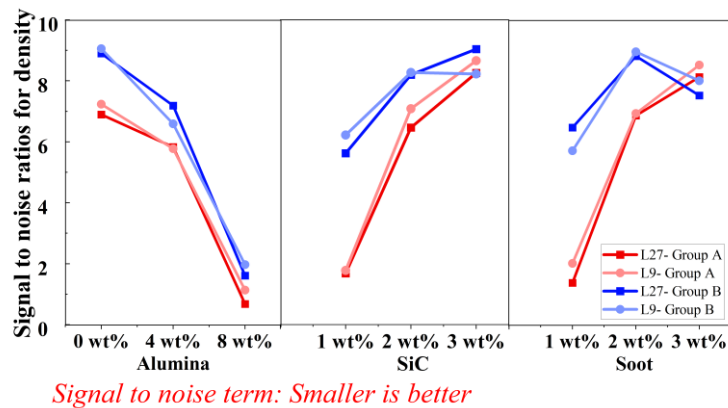
Figure 53. Signal-to-noise ratios for density (group A (L9), group B (L9), group A (L27), and group B (L27))

- Water absorption

Figure 54 shows the water absorption of foam glass. Increasing the alumina content causes less water absorption ("smaller is better "is the term of analyzing) because by increasing the alumina content the viscosity of softened glass increases and increasing the viscosity prevents the cells from forming and expanding.

This phenomenon leads the cells not to connect and less connection of porosity to the surface of the specimen occurs. From another point of view, the increase in viscosity causes an increase in the material's surface energy with the gas phase (either on the surface of the sample or inside the sample, in cells) [248]. This phenomenon in glass-melting tanks also causes corrosion in melting tank refractory [63, 249]. In foam glass samples, due to the lower energy of the furnace air in comparison to the energy of produced CO_2 inside the cells, the surface energy difference with the outside air is greater than the cells inside gas. This energy difference will prevent the formed bubbles from escaping to outer space. Fewer pore connection to the surface leads to less water absorption. On the contrary, increasing the foaming agent content causes increasing in water absorption (which is not desirable for the application of foam glass as CMFGC aggregates).

Likewise, the argumentation that was given for density the intensive of decomposition of soot at the sintering temperature is more than SiC and different contents of soot have a higher effect on water absorption than SiC content. This can be inferred from the difference between the maximum and minimum signal-to-noise ratios corresponding to soot and SiC.
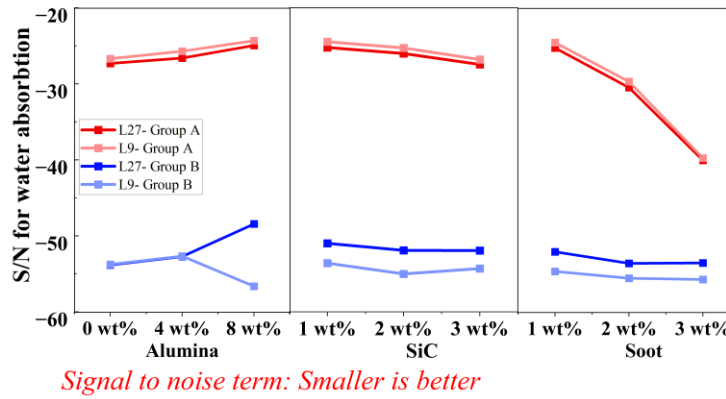
Figure 54. Signal-to-noise ratios for water absorption (group A (L9), group B (L9), group A (L27), and group B (L27))

- **Thermal conductivity**

Figure 54 shows the thermal conductivity signal-to-noise ratios for foam glass. The thermal conductivity is mostly related to the pore structure, as the cells' diameter increases the thermal conductivity decreases. When there is more closed porosity or larger cells, the thermal conductivity is lower. Also, the thermal conductivity of the foam has a direct relationship with the thermal conductivity of its walls. As a result, the thermal conductivity of foam glass in which more intensive decomposition occurred during foaming will be lower compared to the case when the foaming process occurred at a less intensive level. Increasing alumina causes increasing in the thermal conductivity because it prevents the softened glass from becoming foamed completely (due to increasing the viscosity and subsequently decreasing the porosity (vol%)). So, in an equal area, the fraction of the gaseous phase (inside the cells) to the solid phase (wall of cells) will decrease. As a consequence, by increasing the alumina content the thermal conductivity increases. In group B, increasing the SiC to 2 wt% also causes an increase in thermal conductivity.
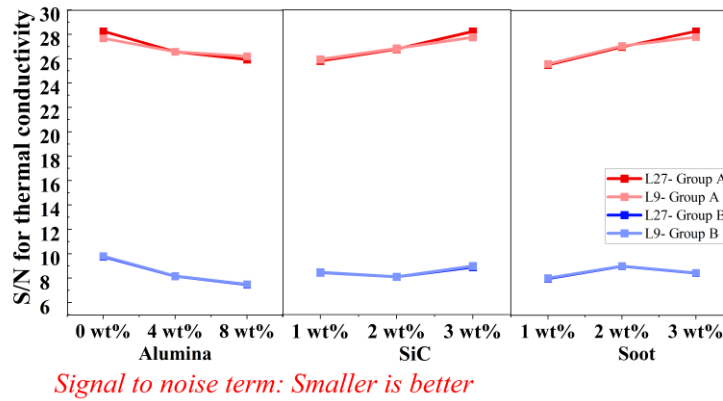
Figure 55. Signal-to-noise ratios for thermal conductivity (group A (L9), group B (L9), group A (L27), and group B (L27))

- **Compressive strength**

The Taguchi analysis signal-to-noise ratios of compressive strength are shown in Figure 56. The compressive strength is affected significantly by the pore structure and the solid phase structure. By increasing the alumina content. the compressive strength increases. However, by increasing the foaming agent content (both SiC and soot) it decreases.
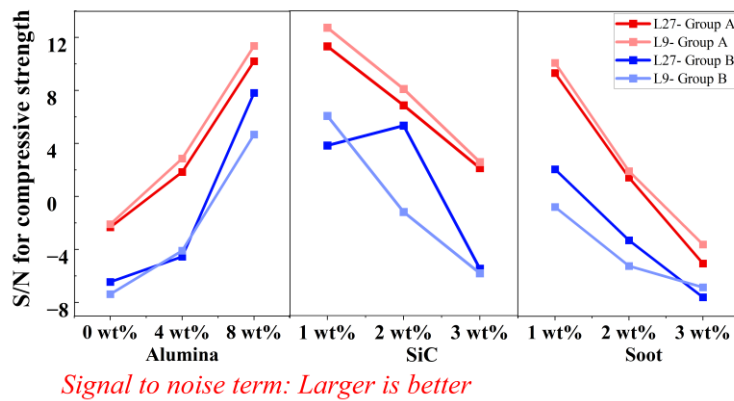
Figure 56. Signal-to-noise ratios for compressive strength (group A (L9), group B (L9), group A (L27), and group B (L27))

Statistical T-test (2-tailed) was performed on all signal-to-noise ratios (for density, thermal conductivity, water absorption, and compressive strength) in each temperature to study if there is a significant difference between the L9 and L27 design of experiments or not. The results are shown in Table 16.

Table 16. P-values of the T-test carried out on L27 and L9 orthogonal array results

Sintering temperature (°C)	p-value			
	Thermal conductivity	Compressive strength	Water absorption	Density
842	0.362	0.559	0.858	0.579
890	0.399	0.179	0.728	0.396

Considering the level of significance equal to 0.05, if calculated p-values (which is between 0 and 1) exceed the 0.05 it can be stated that there is not enough evidence that the means of 2 tested groups are different. According to this argument, it is clear that the difference of signal-

to-noise ratios between L27 and L9 groups is not significant and there is good coincidence matching of L9 and L27 results.

Summary: The investigation on the effects of virgin glass, alumina, and cement factory soot as additives in foam glass contributed to understanding the material's properties. The sintering temperature was identified as a factor influencing the properties of foam glass, with a noticeable difference between the two groups sintered at 842°C and 892°C.

Density, water absorption, thermal conductivity, and compressive strength were all significantly influenced by the additives and their amounts. As alumina content increased, the density of foam glass increased due to reduced expansion, and water absorption decreased because of higher viscosity that inhibited the formation of connected cells. However, higher amounts of foaming agent led to lower density and increased water absorption, which is undesirable for cement matrix composite aggregate applications. Thermal conductivity showed a direct relationship with porosity, where larger and more closed cells resulted in lower conductivity. Alumina's role in increasing thermal conductivity was confirmed as it hindered the complete foaming of the material.

Compressive strength was positively influenced by alumina, while it decreased with higher foaming agent content. Visual and scanning electron microscopy examinations revealed the microstructural effects of additives, where the inclusion of alumina resulted in reduced expansion, while increasing the foaming agent led to more intensive gas production and cell collapse. The formation of unique structures, such as network-like and whisker structures, was observed in certain compositions, enhancing mechanical properties. The findings of this research indicate that cement plant soot can be used as a foaming agent for foam glass production. Additionally, virgin glass powder can serve as a suitable matrix for manufacturing foam glass.

4.6. Selecting the optimal foam glass (multi criteria decision making results)

As mentioned in Section 2.2.5, to determine the optimal foam glass for use in CMFGC, a multi-criteria decision-making (MCDM) approach was employed following a series of tests conducted on foam glass samples produced using various compositions and fabrication methods. The outcome of this analysis provides a ranking of the samples based on the assigned weights specified in Table 5.

The ranking results of the samples are presented in Table of Appendix C. In this analysis, two types of margin errors were considered. Specifically, when the score difference between the two samples exceeded 2%, they were ranked separately. However, when the score difference was less than 2%, both samples shared the same rank. Consequently, two samples

were placed in rank 27. According to this analysis, the sample ranked 1 is shown in row 43 of Table of Appendix C. At this stage, it is important to note that although the sample containing soot achieved the highest rank, the variability of soot, being a waste material with composition dependent on the specific cement factory producing it, may limit the reproducibility of the results in future research. Therefore, this sample was not selected as the optimal choice for producing foam glass granules.

Samples ranked 2, 3, 4, 5, and 6 were also not considered optimal due to insufficient foaming observed during their production. As a result, samples ranked 7, 8, 9, and 10, which are highlighted in red in the Table, were chosen as the optimal candidates for foam glass granule production.

4.7. Results of novel fabrication method for making foam glass granules

In Section 2.2.6 and Table 6, the methodology for producing foam glass granules was outlined. Initially, eight selected compositions were sintered at temperatures between the glass transition temperature (Tg) and the onset of expansion. The resulting hardened preforms were then removed from the furnace, crushed, and re-sintered at a temperature 20°C below the maximum expansion temperature to generate foam glass granules. This subsection presents the outcomes of this fabrication process, detailing the resulting granule characteristics and evaluating the effectiveness of this approach.

The temperature-expansion curve obtained from heating microscopy for the sample with the composition of 2 wt% alumina, 2 wt% SiC, and 96 wt% virgin glass is shown in Figure 57.
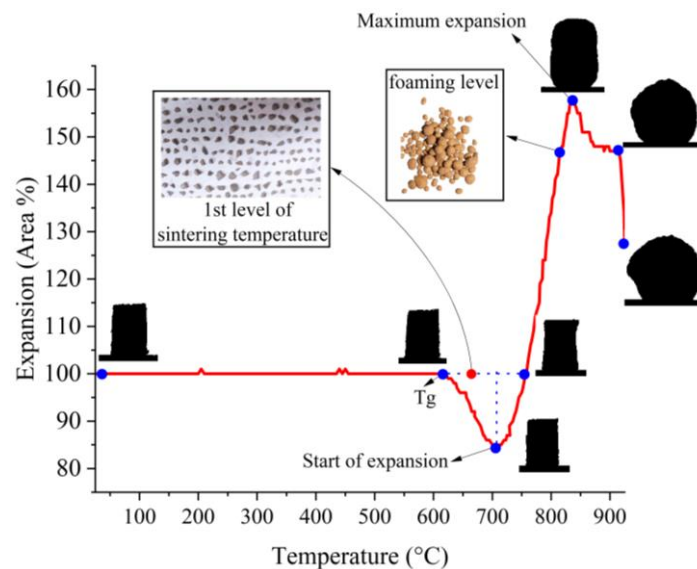
Figure 57. The temperature-expansion curve extracted from heating microscopy for the sample of 2 wt% alumina, 2 wt% SiC, and 96 wt% virgin glass

The diagram illustrates the following key temperatures: glass transition temperature (Tg), start of expansion, temperature at which initial expansion percentage is reached, 1st level of

sintering temperature for preform hardening (for crushing), the temperature of foaming level, and maximum expansion temperature.

The temperature-expansion curves for all the examined samples exhibit a similar trend, with the key difference being the variation in their characteristic temperatures. Up to this point in the study, a crucial conclusion was drawn: by using this method, it is possible to produce foam glass granules of different sizes with surfaces that have low porosity (as shown in Figure 58).

This finding is significant because it confirms the method's capability to create foam glass granules with controlled physical properties, making them suitable for various applications, particularly in construction materials like lightweight CMFGC and concrete.

Figure 58. Granulated foam glass

After the production of foam glass granules, visual observations showed that the surface of the samples was seamless and that the aggregates had a nearly spherical shape. Figure 58 shows the final form of the granules. This foam glass granule manufacturing process creates samples with greater mechanical strength. Also, granules with different diameters can be made using this method. Different granule diameters allow for different concrete and CMFGC mix designs and also for the production of geopolymers with various mix plans that are reinforced with foam glass granules. The results of the tests, presented in Table 17, indicate that the samples made with waste glass (samples number 5 to 8 in Table 6) have a higher density compared to those made from virgin glass (samples number 1 to 4 in Table 6). This suggests that the viscosity of the samples made from waste glass during the sintering temperature is higher than samples made from virgin glass. As a result, the expansion in granules made from waste glass is lower than that of granules made from virgin glass. This reduced expansion leads to an increase in the compressive strength of the waste glass granules.

85

Table 17. The physical and mechanical properties of granular foam glass

Sample code	Glass (Wt%)	SiC (Wt%)	Alumina (Wt%)	Water absorption (Wt%)	Open porosity (Vol%)	Apparent density (g/cm³)	Compressive strength (MPa)
1	96 (virgin)	2	2	0.893	0.227	0.255	1.22
2	94 (virgin)	3	3	8.101	2.033	0.251	0.76
3	95 (virgin)	2	3	79.32	20.781	0.262	0.72
4	95 (virgin)	3	2	26.252	6.379	0.243	0.65
5	96 (waste)	2	2	16.223	10.220	0.63	2.85
6	94 (waste)	3	3	19.596	11.581	0.591	1.47
7	95 (waste)	2	3	22.658	17.106	0.755	1.72
8	95 (waste)	3	2	26.587	13.639	0.513	1

Based on the ASTM C330/C330M standard, which specifies that the acceptable water absorption range for lightweight aggregates is between 5 to 20 percent by weight, only samples 1, 2, and 5 meet the criteria for use in CMFGC. According to this standard, in addition to the water absorption limit, the compressive strength must be greater than 1 MPa. From the test results, it was observed that samples 2, 3, and 4 (see Table 6) don't meet this requirement.

Therefore, among all the granules produced, only samples number 1 and number 5 meet all the standard conditions for use in lightweight aggregate CMFGC. As a result, in the continuation of the research, these granules were used for CMFGC (highlighted in Table 17).

Lower water absorption in aggregates can present both advantages and disadvantages. The positive aspect is that it improves aggregate performance in severe weather conditions by reducing the potential for damage caused by freeze-thaw cycles. This makes the aggregate more stable and durable. However, lower water absorption can also suggest reduced open porosity, which could negatively impact the mechanical bonding between the aggregate and the cement mortar, typically resulting in a reduction in the compressive strength of the lightweight CMFGC produced.

4.7.1. Microstructural characterization of foam glass granules
- Cell structure

To examine the cellular arrangement, the samples' surfaces underwent paper sanding. Figure 59 illustrates the cell structure of samples. The homogeneity of the pores serves as an indicator of effective mixing between glass and foaming agent, as well as uniform heating during the manufacturing process. Uneven heat distribution could lead to localized variations in the foaming agent's decomposition rate, resulting in uneven pore size distribution.

Type of glass	Composition			
	2 wt% SiC + 2 wt% Al_2O_3	3 wt% SiC + 3 wt% Al_2O_3	2 wt% SiC + 3 wt% Al_2O_3	3 wt% SiC+ 2 wt% Al_2O_3
Virgin glass				
Waste glass	1cm			

Figure 59. The structure of the cells of the samples

Based on the observation of the cell structures as shown in Figure 59, it is evident that the samples made from waste glass generally have more asymmetrical shapes compared to those made from virgin glass. This confirms the higher viscosity of the waste glass samples during the foaming process. With the increase of alumina, the cell sizes are observed to become smaller, while increasing silicon carbide results in larger cell sizes. Overall, as seen in all samples, the cells remain uniform in structure.

- **Microstructure**

During SEM analysis of the samples, the cell surfaces appeared mostly smooth and seamless, giving them a glass-like texture that impedes intercellular connectivity, leading to high levels of closed porosity. However, in samples 2 and 4 (see Table 6), multiple connecting channels between cells were observed. The formation of these channels is attributed to the high SiC content in these samples. Since SiC doesn't fully decompose at the sintering temperature, it gradually breaks down during the process, infiltrating the glassy structure and forming connection channels (Figure 60 and Figure 62).
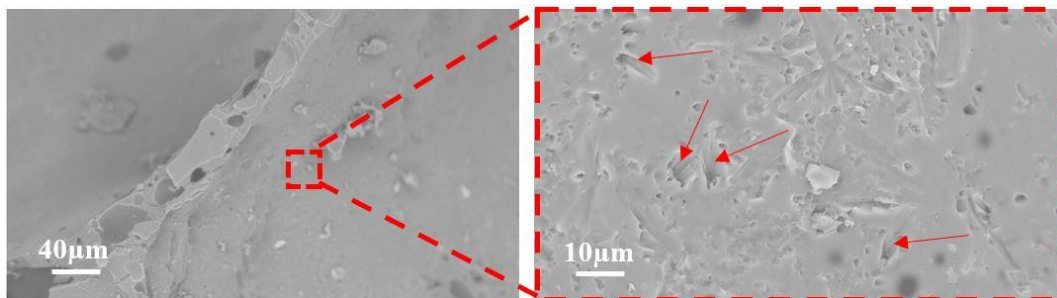
Figure 60. The internal walls of foam glass cells in sample number 2, and the micro-porosity (red arrows) formed because of foaming agent drilling

These holes are formed due to the decomposition of SiC, and the phenomenon behind this occurrence is similar to a process known as upward drilling. Upward drilling is one of the phenomena that leads to the degradation and corrosion of refractory tanks used for molten glass. The mechanism of this occurrence is shown in Figure 61. When the liquid glass contacts the refractory surface and gas bubbles are present, a swirling flow between the bubbles and the refractory surface creates holes in the refractory due to differences in surface tension [250].
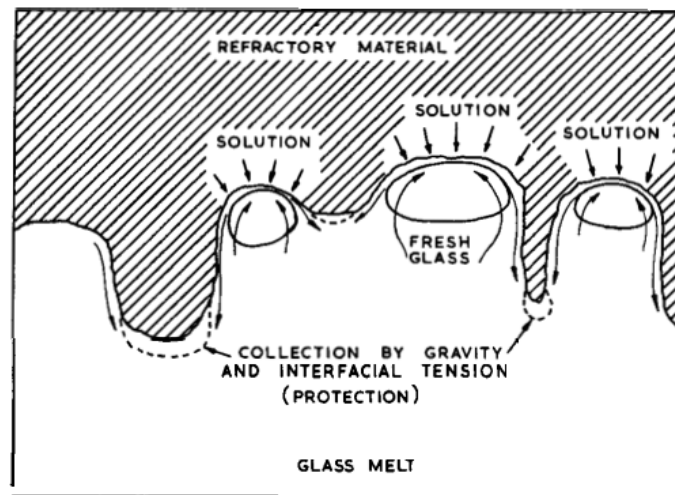
Figure 61. Mechanism of upward drilling caused by gas bubbles showing possible movement of the fresh glass and reaction products as a result of interfacial tension [251]

In sample number 4 (Figure 62), the quantity of these channels is higher, indicating a reduction in the structural resistance of the foam glass. This reduction can be attributed to the lower amount of alumina in these samples.
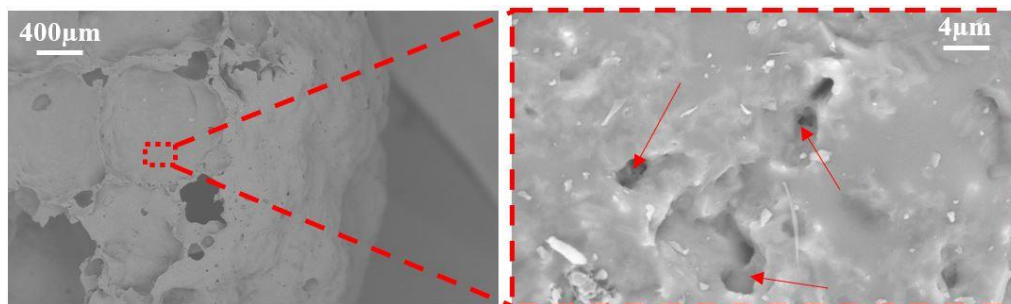
Figure 62. The internal walls of foam glass cells in sample number 4, and the micro-porosity formed (red arrows) because of foaming agent drilling and pore leading of micro whiskers (black arrows)

An interesting observation in these samples was that no crystalline particles were detected during the SEM imaging. This could be attributed to either the melting of the crystals or their small size. To investigate the crystalline structure more precisely, XRD tests were conducted on the samples.

The diffraction pattern in Figure 63 clearly shows that the crystalline content in granules made from waste glass is higher than those made from virgin glass. The analysis indicates the presence of quartz, wollastonite, diopside, and some SiC crystals. Samples made from virgin

glass, on the other hand, only show traces of diopside. The presence of these crystals has contributed to the increased compressive strength of the matrix in foams made from waste glass, which was also confirmed by previous test results.
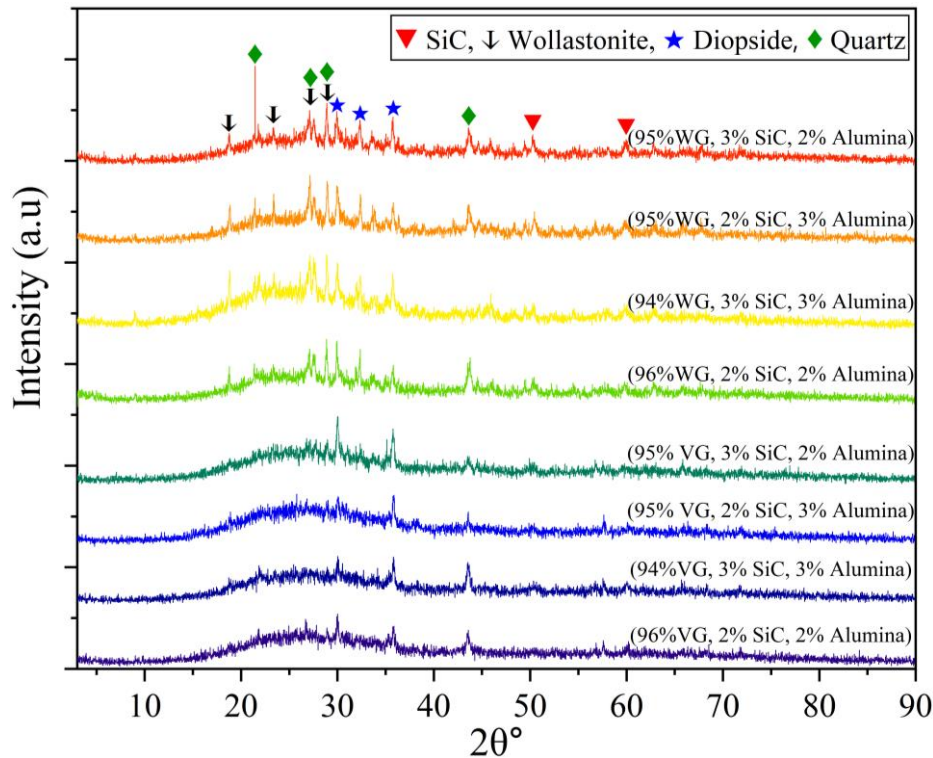
Figure 63. XRD of different granules. WG = waste glass and VG = virgin glass

Up to this point in the research, the best composition and manufacturing method for foam glass granules intended for use in lightweight CMFGC have been examined. As previously detailed, compositions numbered 1 and 5 (see Table 6) were selected as the optimal compositions for making aggregate. Given that the aim of the research is to produce structural CMFGC and the foam glass made from waste glass has higher compressive strength, the composition used in sample number 1 (see Table 6) is prioritized. Moreover, the low crystallinity of the foam glass made from virgin glass increases the likelihood of ASR when exposed to cement paste. In any case, the next phase of the research focused on the crystallization of foam glass to enhance mechanical strength and reduce reactivity with cement paste. The discussion of the results from this investigation is presented in the next section.

Summary: The novel fabrication method successfully produced foam glass granules for use in cement matrix composites as aggregate. The produced aggregates exhibited seamless surfaces, nearly spherical shapes, and varied diameters, making them suitable for tailored applications in lightweight cement matrix composite material. Test results demonstrated that granules made from waste glass had higher density, lower expansion, and greater compressive strength

compared to those made from virgin glass. Based on ASTM C330/C330M standards, only compositions 1(2 wt% of alumina + 2 wt% of SiC and 96 wt% of virgin glass) and 5 (2 wt% of alumina + 2 wt% of SiC and 96 wt% of waste glass) met the criteria for use as aggregate in lightweight cement matrix composite. Microstructural analysis revealed high closed porosity with minimal intercellular connectivity, though samples with higher SiC content exhibited microchannels due to incomplete SiC decomposition. Given these findings, composition 1 (96% virgin glass, 2% alumina, 2% SiC) was selected as the optimal aggregate for using in structural lightweight cement matrix composite.

4.8. Crystallization results of foam glass aggregate

As previously stated in section 2.2.7, to investigate the potential for crystallizing foam glass to enhance mechanical strength and reduce ASR, DSC tests were conducted on granulated foam glass samples made from virgin and waste glass. The results of these tests are shown in Figure 64. As observed, with increasing temperature, foam glass samples made from virgin and waste glass reach the glass transition temperature (Tg) at 572°C and 576°C, respectively. This temperature marks the onset of glass softening without deformation under its own weight. If crystallization is possible, an amorphous-to-crystalline phase change will occur at higher temperatures, resulting in an exothermic peak. Consequently, an exothermic peak should be seen above the glass transition temperature. As the temperature continues to rise, the sample reaches the softening point, where any formed crystals would melt, producing an endothermic peak.

The Tg and softening point peaks are visible in the DSC graphs. However, as evident in the graphs, no crystallization occurred in the samples, and the exothermic peak related to crystallization is absent.
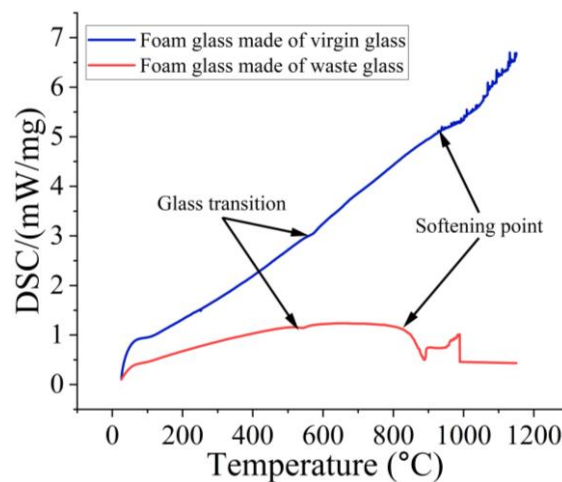
Figure 64. DSC results of foam glass made of virgin glass and waste glass

When float glass crystallizes, devitrite ($Na_2O \cdot 3CaO \cdot 6SiO_2$) and wollastonite ($CaO \cdot SiO_2$) form. Occasionally, SiO_2 polymorphs such as tridymite or cristobalite may appear due to inclusions

of refractory silica materials in the glass melt [252]. If the chemical composition of the glass does not allow for crystallization, as observed in this study, it is advisable to use crystal nuclei to initiate crystallization. Previous research suggests using nucleating agents like TiO_2 and ZrO_2 for crystallizing soda-lime glass [253]. However, our research demonstrated that without nucleating agents, crystallization in foam glass made from soda-lime glass does not occur.

Summary: This part of study examined the potential for crystallization in foam glass aggregates to enhance strength and mitigate alkali-silica reaction. Differential scanning calorimetry analysis showed that foam glass made from virgin and waste glass reached Tg at 572°C and 576°C, respectively, but exhibited no exothermic peak, indicating the absence of crystallization. In soda-lime glass systems, devitrite and wollastonite typically form upon crystallization, but the tested samples remained amorphous due to their chemical composition.

5. Performance of granulated foam glass in cement matrix

5.1. Natural aggregate characteristics

After all the characteristics of the foam glass were identified and the foam glass granules were prepared, the first test conducted on the natural aggregates for CMFGC production was a density test (the methodology is presented in section 2.1.2). The results showed that the density of the fine and coarse aggregates was 2.4 and 1.7, respectively. The fineness modulus was also calculated based on the results from sieving sand shown in Table 18, with a value of 2.62.

Table 18. Natural fine aggregates fineness modulus table

Sieve number	Remained weight (gr)	Remained percentage (wt%)	Cumulative percentage (wt%)	Percentage passing (wt%)
4	0	0	0	100
10	2.77	0.69	0.69	99.31
16	23.43	5.85	6.55	93.45
30	59.10	14.77	21.32	78.67
40	119.58	29.89	51.22	48.78
60	150.89	37.72	88.94	11.06
100	18.63	4.65	93.60	6.40

5.2. Cement matrix composite material mix plan

The ACI method for mix design, as explained in the previous section (see section 2.4.1), was followed, and in the first part of the study, the CMFGC samples were prepared according to the mix plan outlined in Table 19.

Table 19. Specimens cement matrix composite material mix plans in the sample with dimensions of 5cm×5cm ×5cm

Ingredients	Sample type			
	Reference	20% Coarse	40% Coarse	60% Coarse
Water (gr)	25.25	25.25	25.25	25.25
Cement (gr)	33.50	33.50	33.50	33.50
Coarse aggregate (gr)	129.87	104.00	77.92	51.95
Fine aggregate (gr)	47.75	47.75	47.75	47.75
Coarse FGA [3](gr)	0.00	2.81	5.43	8.15

Figure 65 shows the cross-section of the sanded samples. As is clearly visible, the cement paste exhibits excellent adhesion both to the natural aggregates and the foam glass aggregates.

Sample type

Reference	20% Coarse	40% Coarse	60% Coarse
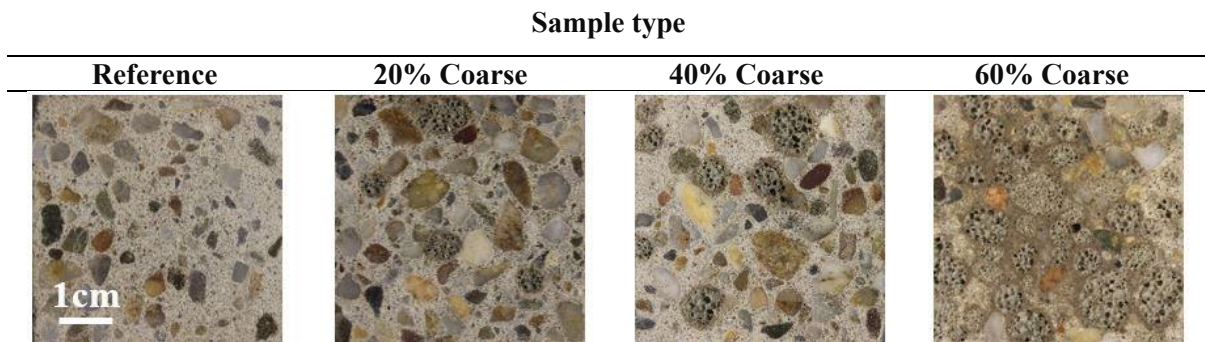
Figure 65. The cross-sectional surface of cement matrix composite specimens after cutting

---

[3] Foam glass aggregate

The density of the 1-day-old and 28-day-old CMFGC, along with their compressive strength, is presented in Table 20. As can be observed, all of the lightweight CMFGC have a density of less than 2000 kg/m³, which means they meet the density requirements for structural concrete.

Table 20. The results of fresh cement matrix composite density, air-dried cement matrix composite density, and compressive strength of the samples

Sample type	Density (kg/m³)				Compressive strength (MPa)			
	Rep. 1	Rep. 2	Rep.3	Avg.	Rep. 1	Rep. 2	Rep.3	Avg.
Reference	2160	2160	2170	2160	28	31	29	29
20% coarse	1850	1840	1910	1860	20	20	21	20
40% coarse	1640	1700	1660	1660	14	19	13	15
60% coarse	1550	1520	1540	1540	9	10	8	9

However, the next factor that needs to be examined to confirm the structural nature of the lightweight concrete (or CMFGC) is its compressive strength, which, according to ISO 22965-1:2007 standards, must be evaluated with at least three repetitions. These compressive strength values are labeled as X_1, X_2, and X_3. The characteristic strength is denoted as F_c, which for structural lightweight concrete must be 17 MPa. To be considered acceptable, the compressive strength of individual repetitions must either exceed 17 MPa, or satisfy the conditions of equation 8. Based on this criterion, only the sample containing 20% virgin foam glass qualifies as structural concrete.

Equation 8. Relationships related to the acceptance of concrete mechanical strength based on characteristic strength.

$$\begin{cases} 1) \ X_{average} \geq \ f_c + 1.5 MPa \\ 2) \ X_{min} \geq \ f_c - 4 MPa \end{cases}$$

5.3. The failure mode of concrete

The failure mode of CMFGC samples also provides valuable insights into the quality of the CMFGC. Figure 66 shows the failed CMFGC samples after the compression test. The conical failure mode, which consists of a cone-shaped core with cracks radiating outward, represents a standard failure mode for CMFGC with acceptable density and good bonding between particles. This failure mode is clearly evident in the reference sample. However, a one-sided conical failure mode is observed in the sample containing 20% foam glass. One possible explanation for this is that, due to the lightness of the foam glass, slight aggregation occurred on one side of the sample. It is also quite evident that the fracture initiated in the foam glass and then propagated into the cement paste.

This highlights a common challenge when working with lightweight aggregates. To mitigate this issue, strategies such as using viscosity-modifying admixtures, optimizing mixing procedures, or pre-saturating the foam glass aggregates can be employed to ensure more uniform dispersion within the matrix.

In this sample (sample containing 20% foam glass), a splitting fracture sheet is also observed, which typically occurs when failure initiates in the aggregate [254]. In the failed section of the sample containing 60% foam glass, it is clear that the crack path passes through the foam granules, causing the foam to fail. The key point is that structural lightweight concrete is designed not solely for maximum strength but for a balance between strength, density, thermal insulation, and sustainability. In many industrial applications, such as in non-load-bearing elements, precast panels, and even structural components with moderate load demands, the compressive strengths obtained with foam glass aggregates (even up to 60%) still meet the necessary design criteria.

The predominant failure mode of the sample containing 40% foam glass is also a splitting fracture sheet, which is attributed to fractures within the foam. It is worth noting that interfacial bonding appears to be relatively strong in all samples, as the fracture path frequently propagated through the foam granules themselves rather than along the interface. This suggests that the bond strength at the interface was sufficient to transfer stress across the cement-aggregate boundary, and that failure was governed more by the internal failure of the foam glass than by debonding. This is a positive indicator of satisfactory interfacial adhesion under the current processing conditions.

Sample type			
Reference	20 vol% coarse	40 vol% coarse	60 vol% coarse
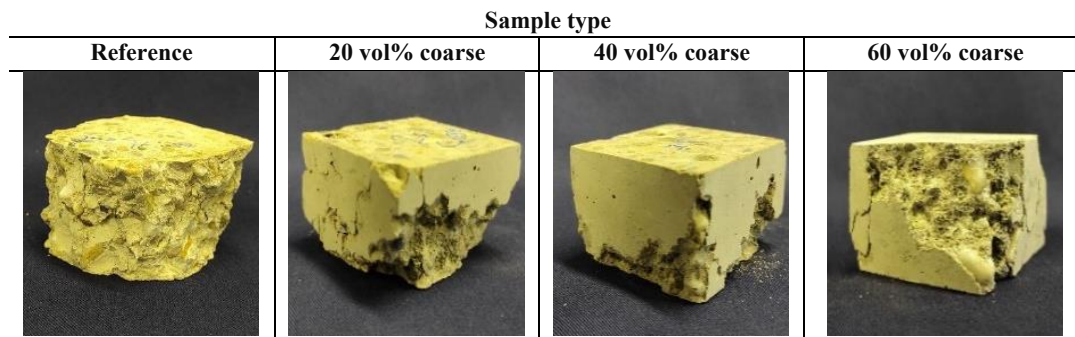
Figure 66. Destruction mechanisms in lightweight cement matrix composite samples made with foam glass granules.

Summary: The mix design follows American Concrete Institute guidelines, with cement matrix composite samples prepared using varying replacement levels (20%, 40%, and 60%) of coarse aggregate with foam glass aggregates.

Results show that all lightweight cement matrix composite mixes meet the density requirement for structural concrete (<2000 kg/m³). However, only the 20% replacement mix meets the ISO 22965-1:2007 structural strength criterion of 17 MPa. The reference sample shows standard conical failure, while the 20% foam glass sample exhibits one-sided conical failure due to aggregate lightness. At 40% and 60% replacement levels, cracks propagate through the foam glass granules, indicating their lower strength compared to cement paste.

5.4. Alkali-silicate reaction (ASR) of cement matrix composite material

As previously mentioned in section 2.5.1, the second part of this study focuses on two topics: the investigation of ASR in CMFGC where natural aggregate is replaced with foam glass made from virgin and waste glass (both granular and crushed types), and the compressive strength of these samples after the ASR test. The changes in the length of the samples, as shown in Table 21, reveal certain facts about the reactivity of the aggregates.

Table 21. The ASR results of foam glass cement matrix composite material prism. W= waste glass, V = virgin glass, L1 = crushed foam glass, and L2 = granulated foam

Sample code	Initial length (mm)	Length after test (mm)	Expansion (%)
WL1	284.6	285.2	0.21
WL2	284.3	284.6	0.10
VL1	284.8	285.3	0.17
VL2	284.8	285.2	0.14

The first observation is that the initial length of the samples is less than 285 mm, indicating some shrinkage during the hydration period of the CMFGC. The increase in the length of the samples also follows an interesting pattern. Firstly, the length increase in all samples is less than 0.22%, meaning that these samples meet the ASTM C1778 standard criteria for ASR resistance. Based on the standards outlined in Table 22, the samples are considered moderately reactive. The change in length for the WL_2 and VL_2 samples is less than that for the WL_1 and VL_1 samples, indicating that CMFGC made with crushed foam glass exhibits greater reactivity.

Table 22. The reactivity classification of aggregates based on ASTM C1778

Reactivity grade of aggregate	Aggregate reactivity description	Expansion of prism according to ASTM C1260 (%)
R0	Non- reactive	Expansion < 0.1
R1	Moderate reactive	$0.1 \leq$ Expansion < 0.22
R2	High reactive	$0.22 \leq$ Expansion < 0.45
R3	Super high reactive	Expansion ≥ 0.45

Furthermore, this standard outline different risk levels according to Table 23.

Table 23. The Alkali-Silica Reaction risk levels of concrete in different environments and dimensions

	Reactivity grade of aggregate			
	R0	R1	R2	R3
Dimensions and using environment	**Level of risk**			
Non-bulky concrete in dry environmental conditions	1	1	2	2
Mass concrete in dry environmental conditions	1	2	3	4
Concrete in moist environmental conditions, buried in soil, or submerged in water	1	3	4	5
Concrete in contact with an alkaline environment	1	4	5	6

According to the definition, a massive member is one with minimum dimensions of 0.9 m. Dry environmental conditions are defined as having an average relative humidity of less than 60%, typically occurring indoors. Additionally, structures in contact with alkalis during service life mainly include marine structures exposed to seawater and transportation infrastructure and roads

exposed to de-icing salts. Based on ASTM C1778, four qualitative risk levels are defined, with lower risk levels being preferable. The relationship between the risk of ASR occurrence and concrete applications is defined in appendix B.

The SEM observations conducted on the samples, as shown in Figure 67, indicate the absence of silica gel formation at the interface between the foam glass and the cement matrix. On the other hand, the adhesion between the cement matrix and the foam glass is remarkably strong. The SEM analysis suggests that the foam glass aggregates (both types, waste, and virgin) are inert. Therefore, it can be concluded that the observed increase in length in the samples is a result of the ASR with the other components of the CMFGC.
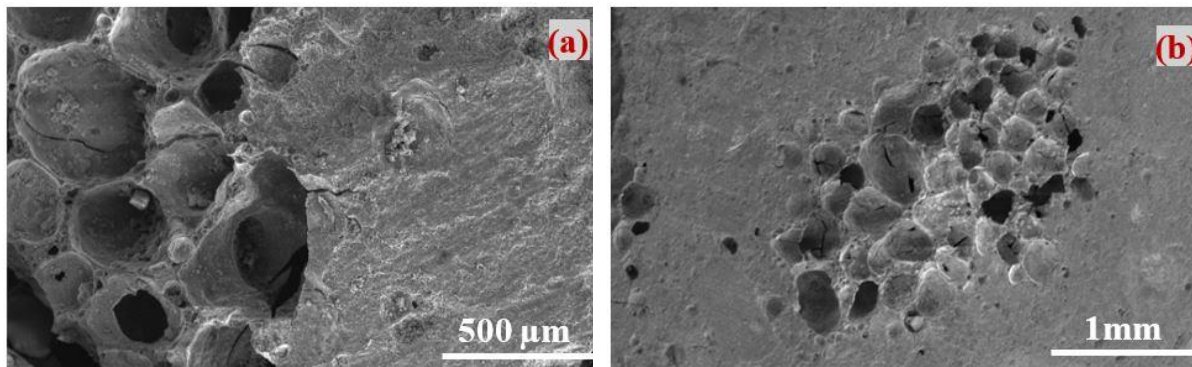
Figure 67. SEM micrographs show strong adhesion between foam glass and cement paste, with no silica gel formation. a) virgin foam glass. b- waste foam glass

5.5. Compressive strength of the cement matrix composite samples

The compressive strength tests conducted at Sapienza University in Rome on the CMFGC samples yielded interesting results, as seen in Figure 68a. This figure shows only one of the repetitions tested from each group.

a

b
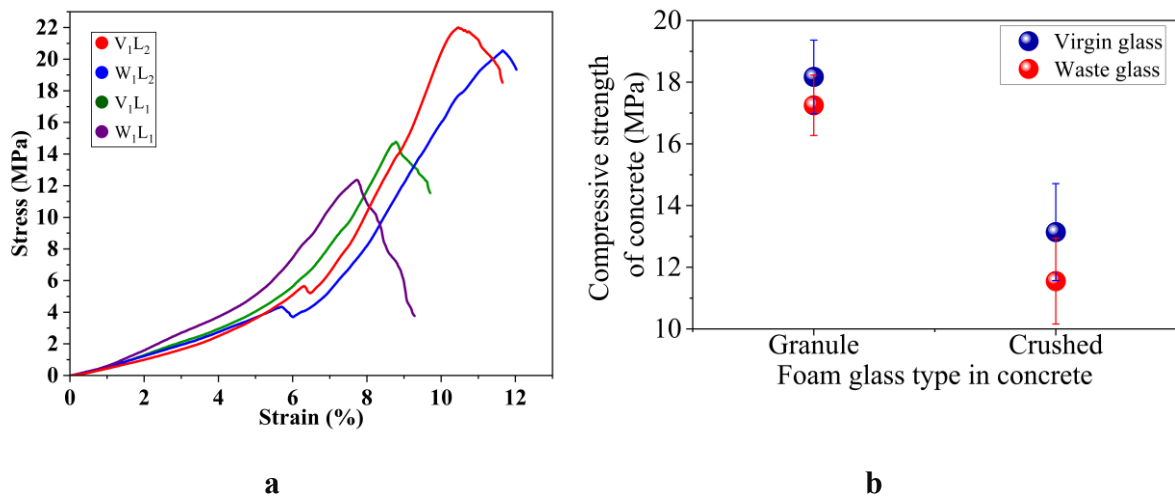
Figure 68. a) The strain-stress curve of cement matrix composite samples. b) The compressive strength

The graph indicates that the compressive strength of CMFGC made from foam glass granules is higher than that of CMFGC made from crushed foam glass. As observed in the graph, the trend of the strain-stress curve shows an initial increase up to about 4 MPa, with strain reaching two percent. After this point, the curve exhibits a steeper increasing trend, indicating a nonlinear increase in the stiffness of the CMFGC due to the presence of foam glass. Following this stage, the graph reaches its maximum compressive strength, and immediately after the maximum point, a momentary drop is observed in the graph. This momentary decrease signifies the failure of the foam glass aggregates, which is clearly depicted in Figure 69, where it occurs in the waste foam glass aggregates.
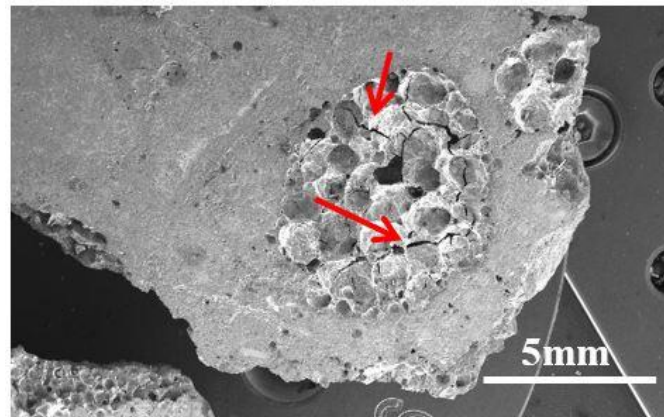
Figure 69. The crack propagation in foam glass aggregates in the cement matrix composite sample.

Interestingly, this failure is more uniform for the CMFGC made from waste foam glass, suggesting better adhesion of the samples containing waste foam glass compared to those made with virgin foam glass to the cement paste. Figure 68b shows the average compressive strength of the tested samples. As indicated, both the foam glass made from virgin glass granules and waste glass granules are acceptable as structural CMFGC. However, it is noteworthy that the compressive strength of samples made with virgin foam glass is higher than that of those made with waste foam glass.

This finding is significant because, as previously mentioned (see Table 17), the compressive strength of granules made from waste glass is greater than that of granules made from virgin glass. Therefore, one would expect the compressive strength of the CMFGC using waste glass to be higher than that of the CMFGC using virgin foam glass. This observation was elucidated by SEM observations and a comparison of the water absorption values of the waste and virgin glass granules presented in Table 17. When observing the pores of the foam glass used in CMFGC under higher magnification, fibers known as ettringite are visible. These ettringite fibers are produced due to the hydration of tricalcium aluminate, present in Portland cement,

in reaction with calcium sulfate and water [255]. The chemical formula of these fibers is represented by equation 9.

Equation 9. The chemical equation of ettringite crystals [255]

$$Ca_6Al_2(SO_4)_3(OH)_{12} \cdot 26H_2O$$
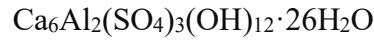
Although the presence of ettringite in conventional concretes generally enhances compressive strength by filling voids, here as shown in Figure 70 ,it is observed that the length and number of needle-like ettringite crystals inside the cracks of waste foam glass are greater than those inside the virgin foam glass. These crystals expand within the foam granules, causing cracks to form before the samples are subjected to compressive strength testing. The granules made from waste glass exhibit significantly higher water absorption than those made from virgin glass, allowing the pore solution to penetrate deeper into the waste glass granules before complete hydration, compared to the virgin glass granules.
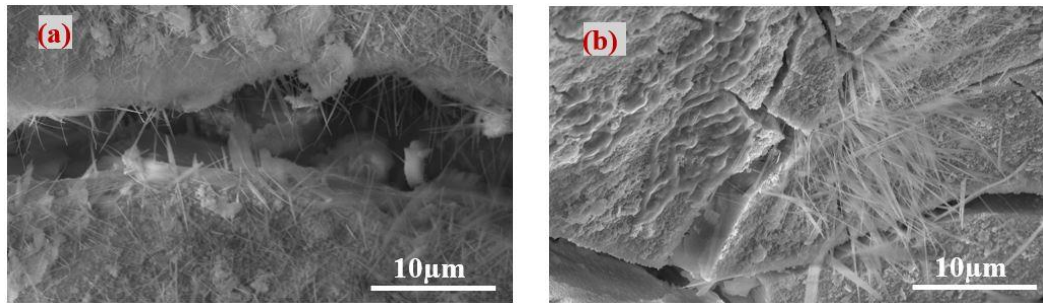
Figure 70. Micrographs of cracks inside the foam glass granules made from a) virgin, b) waste glass

As a result, the cracks formed during the hydration process, due to the formation of ettringite inside the waste glass granules, contribute to the creation of CMFGC with lower compressive strength, even though the waste glass granules themselves exhibit higher compressive strength.

Ultimately, this research concludes that structural lightweight CMFGC can be manufactured using foam glass granules (both virgin and waste glass) that achieve a compressive strength exceeding 17 MPa and a density of less than 2000 kg/m³. For this purpose, the ACI method must be followed for mix design, and23 coarse natural aggregates with a particle size of less than 19 mm should be used, with 20% of these aggregates replaced by foam glass granules of the same particle size. The final part of this research focuses on discussing the results of the tests conducted using the new ASR assessment method (TGA-based method) on foam glass aggregates.

5.6. Thermogravimetry analysis for alkali silica reaction assessment

As detailed in Section 2.3.4, a novel TGA-based method has been employed to evaluate the ASR reactivity of foam glass aggregates. Figure 71a to Figure 71c display the TGA curves acquired at different curing ages (1 day, 7 days, and 28 days respectively). The analyses

highlight the occurrence of two-step degradation mechanism relating with the transformations (decomposition and carbonation) that the unfixed CaOH undergoes.
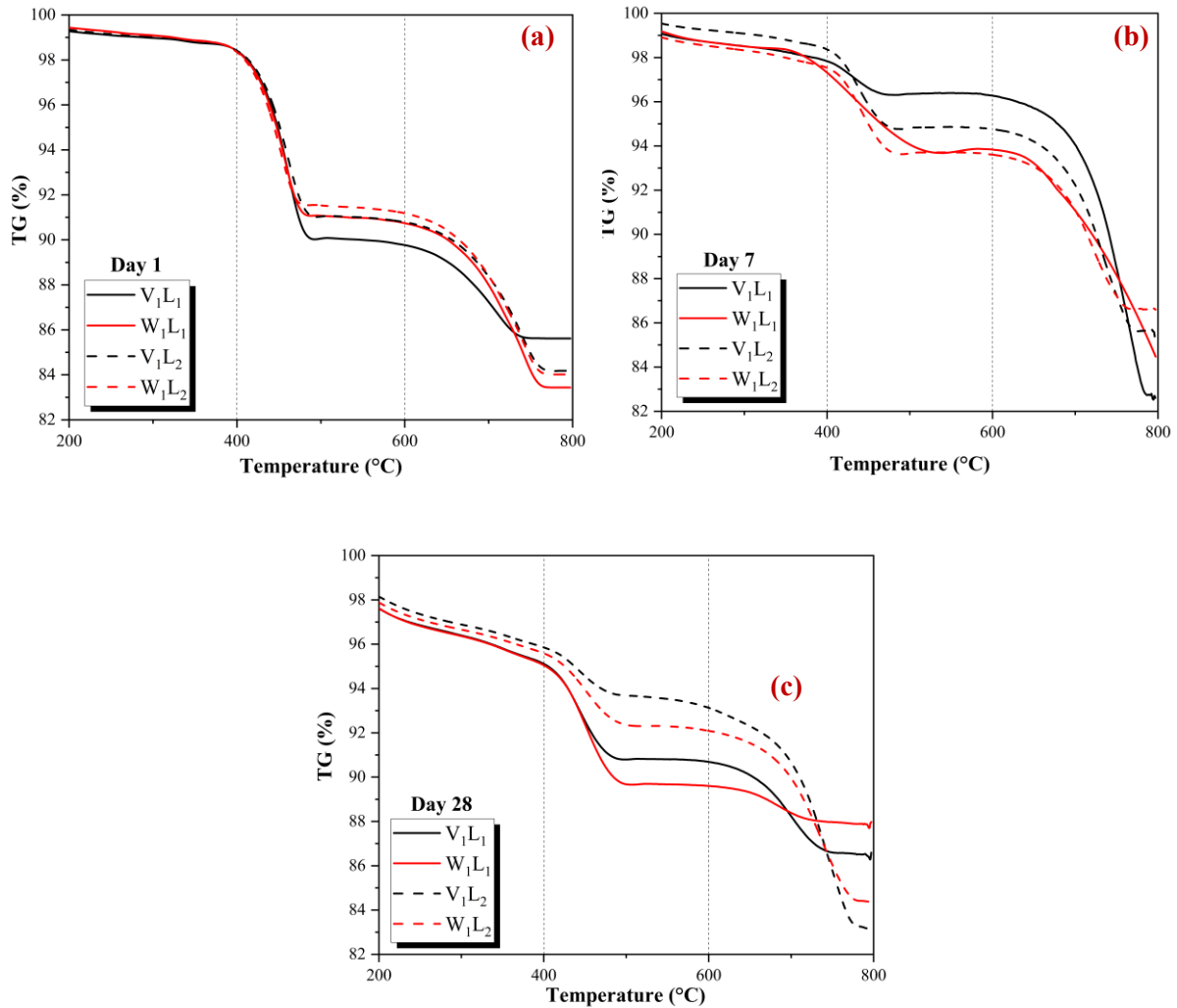
Figure 71. TGA thermograms acquired at a) 1 day of curing, b) 7 days of curing, and c) 28 days of curing

In Figure 72 the pozzolanic reactivity values of the samples are plotted in terms of mg of CaOH fixed (per mg of foam glass powder). Regardless the type of glass and sintering cycles, it can be noted that as the curing age increases there is a gradual increase in the fixing capacity of the CaOH which would demonstrate the pozzolanic reactivity of the foam glass-based powders. After 1 day all samples show pozzolanic activity according to the classification established by Borges et al. [256] who considers glass with pozzolanic behavior when $436 <$ mg CaOH fixed/ g of reactive material < 750. This result supports the feasibility of using the porous glass aggregates produced in the present research without risks in terms of ASR expansion but with the added value to promote the development hydration product for the resulting concrete. In fact, a large content of CaOH in the paste can provide more soluble calcium (Ca) and hydroxide (OH) ions for the ASR sustaining the detrimental expansion and cracking of the material [225]. The capacity of the glass to be reactive reduces the availability of free lime in the paste mitigating this durability issue for concrete materials. By investigating the effect of the sintering cycles, no evident variations in terms of pozzolanic reactivity can be detected.

However, probing the results of the waste glass, it can be noted that a second sintering cycle would help to increase the reactivity of the material, while for the virgin glass there is an expected reverse effect. Indeed, sintering reduces the specific surface area of the powder, make it less prone to react with CaOH [257]. On the other hand, the chemical inhomogeneity of the waste glass may play a crucial role in the influence of the sintering cycles. However, more future research is needed to clarify this finding.
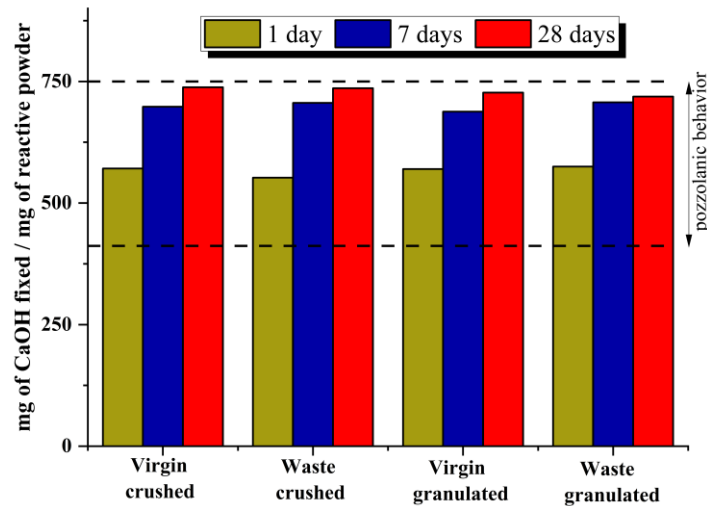
Figure 72. CaOH fixation rate (pozzolanic reactivity) of the foam glass examined samples

Summary: Cement matrix composite (CMFGC) samples were prepared by following American Concrete Institute guidelines using varying replacement levels (20, 40, and 60 vol%) of coarse aggregate with foam glass aggregates. Results show that all lightweight CMFGC mixes meet the density requirement for structural CMFGC (<2000 kg/m³). Only the 20 vol% replacement mix meets the ISO 22965-1:2007 structural strength criterion of 17 MPa. The reference sample shows standard conical failure, while samples with 20 vol% foam glass exhibits one-sided conical failure due to aggregate lightness. At 40 and 60 vol% replacement levels, cracks propagate through the foam glass granules, indicating their lower strength compared to cement paste. ASR tests confirmed that all samples met ASTM C1778 criteria for moderate reactivity, with crushed foam glass showing slightly higher expansion than granulated foam glass. Microstructural analysis revealed no silica gel formation, indicating that foam glass itself was inert. Compressive strength tests showed that CMFGC with granulated foam glass outperformed that with crushed foam glass. Despite the higher strength of waste glass granules, increased water absorption and ettringite-induced cracking reduced the overall CMFGC strength. The findings confirm that structural lightweight CMFGC with foam glass can achieve over 17 MPa compressive strength and a density below 2000 kg/m³. TGA analysis was used to assess alkali-silica reactivity in foam glass aggregates. Thermogravimetry (TGA) curves at different curing ages (1, 7, and 28 days) reveal a

two-step degradation mechanism associated with the decomposition and carbonation of unfixed Ca(OH)$_2$. Pozzolanic reactivity, measured as the amount of Ca(OH)$_2$ fixed per mg of foam glass powder, increases with curing time, demonstrating the pozzolanic behavior of the foam glass. All samples exhibit pozzolanic activity after 1 day, reducing the risk of ASR-induced expansion and cracking by limiting free lime availability.

6. Summary

The research is divided into two main sections: one focused on the properties of the foam glass itself, and the other on the characteristics of the lightweight cement matrix composite reinforced foam glass aggregates.

In terms of foam glass properties, the effects of particle size distribution on materials were analyzed, as well as the influence of sintering parameters. The impact of adding water to the foam glass precursor (preform) was studied, revealing how it affects the properties of the foam. Additionally, a new foaming agent derived from cement plant soot was introduced, which offers a different foaming mechanism compared to traditional agents like silicon carbide (SiC). A new laboratory-scale method for producing foam glass granules was developed, aiming to optimize their shape and size. Furthermore, the Taguchi statistical method was applied to reduce the number of experiments and accurately predict results.

Part of the study was dedicated to exploring the crystallization of foam glass, which was conducted in collaboration with São Carlos University in Brazil. The next section of the research, carried out in close collaboration with Sapienza University, focused on structural lightweight cement matrix/foam glass composite (CMFGC) . A mix design was developed using the American Concrete Institute (ACI) method to produce structural-grade concrete. Various volumetric percentages of foam glass granules were used to replace natural aggregates, and the properties of the resulting CMFGC were examined. In addition, the study compared CMFGC made from foam glass granules and broken foam glass (both from virgin and waste glass sources), investigating the differences in their properties.

The final stage of the research evaluated Alkali-silica reaction in a cementitious environment and introduced a new method for assessing the reactivity of foam glass granules based on thermogravimetry analysis. This approach provided valuable insights into the behavior of foam glass in a cement matrix. The study presents numerous valuable results, which are summarized to highlight the key findings.

- Microscopic heating tests on the foam glass precursor powder revealed that surface area changes in the samples did not align with height changes. The surface area expansion was slightly greater than the height change, with maximum surface expansion occurring 18-60 °C above the temperature of maximum height change.

- Sintering parameter effects showed that changing the sintering temperature accounted for approximately 79% of the foam properties, while holding time influenced about 21% of the properties.

- The study on the effect of adding water to the foam glass precursor powder showed that adding 20% water by weight could eliminate the need for cold pressing (over 80 MPa), impacting foam properties by about 9%. This resulted in a 3% change in open porosity, a 16% change in density, and an 18% change in compressive strength, suggesting that cold pressing could be replaced by water addition.

- Using soot as a foaming agent: Adding up to 3% soot successfully produced foam glass. The mechanism of soot foaming, different from SiC due to the decomposition of calcium carbonate in soot, led to greater expansion, lower water absorption, and higher mechanical strength.

- A multi-criteria decision-making method identified the best composition and processing conditions for foam glass to be used in lightweight CMFGC. The optimal foam glass was made from virgin glass at 30°C below the maximum area temperature from the heating microscope test, with 8% alumina, 1% soot, and 2% SiC, produced by the wet powder method.

- A new method for producing foam glass granules in a lab setting was successfully developed. The precursor foam glass was first heated above Tg but below the expansion temperature for 50 minutes, then ground, and finally sintered again at the expansion temperature. This produced foam glass granules of various sizes and nearly spherical shapes.

- Structural lightweight concrete can be created using natural coarse aggregates (with a maximum particle size of 19 mm), following the ACI mix design method. By replacing 20% of the volume of the aggregates with foam glass granules made from either virgin glass or waste glass (such as window glass), SiC (2% by weight), and alumina (4% by weight), CMFGC with a density below 2000 kg/m³ and compressive strength above 17 MPa can be achieved.

- The mechanical strength of CMFGC made from foam glass granules (both virgin and waste glass) exceeds 17 MPa, while CMFGC made from crushed foam glass (virgin and waste) has a compressive strength below 15.5 MPa.

- Although granules made from waste glass have higher compressive strength than those made from virgin glass, the samples made with virgin glass granules exhibited higher compressive strength due to the formation of ettringite crystals in waste glass granules, which caused cracks during the hydration process.

- ASR tests showed that foam glass has moderate reactivity. The ASR levels in CMFGC made with foam glass granules were lower than those made with crushed foam glass. These compositions for CMFGC could be used in specific environments with a risk rating of 1 or 2 out of 6.

- The study concluded that lightweight structural CMFGC with densities below 2000 kg/m³ and compressive strengths above 17 MPa can be successfully produced using foam glass granules.

- And finally, a new TGA-based method has been implemented to evaluate a double property of foamed glass aggregates: the pozzolanic reactivity and the ability to induce ASR reaction. We proved that the method, in combination with mechanical and microstructural analysis, confirms the inertia of the aggregates to develop ASR but a good pozzolanic activity to be compatible with the cement matrix.

7. Claims and new scientific results

1. Comparative evaluation of foam glass expansion based on maximum silhouette height and maximum projected area temperatures extracted from heating microscopy images

I conducted a comparative evaluation of foam glass characteristics at two distinct temperatures derived from heating microscopy images: one corresponding to the maximum silhouette height and the other to the maximum projected 2D area. Foam glass samples were synthesized using waste window glass combined with 1–3 wt% SiC as the foaming agent. My experimental results demonstrated that sintering at the temperature associated with maximum projected area, typically 18–60 °C higher than that of maximum height, consistently resulted in significantly greater volumetric expansion, ranging from 44% to 57%. In addition, regression analyses revealed a stronger correlation between the projected area ratio (a/a_0) and volumetric expansion $(R^2 = 0.9773)$, compared to the height ratio (h/h_0) $(R^2 = 0.9237)$. These findings highlight the superior predictive capability of the area-based method in identifying the true temperature of maximum expansion. This comparative investigation offers a more accurate and practical approach for determining optimal sintering temperatures in foam glass production through heating microscopy analysis.
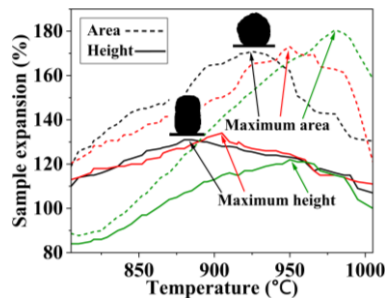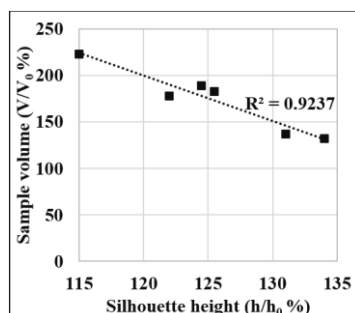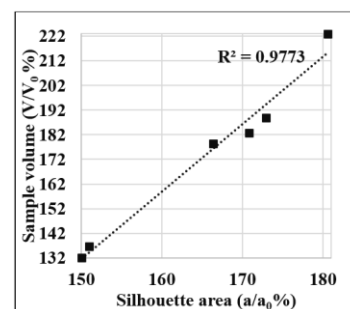
Figure C1. a) The difference in area and height changes graphs for samples made from waste glass powder and, 1 wt% (green lines), 2 wt% (red lines) and 3 wt% (black lines) of SiC. b) Comparison of the same foam glass (1 wt% SiC + waste window glass powder) samplese, which are sintered at maximum height and maximum area temperatures. c) Correlation between height ratio (h/h_0) and volume ratio (V/V_0) of foam glass samples. d) Correlation between area ratio (a/a_0) and volume ratio (V/V_0) of foam glass samples.

2. Application of waste soot originating from a cement factory as a foaming agent in foam glass production[4]

2.1. I demonstrated that cement factory soot, a waste material rich in carbon and calcium carbonate ($CaCO_3$), can be employed as a dual-phase gas-releasing agent in foam glass production. Carbon undergoes oxidation at 475 °C (as confirmed by Thermogravimetry analysis in Figure C.2.1), releasing CO_2 and initiating primary foaming. Subsequently, above 815 °C, $CaCO_3$ starts to decompose and releases additional CO_2, contributing to a secondary foaming. However, this approach requires the glass matrix to be sufficiently softened at the first gas release phase; based on heating microscopy results, the glass transition temperature is in the range of (405 to 505°C), and the softening point of the glass is about 655 °C. Therefore, the first-stage CO_2 evolution from carbon leads to partial pre-foaming and bubble nucleation, but complete swelling requires temperatures higher than 814 °C.

With just 2 wt% soot, foam glass with a low bulk density of 241 kg/m³ was achieved at 840°C. In comparison, a previous study using 4 wt% $CaCO_3$ at 820°C resulted in a higher density of 301 kg/m³, approximately 16% more [60]. Importantly, this method promotes waste valorization and aligns with circular economy goals. Therefore, the use of cement factory soot as a foaming agent can be considered highly practical and industrially applicable.
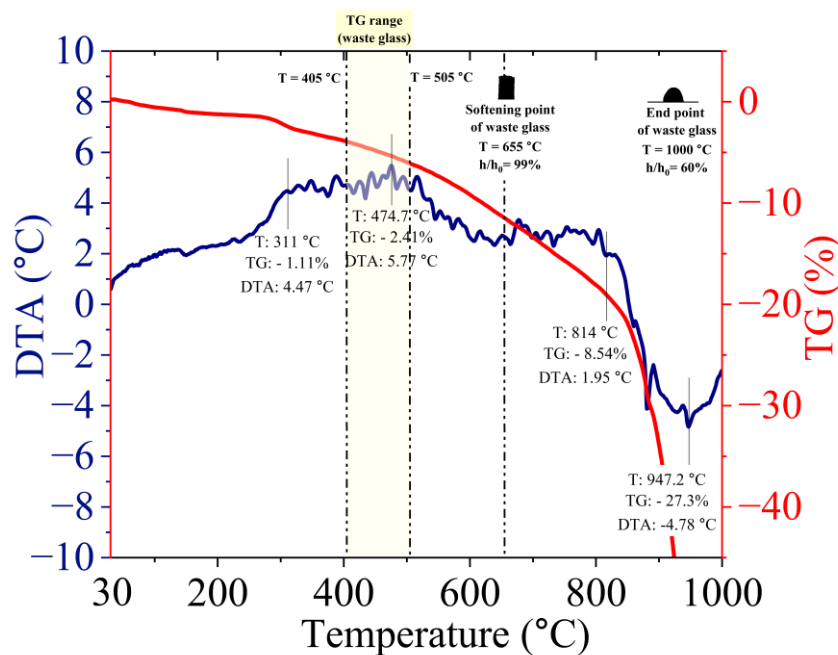
Figure C2.1. Thermogravimetric analysis (TGA) curve of soot alongside the critical temperature points of waste glass. The glass transition temperature of the waste glass is observed in the range of 405°C to 505°C, and its softening point occurs at approximately 655°C. The oxidation temperature of carbon and the decomposition temperature of calcium carbonate in the soot are also clearly indicated on the curve.

---

[4] The results discussed in this claim have been published in the Q1 journal *Ceramics* International and are accessible at https://doi.org/10.1016/j.ceramint.2024.10.152.

2.2. My experimental results demonstrate that the use of cement factory soot as a foaming agent, particularly in combination with silicon carbide (SiC), enhances the compressive strength of foam glass. In our published study [258], I investigated the effects of varying soot and SiC contents (1, 2, and 3 wt%) and found that this hybrid foaming strategy leads to significantly improved mechanical performance. As shown in previous research (summarized in Figure C.2.2, based on the literature), calcium carbonate has traditionally been used as a foaming agent for recycled window glass, resulting in compressive strengths ranging from 0.52 to 6.5 MPa depending on the heating regime and foaming agent dosage [259-261]. In comparison, foam glass produced using cement factory soot achieved compressive strengths between 0.86 and 9.2 MPa [258], representing a notable enhancement.
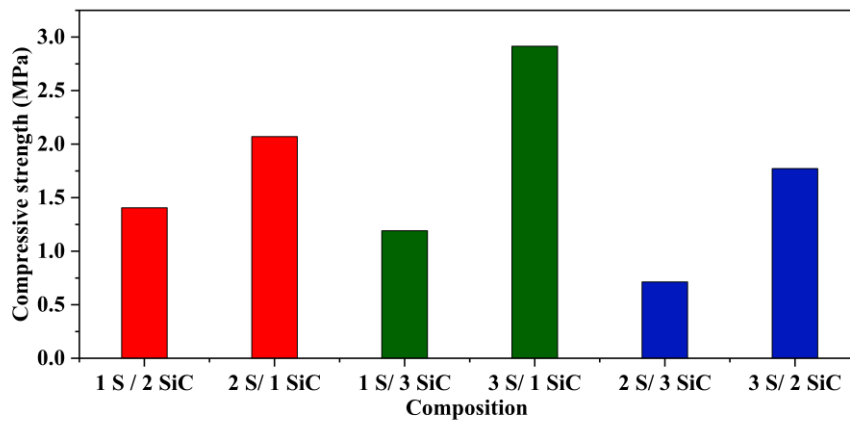
Figure C2.2. Compressive strength variations of foam glass produced from waste glass using a combined foaming agent of soot and SiC. The symbol 'S' denotes soot, and the numbers following it indicate the corresponding weight percentage used in the foam composition

3. Introduction of a simplified laboratory method for making foam glass granules

My research introduces a novel, two-step sintering method for producing foam glass granules, which eliminates the need for pelletizers and rotary furnaces (Figure C3). This method allows for the production of foam glass granules in a wide range of sizes with a uniform pore distribution. The use of the two-step sintering process, which is a significant departure from conventional methods, enables the creation of foam glass granules with a structure resembling that of typical commercial foam glass, without the need for specialized equipment. The outer shell of aggregates in this production method is continuous, with no significant cracks or voids, resulting in improved mechanical strength and a uniform structure.
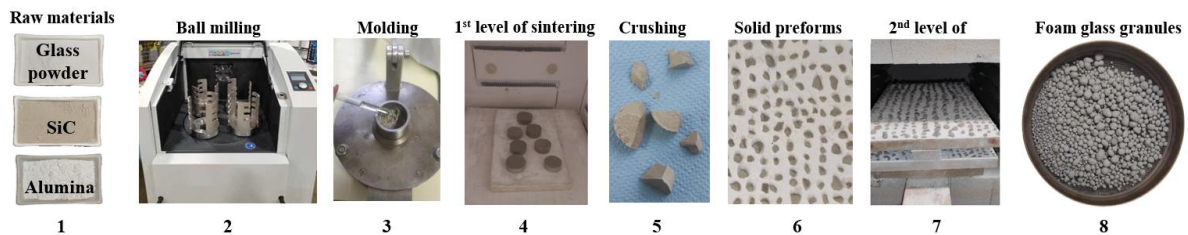
Figure C3. The novel technique for fabricating foam glass granules

4. Application of Thermo-Gravimetric Analysis (TGA) as a predictive tool for indirectly assessing Alkali-Silica Reaction (ASR) by foam glass in cementitious environment[5]

4.1. A new experimental approach was introduced in this research to assess the reactivity of foam glass toward calcium hydroxide $Ca(OH)_2$ as an indirect indication of ASR mitigation potential. In this method, foam glass powder was mixed with reagent-grade $Ca(OH)_2$ in equal proportions by mass and hydrated under controlled conditions. After specified curing durations (1, 7, and 28 days), the residual unreacted $Ca(OH)_2$ was quantified using thermogravimetric analysis. The absence or reduction of the characteristic decomposition peak of $Ca(OH)_2$ at approximately 500 °C is interpreted as an indicator of pozzolanic activity and potential mitigation of ASR. The evaluation criterion is based on the amount of fixed $Ca(OH)_2$, expressed in milligrams per gram of reactive material. These results were benchmarked using values established in previous literature [256], where glass materials fixing more than 436 mg $Ca(OH)_2$/g are considered pozzolanic. The procedural steps of this novel TGA-based method are illustrated in Figure C4.1.

4.2. Experimental results showed that foam glass powders exhibit significant pozzolanic reactivity by absorbing free $Ca(OH)_2$ from the cement paste (Figure C4.2a) and contributing to the formation of calcium-silicate-hydrate (C–S–H) gel. This reduces the availability of free Ca^{2+} and OH^- ions in the pore solution, thereby lowering alkalinity and decreasing the risk of ASR (Figure C4.2b).
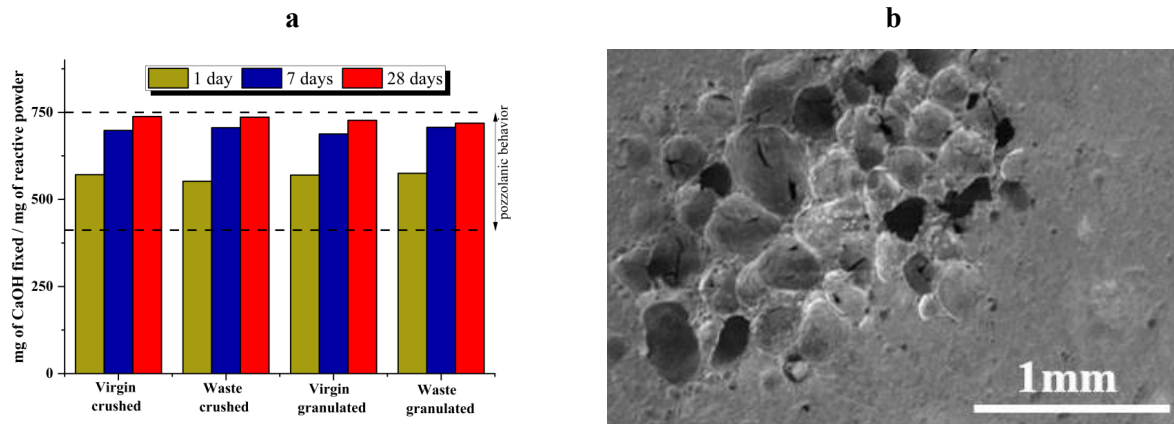
Figure C4.2. a) Calcium hydroxide fixation rate, indicating the pozzolanic reactivity of foam glass particles, as determined by TGA analysis, b) SEM image showing the non-reactive interface between foam glass aggregate and cement paste, with no evidence of ASR gel formation after exposure to ASR testing conditions.

Publications

The detection of porous media volume using the modified Archimedes method

Masoud OSFOURI ▪ Institute of Energy, Ceramics and Polymer Technology, Faculty of Materials and Chemical Engineering, University of Miskolc
Andrea SIMON ▪ Institute of Energy, Ceramics and Polymer Technology, Faculty of Materials and Chemical Engineering, University of Miskolc

Masoud OSFOURI
is PhD student in material science and works on foam glass and light weight concrete at the University of Miskolc in Hungary. His background is mechanical engineering and his MSc thesis dealt with shape memory alloys and fiber metal laminates. He received his MSc degree in applied mechanics in 2017 at the University of Zanjan. His actual research topics are foam glasses, polymer matrix composite materials, and lightweight concrete.

Andrea SIMON
works full-time at ZF Hungary Ltd. as a supplier development engineer, and part-time at the University of Miskolc as an associate professor. She received her PhD degree in materials science and engineering in 2010 at the University of Miskolc. Her actual research topics are foam glasses, waste recycling, and microstructural characterization.

Abstract
Foam glasses are novel materials in engineering that have found a special place in various industries during recent decades. Foam glass is generally produced using recycled glass. By using waste materials, in addition to reducing the amount of waste glass that can harm the environment, it is possible to achieve a lightweight foam that is resistant to compression, corrosion, and heat transfer. The foam glass structure consists of cells that are filled with gas, and the walls of these bubbles are made of solid glass. One of the challenges is to measure its density. Because the samples made in the laboratory generally do not have a conventional shape, and therefore it is difficult to find the volume of the samples geometrically. In this paper, a new, simple, and practical method to find the density of foam glass is presented. The result of the tests showed a very good coincidence between geometrical volume measurements and volumes measured by using this novel method.
Keywords: glass foam, volume, modified Archimedes method, porous materials
Kulcsszavak: üveghab, térfogat, módosított Archimédeszi-módszer, porózus anyagok

1. Introduction

Foam glass is a porous material with a glassy skeleton in which the holes are surrounded by thin glass walls and separated from each other. Foam glass has a unique combination of properties: lightweight, rigid, and strong, compression resistant, thermal insulation, non-flammable, chemically neutral and non-toxic, resistant to rodents and insects, resistant to bacteria, water, and humidity. In addition, it is easy to install, cut, and drill, and it is easily combined with concrete. This combination of properties makes foam glass indispensable in the construction and petrochemical industries (oil and gas transmission lines), railroad foundations, dam constructions, foundations of streets and highways, sports fields, and many other fields [1].

from the material [3]. The glass softening temperature should always be lower than the foaming reaction temperature. But if the composition of the glass is prone to crystallization and the crystallization speed exceeds the sintering speed of the glass, then the crystallization of the glass will increase its viscosity, and as a result, the softening temperature of the glass will be higher than the temperature of the gas exiting the sample. In this case, the possibility of creating closed porosity in the foam glass is reduced, and open porosity increases [3, 4].

The importance of energy conservation on the one hand and the need to lighten the buildings, on the other hand, make the use of lightweight, heat, and sound-insulating but strong and stable materials in building construction more and more essential. But for being an applicable material, they require to

---

Study on the thermal conductivity and density of foam glass

Masoud Osfouri* and Andrea Simon

Institute of Ceramics and Polymer Engineering, Faculty of Materials Science and Engineering, University of Miskolc, Miskolc-Egyetemvaros, Hungary

ORIGINAL RESEARCH PAPER

ABSTRACT

This paper focuses on the relationship between the composition of foam glass and its thermal conductivity and density. In this experimental research, three levels of glass particle size and foaming agent (SiC) quantity were tested. The results showed that the thermal conductivity increased by increasing the ratio of fine glass particles. On the contrary, the thermal conductivity was not affected by changing the foaming agent weight ratio. The density of foam glass increased by decreasing the foaming agent ratio, and there was no linear relation between the size of glass particles and the density of foam glass.

KEYWORDS

foam glass, glass particle size, SiC, foaming agent ratio, thermal conductivity, density

1. INTRODUCTION

In many engineering applications, it is necessary to combine the properties of materials and it is difficult to find a material that proves all of the required properties. For example, in the building industries, materials are needed to have high strength, low density, good sound/heat insulation, high vibration damping, good wettability, and high adhesion capability. Many ceramic materials could be used for thermal insulation in the form of foams or bricks [1, 2]. Foam glass is one of the modern lightweight materials, which can withstand high temperatures, and provide outstanding sound and heat insulation at the same time. The main substances of foam glass are the glass powder and the foaming agent, while the most well-

Nitinol wire-reinforced GLAREs as a novel impact resistant material: An experimental study

Masoud Osfouri, Omid Rahmani

Show more ∨

+ Add to Mendeley   ⦷ Share   " Cite

Get rights and content

Abstract

Glass-fiber-reinforced aluminum layers (GLARE) are one of the excellent impact resistant materials, benefited from both the metal and glass fibers properties. Owing to their high impact damping properties, the shape memory alloys have been also considered as useful materials for arming the conventional impact-exposed materials. In the present paper, the shape memory wires were integrated with GLARE laminate and its response to the Charpy low-velocity impact was experimentally studied. The current study is aimed to determine the effects of three parameters (pre-strain percentage of shape memory alloy (SMA), glass fibers angle and the location of SMA wires within the novel fiber metal laminate) for the first time. Hybrid GLARE specimens of this study were planned by Taguchi design of experiments (DOE) method and contained Nitinol shape memory alloy wires. The results showed that the pre-strain and the angle of glass fibers are the most effective parameters on the impact energy absorption at accepted levels of confidence. Regarding the innovations in the construction of this type of impact-resistant hybrid composites, this study could be used in design of aerospace bodies.

Properties of foam glass produced with the use of soot from a cement factory as a foaming agent: A study based on Taguchi design of experiments

Masoud Osfouri [a c], Jamal-Eldin F.M. Ibrahim [a b], Andrea Simon [a]

Show more ∨

+ Add to Mendeley   ⦷ Share   " Cite

Get rights and content

Abstract

Cellular glass is a lightweight, porous medium with excellent heat transfer resistance that can be used in a variety of industries. This study investigated the use of soot from cement plants as a new foaming agent for producing foam glass. The experiments were designed using the Taguchi Design of Experiments (DOE) method. By applying this approach, instead of creating and testing 27 different groups of samples, only 9 groups were produced. The properties of the remaining 18 sample groups were then predicted based on Taguchi analysis. Soot and silicon carbide were used simultaneously (at weight ratios of 2% and 3%) as foaming agents in the samples. Alumina was also used as a modifier with weight ratios of 4%, and 8%. Mechanical strength, water absorption, density, and thermal resistance were evaluated. The findings indicated a direct correlation between elevated soot content and increased water absorption (open porosity), coupled with a reduction in compressive strength and overall density of the foam glass. Electron microscopy observations revealed a wide range of crystallite morphologies in the resulting foam glass, which results in diverse properties in the material. The developed glass foams exhibit a density spanning from 125 to 700 kg/m^3, with compressive strength varying between 1.2 and 6.7 MPa, and thermal conductivity in the range of 0.08–0.5 W/m·K. The samples with 3% soot, 0% alumina, and 3% SiC exhibited exceptional thermal insulation properties. In contrast, the samples containing 1% soot, 8% alumina, and 1% SiC demonstrated the highest compressive strength. Overall, this study found that soot from cement plants is a viable foaming agent for producing foam glass with desirable properties. The use of soot from cement plants can not only reduce the dispersion of pollution in the environment but also produce a wide range of foam glass with different properties at a lower cost.

Sustainable structural lightweight concrete containing foam glass aggregates

Masoud Osfouri [a],[*], Jamal-Eldin F.M. Ibrahim [a],[b], Matteo Sambucci [c], Marco Valente [c], Jacopo Tirillò [c], Simon Andrea [a]

[a] Institute of Ceramics and Polymer Engineering, University of Miskolc, Egyetemváros, Miskolc, H-3515, Hungary
[b] Department of Materials Technology, University of Bahri, Khartoum, 12217, Sudan
[c] Department of Chemical and Material Engineering, Sapienza University of Rome, Via Eudossiana 18, 00184, Rome, Italy

ABSTRACT

Recently, various types of lightweight concrete have been developed through the combination of different lightweight aggregates and cementitious matrices. This study investigates the replacement of natural coarse aggregates with foam glass to produce lightweight structural concrete, aiming to reduce the environmental footprint of traditional concrete materials. Foam glass aggregates, synthesized from both virgin and recycled glass using an innovative laboratory-scale method, were evaluated as substitutes at replacement levels of 20 %, 40 %, and 60 % by volume. The aggregates were used in granulated and crushed forms to assess their performance compared to conventional natural aggregates. Key findings demonstrate that concrete with 20 % foam glass replacement achieves a bulk density below 2000 kg/m^3 and compressive strength exceeding 17 MPa, meeting the criteria for structural lightweight concrete. Durability tests, including alkali-silica reactivity (ASR) and thermogravimetric analysis (TGA), confirmed the non-reactive behavior of foam glass aggregates, ensuring long-term performance. This research establishes foam glass as a viable alternative to natural aggregates, contributing to sustainable construction practices while maintaining structural integrity and reducing material weight.

1. Introduction

The construction industry is increasingly focusing on sustainable practices, particularly in the development of environmentally friendly building materials that minimize resource consumption and reduce waste [1–4]. Lightweight concrete (LWC) has emerged as a promising solution, valued for its reduced bulk density, thermal insulation properties, and potential for decreasing structural loads [1, 5–7]. However, the widespread production of LWC often relies on synthetic and natural aggregates that may not always align with sustainability goals [8–10]. In response, recent research has explored alternative aggregates derived from recycled materials, with glass waste showing significant potential for producing lightweight aggregates (LWA) suitable for LWC [11–17].

Glass waste, primarily derived from packaging, automotive, and demolition industries, represents a major global waste stream that poses significant disposal and environmental challenges due to its non-degradable nature [18,19]. Traditionally, only a fraction of this waste is recycled, with most discarded in landfills, where it occupies considerable space and risks contaminating soil and water [8,20].

References

1. Thienel, K.C., T. Haller, and N. Beuntner, Lightweight Concrete-From Basics to Innovations. Materials (Basel), 2020. 13(5): p. 1120, DOI: 10.3390/ma13051120. URL: https://www.ncbi.nlm.nih.gov/pubmed/32138207.

2. Newman, J. and P. Owens, Properties of lightweight concrete. Advanced concrete technology, 2003. 3: p. 1-29, DOI: 10.1016/b978-075065686-3/50288-3

3. Li, N., et al., Molding Process Effects on Compressive Strength and Permeability Coefficient of Non-fine Concrete and Its Evaluation Method. International Journal of Science and Research, 2010. 10(4): p. 129-137, DOI: 10.21275/v5i6.nov164304

4. Gu, K., et al., Experimental Study of the Bulge Deformation of Anti-Seepage Geomembranes over Non-Fine Concrete. KSCE Journal of Civil Engineering, 2020. 24(9): p. 2591-2598, DOI: 10.1007/s12205-020-1737-z

5. Chandra, S. and L. Berntsson, Lightweight aggregate concrete. 2002: Elsevier, DOI: 10.1016/S0008-8846(02)00903-1.

6. Clarke, J.L., Structural lightweight aggregate concrete. 1993, DOI: 10.1201/9781482269307-8

7. Agrawal, Y., et al., A comprehensive review on the performance of structural lightweight aggregate concrete for sustainable construction. Construction Materials, 2021. 1(1): p. 39-62, DOI: 10.3390/constrmater1010003

8. Maghfouri, M., et al., Drying shrinkage properties of expanded polystyrene (EPS) lightweight aggregate concrete: A review. Case Studies in Construction Materials, 2022. 16, DOI: 10.1016/j.cscm.2022.e00919

9. pintrest. Foamed Light Weight Concrete - Applications and Advantages. 2021 09 February2024]; Available from: https://www.pinterest.com/pin/foamed-cellular-light-weight-concrete-applications-and-advantages--546905948510844324/.

10. ltd., i.l. no fine concrete. 2023 24 May 2024]; Available from: http://www.idmagroup.co.in/civil.html.

11. Ltd, S.R.M.C.I.P. lightweight concrete. 2023 11 October 2023]; Available from: https://shubhamrmc.com/.

12. Kan, A. and R. Demirboğa, A novel material for lightweight concrete production. Cement and Concrete Composites, 2009. 31(7): p. 489-495, DOI: 10.1016/j.cemconcomp.2009.05.002

13. Holm, T.A. and J.P. Ries, Lightweight concrete and aggregates, in Significance of tests and properties of concrete and concrete-making materials. 2006, ASTM International, DOI: 10.1520/stp37764s

14. Chen, B. and N. Liu, A novel lightweight concrete-fabrication and its thermal and mechanical properties. Construction and building materials, 2013. 44: p. 691-698, DOI: 10.1016/j.conbuildmat.2013.03.091

15. Farina, I., et al., Compressive and Thermal Properties of Non-Structural Lightweight Concrete Containing Industrial Byproduct Aggregates. Materials (Basel), 2022. 15(11): p. 4029, DOI: 10.3390/ma15114029 URL: https://www.ncbi.nlm.nih.gov/pubmed/35683327.

16. Shahpari, M., P. Bamonte, and S.J. Mosallam, An experimental study on mechanical and thermal properties of structural lightweight concrete using carbon nanotubes (CNTs) and LECA aggregates after exposure to elevated temperature. Construction and Building Materials, 2022. 346: p. 128376, DOI: 10.1016/j.conbuildmat.2022.128376

17. Kumar, D., M. Alam, and A.J. Doshi, Investigating the Influence of Thermal Conductivity and Thermal Storage of Lightweight Concrete Panels on the Energy and Thermal Comfort in Residential Buildings. Buildings, 2023. 13(3): p. 720, DOI: 10.3390/buildings13030720

18. Dabbaghi, F., et al., Optimization of Concrete Mixtures Containing Lightweight Expanded Clay Aggregates Based on Mechanical, Economical, Fire-Resistance, and Environmental Considerations. Journal of Materials in Civil Engineering, 2022. 34(2): p. 04021445, DOI: 10.1061/(asce)mt.1943-5533.0004083

19. Bao, J., et al., A state-of-the-art review on high temperature resistance of lightweight aggregate high-strength concrete. Journal of Building Engineering, 2023: p. 106267, DOI: 10.1016/j.jobe.2023.106267

20. Koksal, F., et al., Insulating and fire-resistance performance of calcium aluminate cement based lightweight mortars. Construction and Building Materials, 2023. 362: p. 129759, DOI: 10.1016/j.conbuildmat.2022.129759

21. Amran, M., et al., An ultra-lightweight cellular concrete for geotechnical applications–A review. Case Studies in Construction Materials, 2022. 16: p. e01096, DOI: 10.1016/j.cscm.2022.e01096

22. Assaad, J.J., C. Mikhael, and R. Hanna, Recycling of waste expanded polystyrene concrete in lightweight sandwich panels and structural applications. Cleaner Materials, 2022. 4: p. 100095, DOI: 10.1016/j.clema.2022.100095

23. Smoczkiewicz-Wojciechowska, A., et al., The study on possible applications of lightweight concrete based on waste aggregate in terms of compressive strength and thermal insulation properties. Polish Journal of Environmental Studies, 2022. 31(1): p. 833-841,

24. Wang, F., et al., Study of the structural-functional lightweight concrete containing novel hollow ceramsite compounded with paraffin. Construction and Building Materials, 2022. 342: p. 127954,

25. Islam, M.M.U., et al., Design and strength optimization method for the production of structural lightweight concrete: An experimental investigation for the complete replacement of conventional coarse aggregates by waste rubber particles. Resources, Conservation and Recycling, 2022. 184: p. 106390,

26. Bejan, G., et al., Lightweight concrete with waste-review. Procedia Manufacturing, 2020. 46: p. 136-143, DOI: 10.1016/j.promfg.2020.03.021

27. Hassan, M.K., et al., Experimental study on lightweight concrete made with expanded clay aggregate and lime. Innovative Infrastructure Solutions, 2021. 6: p. 1-11,

28. Vakhshouri, B. and S. Nejadi, Review on the mixture design and mechanical properties of the lightweight concrete containing expanded polystyrene beads. Australian Journal of Structural Engineering, 2018. 19(1): p. 1-23,

29. Vijayan, D., et al. Natural aggregates used for Light weight concrete–A Review. in IOP Conference Series: Materials Science and Engineering. 2020. IOP Publishing,

30. Chica, L. and A. Alzate, Cellular concrete review: New trends for application in construction. Construction and Building Materials, 2019. 200: p. 637-647, DOI: 10.1016/j.conbuildmat.2018.12.136

31. Mo, K.H., et al., Overview of supplementary cementitious materials usage in lightweight aggregate concrete. Construction and Building Materials, 2017. 139: p. 403-418,

32. Rhishi, R.K. and R. Vasudev, A review on the effects of artificial light weight aggregate in concrete. Sustainability, Agri, Food and Environmental Research, 2022. 10,

33. Banawair, A., et al. The strength of lightweight aggregate in concrete–A Review. in IOP Conference Series: Earth and Environmental Science. 2019. IOP Publishing,

34. E Njoku, C., et al., Natural fibers as viable sources for the development of structural, semi-structural, and technological materials–a review. Advanced Materials Letters, 2019. 10(10): p. 682-694, DOI: 10.5185/amlett.2019.9907.

35. Kovler, K. and N. Roussel, Properties of fresh and hardened concrete. Cement and Concrete Research, 2011. 41(7): p. 775-792,

36. Nadh, V.S. and K. Muthumani, Critical review on structural light weight concrete. International Journal of Civil Engineering and Technology, 2017. 8(2): p. 111-127,

37. Adhikary, S.K., D.K. Ashish, and Ž. Rudžionis, Expanded glass as light-weight aggregate in concrete–A review. Journal of Cleaner Production, 2021. 313: p. 127848, DOI: 10.1016/j.jclepro.2021.127848

38. Zorić, D., et al., Thermal conductivity of lightweight aggregate based on coal fly ash. Journal of thermal analysis and calorimetry, 2012. 110(1): p. 489-495,

39. ltd., F.g. foam glass block. 2023 16 Jun 2023]; Available from: https://www.foamglas.com.

40. company, R.m. Foam glass pipe support. 2020 10 September 2024]; Available from: https://www.rilco.com/products/foamglas.

41. surowce, R. foam glass granules. 2022 18 September 2024]; Available from: https://pph-rewa.pl.

42. ltd., B.a.p. Foam glass insulator. 2024 10 October 2024]; Available from: https://bellis.com.au.

43. Rabinovich, E., Preparation of glass by sintering. Journal of Materials Science, 1985. 20(12): p. 4259-4297,

44. Scarinci, G., G. Brusatin, and E. Bernardo, Glass foams. Cellular ceramics: structure, manufacturing, properties and applications. 2005. 158-176, URL: https://www.wiley.com/en-us/Cellular+Ceramics%3A+Structure%2C+Manufacturing%2C+Properties+and+Applications-p-9783527313204.

45. Corning, P. and P.C. Europe, Foamglas industrial insulation handbook. 1992: Editions TECHNIP,

46. Fedosov, S.V., M.O. Bakanov, and S.N. Nikishov, Study and simulation of heat transfer processes during foam glass high temperature processing. International Journal for Computational Civil and Structural Engineering, 2018. 14(3): p. 153-160, DOI: 10.22337/2587-9618-2018-14-3-153-160

47. Janetti, M.B., et al., Thermal Conductivity of Foam Glass Gravels: A Comparison between Experimental Data and Numerical Results. Energy Procedia, 2015. 78: p. 3258-3263, DOI: 10.1016/j.egypro.2015.11.713.

48. Manevich, V. and K.Y. Subbotin, Foam glass and problems of energy conservation. Glass and Ceramics, 2008. 65(3): p. 105-108,

49. Kim, D.-S., et al., Effect of furnace atmosphere on E-glass foaming. Journal of non-crystalline solids, 2006. 352(50-51): p. 5287-5295,

50. Bernardo, E., G. Scarinci, and S. Hreglich, Foam glass as a way of recycling glasses from cathode ray tubes. Glass science and technology (Frankfurt), 2005. 78(1): p. 7-11,

51. Sassi, M., et al., Effect of microstructure on the physicochemical characteristics of foam glass made by soda lime-CRT glasses and aluminium dross. Ceramics International, 2024. 50(19): p. 37085-37095,

52. Bubeník, J. and J. Zach, The use of foam glass based aggregates for the production of ultra-lightweight porous concrete for the production of noise barrier wall panels. Transportation Research Procedia, 2019. 40: p. 639-646, DOI: 10.1016/j.trpro.2019.07.091.

53. Yan, Z., et al., Effect of high titanium blast furnace slag on preparing foam glass–ceramics for sound absorption. Journal of Porous Materials, 2019. 26(4): p. 1209-1215, DOI: 10.1007/s10934-019-00722-0.

54. Liu, Y., et al., Study on factors affecting properties of foam glass made from waste glass. Journal of Renewable Materials, 2021. 9(2): p. 237, DOI: 10.32604/jrm.2021.012228

55. Lim, T.-Y., et al., A study on the fabrication of foamed glass by using refused coal ore and its physical properties. Journal of the Korean Crystal Growth and Crystal Technology, 2011. 21(6): p. 266-273,

56. Lv, D.S., et al. Effect of carbon as foaming agent on pore structure of foam glass. in Advanced Materials Research. 2010. Trans Tech Publ,

57. König, J., R.R. Petersen, and Y. Yue, Influence of the glass particle size on the foaming process and physical characteristics of foam glasses. Journal of Non-Crystalline Solids, 2016. 447: p. 190-197,

58. Ducman, V. and M. Kovacevic, The foaming of waste glass, in Euro ceramics V : extended abstracts of the 5th conference and exhibition of the European Ceramics Society 1997, Trans Tech Publications, Aedermannsdorf: Groupe français de la céramique, Paris, France

59. Ketov, A., An experience of reuse of a glass cullet for production of foam structure material, in Recycling and Reuse of Glass Cullet. 2001, Thomas Telford Publishing. p. 85-91,

60. König, J., R.R. Petersen, and Y. Yue, Influence of the glass–calcium carbonate mixture's characteristics on the foaming process and the properties of the foam glass. Journal of the European Ceramic Society, 2014. 34(6): p. 1591-1598, DOI: 10.1016/j.jeurceramsoc.2013.12.020.

61. Scheffler, M. and P. Colombo, Cellular ceramics: structure, manufacturing, properties and applications. 2006: John Wiley & Sons, URL: https://www.wiley.com/en-us/Cellular+Ceramics%3A+Structure%2C+Manufacturing%2C+Properties+and+Applications-p-9783527313204.

62. Schumacher, K., et al., Lightweight aggregate concrete with an open structure and a porous matrix with an improved ratio of compressive strength to dry density. Construction Building Materials 2020. 264: p. 120167, DOI: 10.1016/j.conbuildmat.2020.120167

63. Velez, M., J. Smith, and R. Moore, Refractory degradation in glass tank melters. A survey of testing methods. Ceramica, 1997. 43: p. 180-184,

64. Spiridonov, Y.A. and L.A. Orlova, Problems of Foam Glass Production. Glass and Ceramics, 2003. 60(9/10): p. 313-314, DOI: 10.1023/B:GLAC.0000008234.79970.2c.

65. Mear, F., et al., Mechanical behaviour and thermal and electrical properties of foam glass. Ceramics international, 2007. 33(4): p. 543-550,

66. Attila, Y., Foaming of waste glass of a glass polishing factory. 2012: Izmir Institute of Technology (Turkey),

67. Fernandes, H.R., et al., The use of egg shells to produce Cathode Ray Tube (CRT) glass foams. Ceramics international, 2013. 39(8): p. 9071-9078, DOI: 10.1016/j.ceramint.2013.05.002

68. Francis, A., M.A. Rahman, and A. Daoud, Processing, structures and compressive properties of porous glass-ceramic composites prepared from secondary by-product materials. Ceramics international, 2013. 39(6): p. 7089-7095,

69. Wu, L., et al. Effect of foaming temperature and holding time on foam glass. in Advanced Materials Research. 2013. Trans Tech Publ,

70. Abbasi, S., et al., The effects of Fe_2O_3 and Co_3O_4 on microstructure and properties of foam glass from soda lime waste glasses. Glass Physics and Chemistry, 2014. 40(2): p. 173-179, DOI: 10.1134/s1087659614020023

71. Ding, L., et al., Preparation and characterization of glass–ceramic foams from blast furnace slag and waste glass. Materials Letters, 2015. 141: p. 327-329, DOI: 10.1016/j.matlet.2014.11.122

72. da Silva, R.C., et al., Recycling of glass waste into foam glass boards: A comparison of cradle-to-gate life cycles of boards with different foaming agents. Science of The Total Environment, 2021. 771: p. 145276, DOI: 10.1016/j.scitotenv.2021.145276

73. Karlsson, S., Viscosity of alumina doped soda lime silicate glasses–observation of anomaly in the linear increase as Al_2O_3 replaces SiO_2. Journal of Non-Crystalline Solids, 2021. 573: p. 121149,

74. Sassi, M. and A. Simon, Waste-to-Reuse Foam Glasses Produced from Soda-Lime-Silicate Glass, Cathode Ray Tube Glass, and Aluminium Dross. Inorganics, 2021. 10(1): p. 1, DOI: 10.3390/inorganics10010001.

75. Owoeye, S.S., et al., Preparation and characterization of foam glass from waste container glasses and water glass for application in thermal insulations. Ceramics International, 2020. 46(8): p. 11770-11775, DOI: 10.1016/j.ceramint.2020.01.211.

76. Saparuddin, D.I., et al., Effect of sintering temperature on the crystal growth, microstructure and mechanical strength of foam glass-ceramic from waste materials. Journal of Materials Research and Technology, 2020. 9(3): p. 5640-5647, DOI: 10.1016/j.jmrt.2020.03.089.

77. Bernardo, E., et al., Reutilization and stabilization of wastes by the production of glass foams. Ceramics International, 2007. 33(6): p. 963-968, DOI: 10.1016/j.ceramint.2006.02.010

78. Yuan, H., H. Wu, and J. Guan. Synthesis of foam glass-ceramic from CRT panel glass using one-step powder sintering. in IOP Conference Series: Earth and Environmental Science. 2018. IOP Publishing,

79. Ali, S.I. and Z. Szalay, Overview and analysis of the overheating effect in modern Sudanese buildings. Pollack Periodica, 2020. 15(3): p. 208-219, DOI: 10.1556/606.2020.15.3.20

80. Fernandes, H.R., D.U. Tulyaganov, and J.M.F. Ferreira, Preparation and characterization of foams from sheet glass and fly ash using carbonates as foaming agents. Ceramics International, 2009. 35(1): p. 229-235, DOI: 10.1016/j.ceramint.2007.10.019. URL: https://doi.org/10.1016/j.ceramint.2007.10.019.

81. Dragoescu, M.F., et al., Foam glass with low apparent density and thermal conductivity produced by microwave heating. Eur. J. Eng. Technol, 2018. 6,

82. Souza, M.T., et al., Glass foams produced from glass bottles and eggshell wastes. Process Safety and Environmental Protection, 2017. 111: p. 60-64,

83. Brusatin, G., E. Bernardo, and G. Scarinci, Production of foam glass from glass waste, in Sustainable Waste Management and Recycling: Glass Waste. 2004, Thomas Telford Publishing. p. 67-82, DOI: 10.1680/cdw.32859

84. Davraz, M., et al., An investigation of foaming additives and usage rates in the production of ultra-light foam glass. Journal of Thermal Analysis and Calorimetry, 2022. 147(5): p. 3567-3576, DOI: 10.1007/s10973-021-10781-8

85. Viktorovna, S.T., Thermal conductivity of highly porous materials. Vestnik MGSU, 2013. 7(3): p. 108-114, DOI: https://doi.org/10.1557/jmr.2013.179

86. Bernardo, E. and F. Albertini, Glass foams from dismantled cathode ray tubes. Ceramics international, 2006. 32(6): p. 603-608, DOI: 10.1016/j.ceramint.2005.04.019

87. Guo, H., Y. Gong, and S. Gao, Preparation of high strength foam glass–ceramics from waste cathode ray tube. Materials letters, 2010. 64(8): p. 997-999,

88. Bai, J., et al., Preparation of foam glass from waste glass and fly ash. Materials Letters, 2014. 136: p. 52-54, DOI: 10.1016/j.matlet.2014.07.028.

89. Yin, H., et al., Fabrication of foam glass from iron tailings. Materials Letters, 2016. 185: p. 511-513,

90. Osfouri, M. and A. Simon, Study on the thermal conductivity and density of foam glass. Pollack Periodica, 2022. 18(1): p. 126-131, DOI: 10.1556/606.2022.00591.

91. García-Ten, J., et al., Glass foams from oxidation/reduction reactions using SiC, Si3N4 and AlN powders. Glass Technology-European Journal of Glass Science and Technology Part A, 2011. 52(4): p. 103-110,

92. Llaudis, A.S., et al., Foaming of flat glass cullet using Si3N4 and MnO2 powders. Ceramics international, 2009. 35(5): p. 1953-1959,

93. Guo, Y., et al., Novel glass ceramic foams materials based on polishing porcelain waste using the carbon ash waste as foaming agent. Construction and Building Materials, 2016. 125: p. 1093-1100,

94. Lee, C.-T., Production of alumino-borosilicate foamed glass body from waste LCD glass. Journal of Industrial and Engineering Chemistry, 2013. 19(6): p. 1916-1925,

95. Semukhin, B., A. Votinov, and O. Kazmina, PROPERTIES OF FOAMGLASS WITH FULLERENE-LIKE MESOSTRUCTURE. Russian Physics Journal, 2020. 63(4): p. 710-713,

96. Østergaard, M.B., et al., Effect of alkali phosphate content on foaming of CRT panel glass using Mn3O4 and carbon as foaming agents. Journal of Non-Crystalline Solids, 2018. 482: p. 217-222,

97. König, J., R.R. Petersen, and Y. Yue, Fabrication of highly insulating foam glass made from CRT panel glass. Ceramics International, 2015. 41(8): p. 9793-9800, DOI: 10.1016/j.ceramint.2015.04.051.

98. Khamidulina, D., S. Nekrasova, and K. Voronin. Foam glass production from waste glass by compression. in IOP Conference Series: Materials Science and Engineering. 2017. IOP Publishing,

99. Suslyaev, V., et al., Electrophysical characteristics of a foam glass crystal material. Russian Physics Journal, 2014. 56(9): p. 990-996,

100. Fokin, V.M., et al., Homogeneous crystal nucleation in silicate glasses: A 40 years perspective. Journal of Non-Crystalline Solids, 2006. 352(26-27): p. 2681-2714,

101. Karandashova, N., B. Goltsman, and E. Yatsenko. Analysis of influence of foaming mixture components on structure and properties of foam glass. in IOP Conference Series: Materials Science and Engineering. 2017. IOP Publishing,

102. Udayakumar, M., et al., Composite Carbon Foams as an Alternative to the Conventional Biomass-Derived Activated Carbon in Catalytic Application. Materials, 2021. 14(16): p. 4540,

103. Jiang, K., et al., Formation of closed pore structure in CaO-MgO-Al2O3-SiO2 (CMAS) porous glass-ceramics via Fe2O3 modified foaming for thermal insulation. Journal of the European Ceramic Society, 2022,

104. Ma, Q., et al. Preparation of high strength and low-cost glass ceramic foams with extremely high coal fly ash content. in IOP Conference Series: Materials Science and Engineering. 2018. IOP Publishing,

105. Kaz'mina, O. and V. Vereshchagin, Physicochemical modeling of composition of foam glass-crystal materials. Glass Physics and Chemistry, 2015. 41: p. 122-126,

106. Kazmina, O. and B. Semukhin, Foam-Glass-Crystal Materials, in Structural Nanocomposites: Perspectives for Future Applications. 2013, Springer. p. 143-164, DOI: 10.1007/978-3-642-40322-4_6

107. Saparuddin, D.I., et al., Effect of sintering temperature on the crystal growth, microstructure and mechanical strength of foam glass-ceramic from waste materials. Journal of Materials Research and Technology, 2020. 9(3): p. 5640-5647,

108. Thenmuhil, D., K. Vignaswaran, and T. Pavithra, Preparation of Wollastonite from Used Plaster of Paris and Quartz through Solid-State Reaction, in International Conference on Multidisciplinary Research & Practice. 2020, IJRSI. p. 540-543

109. Casasola, R., J.M. Rincón, and M. Romero, Glass–ceramic glazes for ceramic tiles: a review. Journal of Materials Science, 2012. 47: p. 553-582, DOI: 10.1007/s10853-011-5981-y

110. pintrest. Material information-Wollastonite. 2020 11 October 2024]; Available from: https://www.pinterest.com/pin/454582156143702822/.

111. Zanotto, E.D., Bright future for glass-ceramics. American Ceramics Society Bulletin, 2010. 89(8): p. 19-27,

112. Zanotto, E.D., Glass crystallization research–A 36-Year retrospective. Part II, methods of study and glass-ceramics. International Journal of Applied Glass Science, 2013. 4(2): p. 117-124,

113. DeCeanne, A.V., et al., Examining the role of nucleating agents within glass-ceramic systems. Journal of Non-Crystalline Solids, 2022. 591: p. 121714, DOI: 10.1016/j.jnoncrysol.2022.121714

114. Ojovan, M.I. and S.V. Yudintsev, Glass, ceramic, and glass-crystalline matrices for HLW immobilisation. Open Ceramics, 2023. 14: p. 100355,

115. Wang, H., et al., A novel and clean utilization of multiple solid wastes to produce foam glass-ceramic. Construction and Building Materials, 2023. 370: p. 130711,

116. Zhang, J., B. Liu, and S. Zhang, A review of glass ceramic foams prepared from solid wastes: Processing, heavy-metal solidification and volatilization, applications. Sci Total Environ, 2021. 781: p. 146727, DOI: 10.1016/j.scitotenv.2021.146727. URL: https://www.ncbi.nlm.nih.gov/pubmed/33812111.

117. Bernardo, E., G. Scarinci, and S. Hreglich, Foam glass as a way of recycling glasses from cathode ray tubes. Glass Science and Technology, 2005. 78(1): p. 7-11, DOI: 10.1016/j.ceramint.2005.04.019

118. Ibrahim, J.E.F., et al., Innovative glass-ceramic foams prepared by alkali activation and reactive sintering of clay containing zeolite (zeolite-poor rock) and sawdust for thermal insulation. Journal of Building Engineering, 2022. 59: p. 105160, DOI: 10.1016/j.jobe.2022.105160

119. Hesky, D., et al., Water and waterglass mixtures for foam glass production. Ceramics International, 2015. 41(10): p. 12604-12613, DOI: 10.1016/j.ceramint.2015.06.088

120. Goyal, S. and I.B. Cutler, Absorption of water in waste glass as a precursor for foam formation, in Glass Surfaces. 1975, Elsevier. p. 311-320,

121. Yatsenko, E.A., et al., Peculiarities of foam glass synthesis from natural silica-containing raw materials. Journal of Thermal Analysis and Calorimetry, 2020. 142: p. 119-127,

122. Silverman, A., Glass: Historical notes 1900 to 1950. Journal of Chemical Education, 1953. 30(1): p. 32, DOI: 10.1021/ed030p32.

123. Shuster, R.L., Experience in the utilization of foam glass wastes. Glass and Ceramics, 1956. 13(9): p. 417-417, DOI: 10.1007/bf00669461.

124. Berke, N., Microsilica and concrete durability. Transportation Research Record, 1988. 1204: p. 21-26, URL: https://onlinepubs.trb.org/Onlinepubs/trr/1988/1204/1204-004.pdf.

125. Corigliano, A., E. Rizzi, and E. Papa, Experimental characterization and numerical simulations of a syntactic-foam/glass-fibre composite sandwich. Composites Science and Technology, 2000. 60(11): p. 2169-2180, DOI: 10.1016/s0266-3538(00)00118-4.

126. Nemes, R. and Z. Józsa, Strength of lightweight glass aggregate concrete. Journal of materials in civil engineering, 2006. 18(5): p. 710-714, DOI: https://doi.org/10.1061/(ASCE)0899-1561(2006)18:5(710).

127. Atrushi, D.S., Structural behavior of reinforced concrete beams incorporating foamed glass as aggregates. ARO-The Scientific Journal of Koya University, 2021. 9(1): p. 40-50, DOI: 10.14500/aro.10746

128. Bubeník, J., et al., Behavior and properties of ultra-lightweight concrete with foamed glass aggregate and cellulose fibres under high temperature loading. Journal of Building Engineering, 2023. 72: p. 106677, DOI: 10.1016/j.jobe.2023.106677

129. Sharma, L., N. Taak, and M. Bhandari, Influence of ultra-lightweight foamed glass aggregate on the strength aspects of lightweight concrete. Materials Today: Proceedings, 2021. 45: p. 3240-3246,

130. Mustafa, W.S. and J. Szendefy, Effect of Static Loading States on the Compressional Behavior of Foam Glass Aggregate. Periodica Polytechnica Civil Engineering, 2023. 67(4): p. 1203-1213,

131. Mustafa, W.S., J. Szendefy, and B. Nagy, Thermal performance of foam glass aggregate at different compaction ratios. Buildings, 2023. 13(7): p. 1844,

132. Nguyen, D., Performance of granulated foam glass aggregates in concrete. 2023,

133. Marinov, M., L. Lakov, and T. Kr, Granulated foam glass. Production, physical and mechanical properties. Machines. Technologies. Materials., 2016. 10(12): p. 42-44, URL: https://stumejournals.com/journals/mtm/2016/12/42.

134. Nikolenko, S., et al. Dust cleaning of working areas in the production of granulated foam glass ceramics. in AIP Conference Proceedings. 2021. AIP Publishing LLC, DOI: https://doi.org/10.1063/5.0072038.

135. Gol'tsman, B.M. and E.A. Yatsenko, Modern Methods for Foaming of Glass and Silicate Raw Materials: Review and Analysis. Theoretical Foundations of Chemical Engineering, 2022. 56(5): p. 678-686, DOI: 10.1134/s0040579522050232.

136. Savić, V., et al. Recycling of glass waste into foam glass: A review. in 9th International Conference Mining and Environmental Protection MEP-23. 2023. Belgrade: University of Belgrade, Faculty of Mining and Geology, URL: https://ritnms.itnms.ac.rs/handle/123456789/784.

137. Mustafa, W.S., B. Nagy, and J. Szendefy, Impact of compaction ratio and loading period on compressional behavior of foam glass aggregates. Construction and Building Materials, 2022. 343(1): p. 128111, DOI: 10.1016/j.conbuildmat.2022.128111.

138. Osfouri, M. and A. Simon, The detection of porous media volume using the modified Archimedes method. Epitoanyag - Journal of Silicate Based and Composite Materials, 2023. 75(2): p. 48-51, DOI: 10.14382/epitoanyag-jsbcm.2023.07.

139. Papadopoulos, A.M., State of the art in thermal insulation materials and aims for future developments. Energy and Buildings, 2005. 37(1): p. 77-86, DOI: 10.1016/j.enbuild.2004.05.006.

140. Siddika, A., A. Hajimohammadi, and V. Sahajwalla, Powder sintering and gel casting methods in making glass foam using waste glass: A review on parameters, performance, and challenges. Ceramics International, 2022. 48(2): p. 1494-1511, DOI: 10.1016/j.ceramint.2021.10.066.

141. Spiridonov, Y.A. and L. Orlova, Problems of foam glass production. Glass and ceramics, 2003. 60(9-10): p. 313-314, DOI: 10.1023/B:GLAC.0000008234.79970.2c.

142. Wang, W., J. Chi, and S. Niu. On the Application of foam Glass in Interior Design. in E3S Web of Conferences. 2023. EDP Sciences, DOI: https://doi.org/10.1051/e3sconf/202340604033

143. Lebullenger, R., et al., Glass foams for environmental applications. Journal of Non-Crystalline Solids, 2010. 356(44-49): p. 2562-2568, DOI: 10.1016/j.jnoncrysol.2010.04.050.

144. SOOKSAEN, P., et al., Fabrication of granular foam glass aggregates from soda lime silicate glass waste. Journal of Metals, Materials and Minerals, 2023. 33(4): p. 1671-1671,

145. Shi, X., et al., Utilizing multi-solid waste to prepare and characterize foam glass ceramics. Ceramics International, 2023. 49(22): p. 35534-35543, DOI: 10.1016/j.ceramint.2023.08.232.

146. Bessonov, I., et al. Lightweight concrete based on crushed foam glass aggregate. in IOP Conference Series: Materials Science and Engineering. 2021. IOP Publishing, DOI: 10.1088/1757-899X/1083/1/012038.

147. Chahour, K., et al., Granulated foam glass based on mineral wastes used for building materials. Building Acoustics, 2017. 24(4): p. 281-294, DOI: 10.1177/1351010x17739434.

148. Zach, J., et al., Development of Light-Weight Concrete with Utilization of Foam Glass Based Aggregate. Solid State Phenomena, 2018. 276: p. 276-281, DOI: 10.4028/www.scientific.net/SSP.276.276.

149. Asztalos, F. and I. Kocserha. Laminar foam glass as a lightweight concrete aggregate. in Journal of Physics: Conference Series. 2020. IOP Publishing, DOI: 10.1088/1742-6596/1527/1/012041.

150. Sedlmajer, M., J. Zach, and J. Bubeník. Utilization and study of lightweight concrete properties with foam glass-based aggregate in the field of civil engineering. in AIP Conference Proceedings. 2023. AIP Publishing, DOI: https://doi.org/10.1063/5.0136923

151. Kasperkiewicz, J., A review of concrete mix design methods. Optimization methods for material design of cement-based composites, 1998: p. 60-114,

152. Shafigh, P., M.Z. Jumaat, and H. Mahmud, Mix design and mechanical properties of oil palm shell lightweight aggregate concrete: a review. International journal of the physical sciences, 2010. 5(14): p. 2127-2134,

153. Wattanasiriwech, D., et al. Foam glass from municipal waste as a lightweight aggregate for cement mortar. in IOP conference series: earth and environmental science. 2019. IOP Publishing, DOI: DOI: 10.1088/1755-1315/351/1/012008

154. Smirnov, Y.M., et al., Energetics Metrics for Foam-Glass Concrete Building Products. Glass and Ceramics, 2020. 77: p. 267-271,

155. Šeputytė-Jucikė, J., et al., Evaluation of the Effect of the Composition of the Foam Glass Concrete on Its Flammability and Moisture Characteristics. Journal of Composites Science, 2024. 8(3): p. 105,

156. Mohammed, S.K. and R. Géber, Production of lightweight geopolymer concrete with foam glass aggregate derived from cathode-ray glass waste. Case Studies in Construction Materials, 2024: p. e03888,

157. da Silva Fernandes, F.A., et al., Glass foams produced from soda-lime glass waste and rice husk ash applied as partial substitutes for concrete aggregates. Process Safety and Environmental Protection, 2019. 128: p. 77-84, DOI: 10.1016/j.psep.2019.05.044.

158. Gopinath, S., et al., Optimised Mix Design for Normal Strength and High Performance Concrete Using Particle Packing Method. Archives of Civil Engineering, 2011. 57(4): p. 357-371, DOI: 10.2478/v.10169-011-0026-0.

159. Sohail, M.G., et al., Advancements in concrete mix designs: high-performance and ultrahigh-performance concretes from 1970 to 2016. Journal of Materials in Civil Engineering, 2018. 30(3): p. 04017310, DOI: https://doi.org/10.1061/(ASCE)MT.1943-5533.000214.

160. Ashish, D.K. and S.K. Verma, An overview on mixture design of self-compacting concrete. Structural Concrete, 2018. 20(1): p. 371-395, DOI: 10.1002/suco.201700279.

161. Deshpande, V.D., P. Pawade, and K. Dabhekar. A review on self compacting concrete with metakaolin and fly ash as partial replacement. in AIP Conference Proceedings. 2023. AIP Publishing, DOI: 10.1063/5.0144143

162. Murthy, N.K., et al., Mix Design procedure for self-compacting concrete. IOSR Journal of Engineering, 2012. 2(9): p. 33-41,

163. Meng, D., et al., A strength-based mix design method for recycled aggregate concrete and consequent durability performance. Construction and Building Materials, 2021. 281: p. 122616,

164. Kumbhar, P.D. and P.B. Murnael, Assessment of suitability of existing mix design methods of normal concrete for designing high performance concrete mixes. International Journal of Civil & Structural Engineering, 2012. 3(1): p. 158-167,

165. Kosmatka, S.H., B. Kerkhoff, and W. Panarese, Design and control of concrete mixtures 14th editi. Skokie, IL: Portland Cement Assosiation. 2003,

166. Barreto Santos, M., J. De Brito, and A. Santos Silva, A Review on Alkali-Silica Reaction Evolution in Recycled Aggregate Concrete. Materials (Basel), 2020. 13(11): p. 2625, DOI: 10.3390/ma13112625. URL: https://www.ncbi.nlm.nih.gov/pubmed/32526866.

167. Moreira, K.M.d.V., et al., Alkali-silica reaction: understanding the phenomenon. Journal of Building Pathology and Rehabilitation, 2021. 6(1): p. 5, DOI: 10.1007/s41024-020-00100-3.

168. Salim, M.U. and M.A. Mosaberpanah, The mechanism of alkali-aggregate reaction in concrete/mortar and its mitigation by using geopolymer materials and mineral admixtures: a comprehensive review. European Journal of Environmental and Civil Engineering, 2021. 26(14): p. 6766-6806, DOI: 10.1080/19648189.2021.1960899.

169. Torres-Carrasco, M. and F. Puertas, Alkaline activation of different aluminosilicates as an alternative to Portland cement: alkali activated cements. Revista ingenieria de construccion, 2017. 32(2): p. 5-12, DOI: https://doi.org/10.4067/S0718-50732017000200001

170. Selman, M.M. and A.M. Ali, The effect of alkalis on the properties of portland cement. Anbar J Eng Sci, 2012: p. 25-38,

171. Junsomboon, J. and J. Jakmunee, Determination of potassium, sodium, and total alkalies in portland cement, fly ash, admixtures, and water of concrete by a simple flow injection flame photometric system. J Autom Methods Manag Chem, 2011. 2011: p. 742656, DOI: 10.1155/2011/742656. URL: https://www.ncbi.nlm.nih.gov/pubmed/21747733.

172. Goethals, J., et al., Phenomenological description of the effect of glass dissolution on cement paste evolution in an integrated glass dissolution experiment. Applied Geochemistry, 2024. 168: p. 106012, DOI: 10.1016/j.apgeochem.2024.106012.

173. Balachandran, C., et al., A multianalytical approach to understand the relationship between ASR mitigation mechanisms of class F fly ash in highly reactive systems. Materials and Structures, 2024. 57(4): p. 62, DOI: 10.1617/s11527-024-02342-w.

174. Zapala-Slaweta, J., Impact of Aggregate Grain Size on ASR-Induced Expansion. Materials (Basel), 2023. 16(24): p. 7506, DOI: 10.3390/ma16247506. URL: https://www.ncbi.nlm.nih.gov/pubmed/38138653.

175. budov, T.z. ASR gel. 2024 10 October 2024]; Available from: https://m.tzb-info.cz.

176. Ma, P., et al., Characterization of alkali-silica reaction (ASR) products and C-S-H using SWIR spectroscopy for nondestructive detection of ASR. Construction and Building Materials, 2024. 416: p. 135207, DOI: 10.1016/j.conbuildmat.2024.135207.

177. Lu, G., et al., Adsorption and Desorption Characteristics of K+ and Na+ Ions in Fly Ash Blended Cement Pastes. Journal of Wuhan University of Technology-Mater. Sci. Ed., 2020. 35(3): p. 571-578, DOI: 10.1007/s11595-020-2294-5.

178. Wang, W. and T. Noguchi, Alkali-silica reaction (ASR) in the alkali-activated cement (AAC) system: A state-of-the-art review. Construction and Building Materials, 2020. 252: p. 119105, DOI: 10.1016/j.conbuildmat.2020.119105.

179. Leemann, A., Z. Shi, and J. Lindgård, Characterization of amorphous and crystalline ASR products formed in concrete aggregates. Cement and Concrete Research, 2020. 137: p. 106190, DOI: 10.1016/j.cemconres.2020.106190.

180. Hanson, W. Studies Relating To the Mechanism by Which the Alkali-Aggregate Reaction Produces EXPANSION IN CONCRETE. in Journal Proceedings. 1944. DOI: 10.14359/8657.

181. Mohammadi, A., E. Ghiasvand, and M. Nili, Relation between mechanical properties of concrete and alkali-silica reaction (ASR); a review. Construction and Building Materials, 2020. 258: p. 119567, DOI: 10.1016/j.conbuildmat.2020.119567.

182. Francklin, I., Jr., R.P. Ribeiro, and F.A. Correa, Quartzite Mining Waste: Diagnosis of ASR Alkali-Silica Reaction in Mortars and Portland Cement Concrete. Materials (Basel), 2021. 14(24): p. 7642, DOI: 10.3390/ma14247642. URL: https://www.ncbi.nlm.nih.gov/pubmed/34947240.

183. Strack, C.M., et al., Impact of aggregate mineralogy and exposure solution on alkali-silica reaction product composition and structure within accelerated test conditions. Construction and Building Materials, 2020. 240: p. 117929, DOI: 10.1016/j.conbuildmat.2019.117929.

184. Rajabipour, F., et al., Alkali–silica reaction: Current understanding of the reaction mechanisms and the knowledge gaps. Cement and Concrete Research, 2015. 76: p. 130-146, DOI: 10.1016/j.cemconres.2015.05.024.

185. Sanchez, L.F.M., et al., Condition assessment of an ASR-affected overpass after nearly 50 years in service. Construction and Building Materials, 2020. 236: p. 117554, DOI: 10.1016/j.conbuildmat.2019.117554.

186. Adesina, A.D., Influence of Moisture on Alkali Silica Reaction. 2016, Concordia University

187. Fairbairn, E.M.R., et al., Modelling the structural behaviour of a dam affected by alkali–silica reaction. Communications in Numerical Methods in Engineering, 2005. 22(1): p. 1-12, DOI: 10.1002/cnm.788.

188. Ekolu, S. Contribution to diagnosis of alkali-silica reaction in a bridge structure. in 2nd International Conference on Concrete Repair, Rehabilitation and Retrofitting, ICCRRR. 2009. DOI: 10.1201/9781439828403-93

189. De Ceukelaire, L. Alkali-silica reaction in a lightweight concrete bridge. in The 9th International Conference on Alkali-Aggregate Reaction in Concrete. 1992.

190. Diamond, S., Alkali silica reactions — Some paradoxes. Cement and Concrete Composites, 1997. 19(5-6): p. 391-401, DOI: 10.1016/s0958-9465(97)00004-8.

191. Figueira, R.B., et al., Alkali-silica reaction in concrete: Mechanisms, mitigation and test methods. Construction and Building Materials, 2019. 222: p. 903-931, DOI: 10.1016/j.conbuildmat.2019.07.230.

192. Helmuth, R., et al., Alkali-silica reactivity: an overview of research. Contract, 1993. 100: p. 202,

193. Lindgård, J., et al., Alkali–silica reactions (ASR): Literature review on parameters influencing laboratory performance testing. Cement and Concrete research, 2012. 42(2): p. 223-243,

194. Touma, W.E., et al., Characterizing Alkali-Silica Reactivity of Aggregates Using ASTM C 1293, ASTM C 1260, and Their Modifications. Transportation Research Record: Journal of the Transportation Research Board, 2001. 1757(1): p. 157-165, DOI: 10.3141/1757-18.

195. Shon, C.-S., D.G. Zollinger, and S.L. Sarkar, Evaluation of modified ASTM C 1260 accelerated mortar bar test for alkali–silica reactivity. Cement and Concrete Research, 2002. 32(12): p. 1981-1987, DOI: 10.1016/s0008-8846(02)00903-1.

196. Alexander, M.G., et al., Outdoor exposure site testing for preventing Alkali-Aggregate Reactivity in concrete – a review. MATEC Web of Conferences, 2018. 199, DOI: 10.1051/matecconf/201819903002

197. Ideker, J.H., et al., Preventing Alkali-Silica Reaction in Concrete. ce/papers, 2023. 6(6): p. 1101-1109, DOI: 10.1002/cepa.2935.

198. Tanesi, J., et al., Divergence between Performance in the Field and Laboratory Test Results for Alkali-Silica Reaction. Transportation Research Record: Journal of the Transportation Research Board, 2020. 2674(5): p. 120-134, DOI: 10.1177/0361198120913288.

199. Halsey, L. and W. Heyen, Evaluation of Nebraska's Aggregate Reactivity by the Miniature Concrete Prism Test Method–AASHTO T380. 2019,

200. Rønning, T.F., et al., Recommendation of RILEM TC 258-AAA: RILEM AAR-0 outline guide to the use of RILEM methods in the assessment of the alkali-reactivity potential of concrete. Materials and Structures, 2021. 54(6): p. 1-25, DOI: 10.1617/s11527-021-01687-w.

201. Krattiger, N., B. Lothenbach, and S.V. Churakov, Sorption and electrokinetic properties of ASR product and C-S-H: A comparative modelling study. Cement and Concrete Research, 2021. 146: p. 106491, DOI: 10.1016/j.cemconres.2021.106491.

202. Chappex, T. and K.L. Scrivener, The effect of aluminum in solution on the dissolution of amorphous silica and its relation to cementitious systems. Journal of the American Ceramic Society, 2013. 96(2): p. 592-597, DOI: 10.1111/jace.12098

203. Limbachiya, M., M.S. Meddah, and S. Fotiadou, Performance of granulated foam glass concrete. Construction and building materials, 2012. 28(1): p. 759-768,

204. Kazantseva, L. and I. Puzanov, Crystallization of the amorphous phase in foam glass as a method of decreasing the alkali-silicon reaction. Glass and Ceramics, 2016. 73: p. 77-81,

205. Mladenovič, A., et al., Alkali–silica reactivity of some frequently used lightweight aggregates. Cement and concrete research, 2004. 34(10): p. 1809-1816,

206. Gorospe, K., et al., Effect of various glass aggregates on the shrinkage and expansion of cement mortar. Construction and Building Materials, 2019. 210: p. 301-311,

207. Bai, W., et al., Study on mechanical properties and damage mechanism of alkali-activated slag concrete. Journal of Building Engineering, 2024. 96: p. 110357, DOI: 10.1016/j.jobe.2024.110357

208. Al-Otaibi, S., Durability of concrete incorporating GGBS activated by water-glass. Construction and building materials, 2008. 22(10): p. 2059-2067, DOI: 10.1016/j.conbuildmat.2007.07.023

209. Shi, C. On the state and role of alkalis during the activation of alkali-activated slag cement. in Proceedings of the 11th International Congress on the Chemistry of Cement. Durban (South Africa). 2003.

210. Shi, Z., et al., Comparison of alkali–silica reactions in alkali-activated slag and Portland cement mortars. Materials and Structures, 2015. 48: p. 743-751,

211. Shi, C., A.F. Jiménez, and A. Palomo, New cements for the 21st century: The pursuit of an alternative to Portland cement. Cement and concrete research, 2011. 41(7): p. 750-763,

212. Glasser, L.D. and N. Kataoka, On the role of calcium in the alkali-aggregate reaction. Cement and Concrete Research, 1982. 12(3): p. 321-331,

213. Gaboriaud, F., et al., Aggregation and gel formation in basic silico− calco− alkaline solutions studied: a SAXS, SANS, and ELS study. The Journal of Physical Chemistry B, 1999. 103(28): p. 5775-5781,

214. Leemann, A., et al., Alkali–silica reaction: the influence of calcium on silica dissolution and the formation of reaction products. Journal of the American Ceramic Society, 2011. 94(4): p. 1243-1249,

215. Urhan, S., Alkali silica and pozzolanic reactions in concrete. Part 1: Interpretation of published results and an hypothesis concerning the mechanism. Cement and concrete research, 1987. 17(1): p. 141-152,

216. Struble, L.J. and S. Diamond, Swelling properties of synthetic alkali silica gels. Journal of the American ceramic society, 1981. 64(11): p. 652-655,

217. Thomas, M. Microstructural studies of alkali-silica reaction in fly ash concrete. in Fuel and Energy Abstracts. 1996.

218. Vayghan, A.G., F. Rajabipour, and J.L. Rosenberger, Composition–rheology relationships in alkali–silica reaction gels and the impact on the gel's deleterious behavior. Cement and Concrete Research, 2016. 83: p. 45-56,

219. Wang, H. and J. Gillott, Mechanism of alkali-silica reaction and the significance of calcium hydroxide. Cement and Concrete Research, 1991. 21(4): p. 647-654,

220. Chatterji, S., et al., Studies of alkali-silica reaction. Part 3. Mechanisms by which NaCl and Ca (OH) 2 affect the reaction. Cement and concrete research, 1986. 16(2): p. 246-254, DOI: 10.1016/0008-8846(86)90141-9

221. Hou, X., et al., Structural investigations of alkali silicate gels. Journal of the American Ceramic Society, 2005. 88(4): p. 943-949,

222. Kim, T., J. Olek, and H. Jeong, Alkali–silica reaction: kinetics of chemistry of pore solution and calcium hydroxide content in cementitious system. Cement and Concrete Research, 2015. 71: p. 36-45,

223. STRUBLE, L.J., The influence of cement pore solution on alkali-silica reaction. 1987: Purdue University,

224. Pallagi, A., et al., The solubility of Ca (OH) 2 in extremely concentrated NaOH solutions at 25 C. Central European Journal of Chemistry, 2012. 10: p. 332-337,

225. Lei, J., W.W. Law, and E.-H. Yang, Effect of calcium hydroxide on the alkali-silica reaction of alkali-activated slag mortars activated by sodium hydroxide. Construction and Building Materials, 2021. 272: p. 121868,

226. Afshinnia, K. and P.R. Rangaraju, Influence of fineness of ground recycled glass on mitigation of alkali–silica reaction in mortars. Construction and Building Materials, 2015. 81: p. 257-267, DOI: 10.1016/j.conbuildmat.2015.02.041

227. Ukala, D., Effects of combined aggregate gradation on the compression strength and workability of concrete using fineness modulus. Journal of Applied Sciences and Environmental Management, 2019. 23(5): p. 851-856,

228. Ring, T.A., Fundamentals of ceramic powder processing and synthesis. 1996: Elsevier,

229. Fishburn, P.C., Utility theory for decision making. 1970, Research analysis corp McLean VA.10.21236/ad0708563

230. Hiramatsu, Y. and Y. Oka. Determination of the tensile strength of rock by a compression test of an irregular test piece. in International Journal of Rock Mechanics and Mining Sciences & Geomechanics Abstracts. 1966. Elsevier,

231. Prestera, J.R., et al., Standard Practice for Selecting Proportions for Structural Lightweight Concrete (ACI 211.2-98). 1998,

232. Al-Saudi, S.K.M. and R. Géber, Production of lightweight geopolymer concrete with foam glass aggregate derived from cathode-ray glass waste. Case Studies in Construction Materials, 2024. 21: p. e03888,

233. Lin, C.-C., et al., Elasticity and structure of the compounds in the wollastonite (CaSiO 3)–Na 2 SiO 3 system: from amorphous to crystalline state. Journal of Materials Science: Materials in Medicine, 2015. 26: p. 1-14,

234. Barsoum, M., Fundamentals of ceramics. 2019: CRC press,

235. Ligabue, M.L., et al., Innovative use of thermally treated cement-asbestos in the production of foaming materials: Effect of composition, foaming agent, temperature and reaction time. Construction and Building Materials, 2022. 335: p. 127517,

236. Al-Qasem, I.A., Effect of Glass Powder on the Mechanical Properties of Mortar. 2009, Master Thesis, Department of Civil Engineering, Jordan University of Science …

237. Cooper Jr, A. and W. Kingery, Dissolution in ceramic systems: I, molecular diffusion, natural convection, and forced convection studies of sapphire dissolution in calcium aluminum silicate. Journal of the American Ceramic Society, 1964. 47(1): p. 37-43, DOI: 10.1111/j.1151-2916.1964.tb14638.x.

238. Chappex, T., K.L. Scrivener, and H. Jennings, The Effect of Aluminum in Solution on the Dissolution of Amorphous Silica and its Relation to Cementitious Systems. Journal of the American Ceramic Society, 2012. 96(2): p. 592-597, DOI: 10.1111/jace.12098.

239. Swiler, D.R. and O. Perrysburg. SURFACE VISCOSITY AND THE MELTING OF GLASS. in 81St Conference on Glass Problems: Ceramic Transactions. 2021. Wiley Online Library,

240. Saulat, H., et al., Preparation and applications of calcium carbonate whisker with a special focus on construction materials. Construction and Building Materials, 2020. 236: p. 117613,

241. Lombardo, T., et al., Characterisation of particulate matter deposition inducing soiling of modern glass. Air Pollution and Cultural Heritage; Saiz-Jimenez, C., Ed, 2004: p. 209-214,

242. Feng, Q., Principles of calcium-based biomineralization, in Molecular Biomineralization. 2011, Springer. p. 141-197, DOI: 10.1007/978-3-642-21230-7_6

243. Chen, Q., et al., Synthesis and characterization of calcium carbonate whisker from yellow phosphorus slag. Open Chemistry, 2020. 18(1): p. 347-356, DOI: 10.1515/chem-2020-0036

244. Holman, J.P., Heat transfer. 2010, McGraw Hill Higher Education

245. Zanotto, E.D. and J.C. Mauro, The glassy state of matter: Its definition and ultimate fate. Journal of Non-Crystalline Solids, 2017. 471: p. 490-495,

246. Dhami, N.K., M.S. Reddy, and A. Mukherjee, Biomineralization of calcium carbonates and their engineered applications: a review. Frontiers in microbiology, 2013. 4: p. 314, DOI: 10.3389/fmicb.2013.00314

247. Guo, X., et al., Controlled crystallization of hierarchical and porous calcium carbonate crystals using polypeptide type block copolymer as crystal growth modifier in a mixed solution. CrystEngComm, 2011. 13(6): p. 2054-2061,

248. Nath, M., A. Ghosh, and H.S. Tripathi, Hot corrosion behavior of Al2O3–Cr2O3 refractory by molten glass at 1200° C under static condition. Corrosion Science, 2016. 102: p. 153-160,

249. Manfredo, L. and R. McNally, The corrosion resistance of high ZrO2 fusion-cast Al2O3-ZrO2-SiO2 glass refractories in soda lime glass. Journal of materials science, 1984. 19(4): p. 1272-1276,

250. Preston, F. and J. Turnbull, The physics of upward drilling. American Journal of Science, 1941. 239(2): p. 92-105,

251. Busby, T. and J. Barker, Simulative studies of upward drilling. Journal of the American Ceramic Society, 1966. 49(8): p. 441-446, DOI: 10.1111/j.1151-2916.1966.tb15413.x

252. Aboud, T.K., L. Stoch, and M. Šroda, Quartz crystallization in soda-lime-silica glass. Optica Applicata, 2005. 35(4), DOI: 10.1007/978-3-642-41714-6_35862

253. Smiljanić, S., et al., Influence of additives on the crystallization and thermal conductivity of container glass cullet for foamed glass preparation. Ceramics International, 2021. 47(23): p. 32867-32873, DOI: 10.1016/j.ceramint.2021.08.183.

254. Bogas, J.A. and A. Gomes, Compressive behavior and failure modes of structural lightweight aggregate concrete–Characterization and strength prediction. Materials & Design (1980-2015), 2013. 46: p. 832-841, DOI: 10.1016/j.matdes.2012.11.004

255. Hirsch, T., T. Matschei, and D. Stephan, The hydration of tricalcium aluminate (Ca3Al2O6) in Portland cement-related systems: A review. Cement and Concrete Research, 2023. 168: p. 107150,

256. Borges, A.L., et al., Evaluation of the pozzolanic activity of glass powder in three maximum grain sizes. Materials Research, 2021. 24: p. e20200496,

257. Souri, A., et al., Pozzolanic activity of mechanochemically and thermally activated kaolins in cement. Cement and Concrete Research, 2015. 77: p. 47-59,

258. Osfouri, M., J.-E.F. Ibrahim, and A. Simon, Properties of foam glass produced with the use of soot from a cement factory as a foaming agent: A study based on Taguchi design of experiments. Ceramics International, 2024, DOI: 10.1016/j.ceramint.2024.10.152.

259. Zifang, X., et al., Development and Performance Characterization of Lightweight Foam Glass Mixed with Coal Waste. Integrated Ferroelectrics, 2023. 234(1): p. 1-7,

260. Wu, L., et al., Influence of the heat treatment on the structure and property of the foam glass. Applied Mechanics and Materials, 2014. 488: p. 90-93,

261. Qu, Y.-N., et al., High porosity glass foams from waste glass and compound blowing agent. Journal of Porous Materials, 2016. 23: p. 1451-1458,